Department für Biotechnologie

Institut für angewandte Mikrobiologie

Vorstand:

Ao.Univ.Prof. Dipl.-Ing. Dr.nat.techn. Florian Rüker

Betreuer:

Ao.Univ.Prof. Dipl.-Ing. Dr.nat.techn. Alois Jungbauer

SURFACE ENERGY OF HYDROPHOBIC CHROMATOGRAPHIC MEDIA AND THE IMPACT OF RADIAL FLOW DIRECTION TO THE PEAK DISTRIBUTION IN CHROMATOGRAPHY

Dissertation

zur Erlangung des Doktorgrades
an der Universität für Bodenkultur Wien

Eingereicht von
DI Ingeborg Bednar

Wien, im November 2014

Abstract

An inverse liquid chromatography method to determine the surface energy of hydrophobic interaction chromatography media was developed and applied to several beaded chromatographic media and, after enhancements, also to monoliths. Subsequently also the hydrophobicity of the media, represented by the free energy of interaction between chromatography material and water, was determined. So a ranking according to the surface energy and particularly to the hydrophobicity of chromatographic media, instead of a relative ranking regarding the retention of model proteins, was done for the first time. The results do agree with literature data and data from manufacturers, respectively. Further benefits of this method are its appliance within the usual working environment and the possibility to compare chromatography materials with different flow direction and column volumes. For monolithic materials the conventional method, namely contact angle measurements, to determine surface energies was applied by using non-porous monolithic sheets. These results were compared with the outcome of the inverse liquid chromatography method. Apart from an additive constant, the findings are in accordance with each other. Additionally, a model to fit protein retention for radial monoliths was introduced. This model is physically motivated and can substitute the exponentially modified Gaussian function, which is generally used, but not physically justified.

Keywords

Agarose, Poly(meth acrylate), Monoliths, Surface energy, Hydrophobicity, Inverse Liquid Chromatography, Contact angle measurements, radial Chromatography

Kurzfassung

Um die Ober ächenenergie von hydrophoben Interaktionschromatographie-Materialien zu bestimmen wurde eine inverse Flüssigchromatographie-Methode entwickelt. Diese wurde auf konventionelle Säulenmaterialien und, nach einer Weiterentwicklung, auch auf Monolithen angewendet. Im Weiteren wurde die Hydrophobizität der Chromatographiemedien, die durch die freie Energie der Wechselwirkung zwischen Chromatographiematerial und Wasser gegeben ist, bestimmt. Dadurch konnten die Materialien erstmals bezüglich ihrer Ober ächenengie und Hydrophobizität gereiht werden, anstatt basierend auf der Retention von Modellproteinen, wie bislang üblich. Die Ergebnisse stimmen mit Literaturdaten beziehungsweise den Herstellerangaben überein. Die Vorteile dieser Methode sind, dass sie unter üblichen chromatographischen Bedingungen durchgeführt wird und au erdem Vergleiche zwischen Chromatographiematerialien mit axialer und radialer Flussrichtung sowie Säulen mit unterschiedlichen Volumen möglich sind. Für monolithische Materialien konnte zusätzlich die konventionelle Methode, die Kontaktwinkelmethode, um Ober ächenenergien zu bestimmen, angewandt werden. Dafür wurden nicht-poröse monlithische Filme hergestellt. Abgesehen von einer additiven Konstante stimmten die Ergebnisse beider Messmethoden überein. Au erdem wird ein Modell zur Beschreibung der Proteinretention durch radiale Monolithen vorgestellt, das die exponentiell modi zierte Gau funktion, die zwar vielfach verwendet, aber nicht physikalisch begründet ist, ersetzt.

Schlüsselwörter

Agarose, Polymethacrylat, Monolithen, Ober ächenenergie, Hydrophobizität, Inverse Flüssigkeitschromatographie, Kontaktwinkelmessung, radiale Chromatographie

many thanks to …

my advisor, Alois Jungbauer, for giving me the opportunity to conduct my thesis in his working group, for his con dence and cheerful disposition particularly in di cult times

Rupert Tscheliessnig for his support based on his expert knowledge and the many things I was able to learn from him and through working with him

Verena Beck, for enriching the project work with her management qualities

my company partner BIA separations for the trouble-free collaboration; especially Nika Lendero Krajnc and Ale Podgornik for fruitful discussions and sharing their expertise

the working group Downstream Processing for their kindly admittance as well as professional and amicable conversations, especially Nikolaus Hammerschmidt, Beate Hintersteiner, Moritz Imendör er, Nico Lingg (special thanks for chromatography tutoring), Svjetlana Medjacovic, Agnes Rodler, Ralf Sommer, Petra Steppert, Cornelia Walther and Martin Wellhöfer

the Austrian Centre of Industrial Biotechnology, I am grateful for the nancial support

all those who accompanied me through the good and tough times doing my thesis, particularly Agnes Rodler, for her encouragement; on the basis of her staying power and gentleness she is a shining example to me

my friends Matthias Berger, Jochen Billinger, Oliver Geppert, Marcel Janczer, Veronika Magerl, Anne Neumann, Nora Odabas, Bernhard Schott, Katharina Schott (special thanks for proofreading), Claudia Stefan, Michael Traub, Maria Vogt, Cornelia Walther

all fellows (formerly) from the TU Vienna, especially Matthias Ikeda, Walter Kantor, Friedrich Kneidinger, Karl-Anton Lorenzer, Alexander Zavarsky and my former advisor Ernst Bauer

the gorgeous and brilliant Waltraud Emhofer, Michaela Königshofer and Dorit Mersmann from the "writing marathon group"

Marianne und Bernd Plibrsek for providing a place of refuge when I needed it the most

my friend Kathrin Kurzbauer, I appreciate her attitude of continuous honesty and asking inconvenient questions, I am grateful for her beeing at my side

my family, particularly my parents for their everlasting support, my beloved grandfather for sharing his experience of life and my brother for sharing chocolate, library tables as well as jolly lunch and co ee breaks with me

List of Symbols

ΔG change in Gibbs free energy

ΔG^{AB} Lewis acid-base contribution to the change in Gibbs free energy

ΔG^{LW} Lifshitz-van der Waals contribution to the change in Gibbs free energy

ΔG_{ijk} change in free energy of interaction for a system of three components indicated by i, j and k

ΔG_{lk} change in Gibbs free energy of two substances l and k

ΔH change in enthalpy

ΔS change in entropy

δ Dirac delta function

ϵ porosity

γ surface energy

γ^{+} Lewis acid contribution to the surface energy

γ^{-} Lewis base contribution to the surface energy

γ^{AB} Lewis acid-base contribution to the surface energy

γ^{LW} Lifshitz-van der Waals contribution to the surface energy

μ_0 peak area

μ_1 rst raw moment

ν volumetric velocity

∂_t partial di erentiation with respect to time t

ρ_i densitiy of substance i

ϑ_{lk} contact angle between a solid, indexed by k and a liquid, indexed by l

A_i (theoretical) area an adsorbed molecule of substance i covers on the surface, $A_i/\sqrt[3]{\pi^2} = 3(MW_i)/(4\rho_i N_A))^{2/3}$

$c'(t)$ partial differentiation of $c(t)$ with respect to time t

$c(t)$ time dependent concentration

c_0 peak height

$c_{k'}$ concentration of the molecular probe in the mobile phase

D dispersion coefficient

D_i innner diameter

D_o outer diameter

H Henry constant, $H = k'\varepsilon/(1-\varepsilon)$

I_0 Bessels function of the first kind, order zero

k' retention factor

k_B Boltzmann constant

L column length

MW_i molecular weight of substance i

N_A Avogadro constant

T temperature in Kelvin

t_0 dead time

t_R retention time

u chromatographic velocity, $u = L/t_R$

z dimension in axial direction of the column

Table of Contents

1. Introduction

1.1. Preface

The surface free energy of a material is known as the basic parameter for adsorption, adhesion and wetting [1]. These surface properties are an issue in several disciplines, e.g. in painting where organic binders are used to x pigments on canvas, wood, metals, stone, fresco or grounding; wherever the painter wants to present the work of art [2, 3, 4]. Further applications are the surface coating of cars and aerospace bodies, containers, wind turbines, bridges, rail cars, petrochemical plants, engine rooms on ships and many more [5, 6]. In dental practice the preparation of dentin to obtain the appropriate surface free energy of the teeth to establish a durable bonding with a crown is a crucial issue [7] . In all this applications the adsorption or adhesion of molecules should last independently of changes in their physical or chemical environment, for several years, decades or in the case of art work even for centuries.

In particular cases the adsorption or adhesion of certain molecules should be avoided, e.g. in facade coatings to prevent growth of alga for aesthetic reasons [8, 9]. Microbes or bacterial adhesion as well as bio lm formation should be prevented on surfaces where a hygiene risk is present, e.g. in processing equipment for cooling water or food [10, 11]. Also the surface properties of medical devices like implants, cardiovascular devices and many other biomedical aids should be designed to prohibit protein adsorption, which leads to a consecutive adsorption of brous proteins, originating an immune reaction [12, 13, 14].

Contrary, in other disciplines there is the desire to desorb previously adsorbed molecules from a surface, particularly in chromatography, where these processes are induced to separate molecules. In this eld the challenge is to adjust the adsorption strength of certain molecules by their physical or chemical environment. The molecules ad- and desorbed are most often very complex, e.g. proteins. The adsorption ability and selectivity are a crucial factors to the decision of using a particular chromatography material e.g. in a puri cation

step. Up to now the adsorption strength of a chromatography column to a certain protein or molecule has been estimated by considering the different retention behavior of certain model or reference proteins. This method needs loads of intuition and experience of the experimenter and is therefore, above all, subjectively biased.

The selective adsorption of certain molecules is a method to separate molecule mixtures by chromatography. This can be realized by size exclusion (SEC), normal phase chromatography (NPC), reversed phase chromatography (RPC), metal ion interaction (MIC), biospecific or affinity (BIC), ion exchange (IEC) and hydrophobic interaction chromatography (HIC). Also so-called mixed mode or mulitmodal interaction chromatography do exist, where electrostatic and hydrophobic interactions or positive and negative charged ligands are combined.

In size exclusion chromatography only the steric exclusion of large molecules takes place, no further interactions between molecules and chromatography material are responsible for a separation, at least in theory. For other types of chromatography the strength of interaction of molecules with a column can vary from being very different to a gradual change or even to be not specific at all. Of course, for the latter case no separation of molecules would take place, apart from their size. If such molecules should be separated, another chromatography method or a modification of the applied method should be considered. But, if a certain bunch of molecules, e.g. different impurities, should be separated from a target protein, this might be as desired. The chromatographic parameters like the stationary phase, mobile phase composition, salt, organic solvent or competitively bound species concentration of the eluent, pH and temperature have to be adjusted to obtain the optimal effect [15, 16].

But how is the adsorption behavior related to the surface energy? Generally, a reaction, e.g. adsorption of a molecule, takes places spontaneously if the Gibbs free energy decreases within this process [17]. Since the surface free energy is directly related to the difference of the Gibbs free energy, it is interconnected also with the adsorption behavior. Information on the surface free energy of chromatography materials may be used to predict adsorption respectively retention as well as desorption. Of course, to undertake that, all relevant properties of the adsorbents and mobile phases have to be known.

Are other properties of a chromatography medium connected with the surface energy? The surface energy is related to certain interaction forces via the Gibbs free energy. According to Van Oss [18] these interactions can be split into apolar Lifshitz-van der

Waals and polar Lewis acid and base inter- and intraactions. Fowkes et al. [19] found that London dispersion forces (a part of Lifshitz-van der Waals forces) and Lewis acid and base interactions are responsible for the solubility, how plasticizers can act, the wettability, the reinforcement, crystallinity, and mechanical properties of polymers. Additionally, steric restrictions do in uence these properties as well.

Generally, the surface energy of a material is responsible for the wetting properties of a material. This holds of course also for chromatography media. Typically, if the term wettability is used, the wettability of the surface with water is meant. Wettability in general is dependent on the surface energy of the material to be wetted (a solid) and on the interfacial energy between the liquid and the solid, but also on the surface roughness. Widely known are the hydrophobic properties of the lotus leaf, which surface structure in uences the wettability behavior of the surface regarding water, so that water drops immediately roll o [20].

Furthermore, the aging of materials like oxidation, degradation and recrystallization alters the bonds between bulk molecules of a material and this in uences the surface properties, including the surface energy. Also chemical deposition can happen while materials mature, so the surface energy can be a measure for the progress of material aging. Moreover, the coating of a surface with molecules will also in uence its surface energy [21]. That results in the fact that, if a chromatography material had aged or is loaded with non-desorbable molecules, this has an irreversible impact on the surface energy and on the ability to adsorb molecules. Thus, the surface energy may be used as a measure of the column contamination and used to estimate its expectable performance regarding a certain chromatography step.

1.2. Introduction and Motivation

Besides the physical characterization of chromatography media, characterization of the surface respectively the chemistry of the material is needed to achieve a comprehensive picture.

The physical parameters of any stationary phase are its particle size and distribution, its pore size and distribution as well as its mechanical stability (compressibility, resistance to abrasive forces). The surface and chemical properties of chromatographic media are the ligand type, the ligand density and its distribution, the coverage of the backbone with the

1. Introduction

ligand, the ligand stability as well as the backbone material. These properties induce a certain surface energy of the material, which is another physical parameter. It can be used to describe the adsorption strength of surfaces with molecules and to rank chromatography media. Today ranking of chromatographic media is routinely done by measuring the retention of reference molecules, particularly proteins. Within this work a new method is presented, replacing the relative ranking of hydrophobic interaction chromatography (HIC) materials by a physical parameter.

Usually the surface energy is obtained via contact angle measurements. To determine the contact angle of a material a at surface is necessary, which is not available for beaded chromatography media. In addition, soaking e ects of porous materials make the measurement of contact angles unfeasible. Therefore, also porous monolithic materials can not be investigated by contact angle measurements, although the production of a at surface would be possible. Above all, di erent theoretical approaches lead to di erent surface energies [22].

A novel method to quantify surface energy of porous surfaces is needed. Inverse Liquid Chromatography (ILC) together with the acid-base theory (according to van Oss [18]) allows to determine the surface energy of the column material within its usual working environment. The area occupied by adsorbed molecules, the molecular properties of these molecules as well as their chromatographic retention factor are the parameters which are included in the theory.

ILC is a method to characterize a chromatography column (material) by the use of substances with known properties. If the molecular sizes of the substances are the property to characterize the column, the method is named Inverse Size Exclusion Chromatography (ISEC). ISEC is used to determine the pore-size distribution or just the external, internal, and total porosities of conventional packed columns as well as monoliths [23, 24, 25]. By determining the number of plates and the height equivalent of a theoretical plate (HETP) of a column regarding to a certain protein or molecule, respectively, ILC is practiced as well [15].

1.3. Objective

Due to soaking e ects and the uneven surface of beaded media, contact angle measurements, being the conventional method to determine the surface energy, would lead to wrong results. So the rst aim of this thesis was to establish an ILC method to determine the surface energy of chromatographic materials. Up to now chromatographic media are ranked according to the retention of model proteins. Therefore a comparison between varying column sizes or columns with di erent ow directions (axial and radial) is di cult if not impossible. The new method to determine the surface energy should be applicable to all these di erent chromatography columns. Additionally, in HIC often certain proteins and columns do exhibit stronger interaction than expected, indicating a kind of particular bio-speci c a nity. It is not possible to derive di erences in hydrophobicity of chromatography columns equitable by such results [26]. An approach to compare the hydrophobicity of chromatography media on an objective basis is desired. Furthermore, peak distributions in monoliths often show tailing and tailed peaks were described traditionally by an exponentially modi ed Gaussian (EMG) function. For axial chromatography this is physically justi ed in certain cases, but not for radial chromatography, although still applied. A physically motivated model to describe protein retention in radial chromatography is missing.

The objectives in particular were:

1. Development of an ILC method to determine the surface energy of beaded HIC media with axial ow

2. Enhancement of this method to determine the surface energy of HIC monoliths with radial ow

3. Ranking of HIC media according to their surface energy and hydrophobicity

4. Comparison of the results obtained by the developed ILC method and by contact angle measurements to determine the surface energy of monolithic materials

5. Description of the peak distribution of protein retention caused by monoliths with radial ow direction to determine the height of a theoretical plate more precisely

2. Theory

A complicacy for the calculation of surface energies is that different concepts lead to different surface energies, which was investigated by Gindl et al. [22]. Their comparison between the Zisman approach, the equation of state, the harmonic mean equation, the geometric mean equation and the acid-base theory showed that the most detailed information was provided by the last approach. Therefore the acid-base theory by van Oss was taken as the theoretical fundament to determine surface energies.

2.1. Thermochemistry & van Oss' approach

2.1.1. Relation between retention factor and surface energy contributions

Van Oss [18] postulated that interactions between molecules can be divided into short range, electron acceptor and donor, namely Lewis acid and base (AB), and long range Lifshitz-van der Waals (LW) interactions, between different molecules and those of the same kind. Lewis acid base interactions are polar, but non-electrostatic interactions, as e.g. hydrogen bonds. The apolar Lifshitz-van der Waals interactions comprise van der Waals-Keesom (permanent dipole-dipole), van der Waals-Debye (permanent dipole-induced dipole) and van der Waals-London (fluctuating dipole-induced dipole) interactions [27].

The Gibbs free energy (G) consists of these contributions and this holds also for a change in Gibbs free energy (ΔG)

$$\Delta G = \Delta G^{LW} + \Delta G^{AB}. \tag{2.1}$$

Since the surface energy (γ) is a linear function of the Gibbs free energy ($\Delta G = -2\gamma$), this partition holds for the surface energy as well:

$$\gamma = \gamma^{LW} + \gamma^{AB}. \tag{2.2}$$

The polar contribution to the surface energy includes Lewis acid $(+)$ and Lewis base $(-)$ contributions and is de ned according to van Oss by

$$\gamma^{AB} = 2\sqrt{\gamma^+ \gamma^-}. \tag{2.3}$$

For a system of three substances, a molecular probe (index i), immersed in a liquid (index j), adjacent to a surface (index k), the free energy of interaction covering this system (ΔG_{ijk}) can be expressed by the individual contributions of the surface energy of all three partners:

$$\Delta G_{ijk}/2 = -\gamma_j^{LW} + \sqrt{(\gamma_i^{LW}\gamma_j^{LW})} + \sqrt{(\gamma_j^{LW}\gamma_k^{LW})} - \sqrt{(\gamma_i^{LW}\gamma_k^{LW})}+ \tag{2.4}$$
$$\sqrt{\gamma_j^+}\left(\sqrt{\gamma_i^-} - \sqrt{\gamma_j^-} + \sqrt{\gamma_k^-}\right) + \sqrt{\gamma_j^-}\left(\sqrt{\gamma_i^+} - \sqrt{\gamma_j^+} + \sqrt{\gamma_k^+}\right) +$$
$$-\sqrt{\gamma_i^+ \gamma_k^-} - \sqrt{\gamma_i^- \gamma_k^+}$$

Additionally, the free energy of interaction can be related to a chromatographic parameter, the retention time, if certain preconditions are ful lled [28]

$$\Delta G_{ijk} = -k_B T/A_i \ln k'_{ijk} \frac{\varepsilon}{(1-\varepsilon)}. \tag{2.5}$$

Here k_B stands for Boltzmann s constant and T for the temperature in Kelvin. A_i symbolizes the (theoretical) area an adsorbed molecule of substance i covers on the surface: $A_i/\sqrt[3]{\pi^2} = 3(MW_i)/(4\rho_i N_A))^{2/3}$. It is calculated by using the molecular weight MW_i, its density ρ_i, the Avogadro constant, N_A and by assuming a spherical molecule. The retention factor can be determined by ILC via pulse response experiments.

The contributions of the molecular probes to the surface energy $(\gamma_i^{LW}, \gamma_i^+$ and $\gamma_i^-)$ as well as the parameters for the mobile phase, HQ-water in this case, $(\gamma_j^{LW}, \gamma_j^+$ and $\gamma_j^-)$ have to be known. The retention factors are obtained by pulse experiments. If the total porosity of the column is known, three molecular probes with known surface energy contributions are necessary to determine the three contributions to the surface energy of the chromatography material $(\gamma_k^{LW}, \gamma_k^+$ and $\gamma_k^-)$. By equalizing the right sides of eq. 2.4 and 2.5 and insertion of all known parameters a system of three equations is formed which has to be solved to

obtain γ_k^{LW}, γ_k^+ and γ_k^-.

By applying an additional mathematical move it is not necessary to know the exact value of the total porosity. Instead the retention of a fourth molecular probe has to be measured. Beyond that, it is necessary to know the polar and apolar surface energy contributions of this fourth molecular probe as well. This approach is executed more detailed in subsection 2.1.3.

2.1.2. Determination of the retention factor

For conventional chromatography columns the UV-response over time is described by the solution of the mass balance equation

$$c_{k'} = c_0 \frac{1}{2\sqrt{D\pi\dfrac{t}{1+k'}}} \exp\left(-\frac{\left(z - u\dfrac{t}{1+k'}\right)^2}{4D\dfrac{t}{1+k'}}\right). \tag{2.6}$$

The parameter $c_{k'}$ represents the concentration of the particular molecular probe in the mobile phase. It is dependent on time t and dimension z in the direction of the column. D, the axial dispersion coefficient, comprises all contributions to peak broadening. The parameter u represents the chromatographic velocity and is calculated by the retention time t_R (location of the peak maximum) of glucose together with L, the column length: $u = L/t_R$. The overall peak height is determined by c_0.

It is assumed that the response consists of two parts, the molecular probes that have interacted with the surface exhibit a retention factor of $k'' > 0$, those that have not interacted are represented by a retention factor of $k'' = 0$

$$c_{k'} = \int_0^\infty (\delta(k'') + \delta(k'' - k'))c_{k''}dk''. \tag{2.7}$$

Therein δ represents the Dirac delta function. The retention factors k' are obtained by fitting eq. 2.7 to the experimental data [28].

An analytical solution to describe the retention of small molecules as discussed for conventional chromatography columns is missing for monoliths. Therefore the retention time t_R is obtained by the first raw moment, μ_1, which depends also on μ_0, the peak area, acting as scaling factor.

$$\mu_1 = \frac{1}{\mu_0} \int_0^\infty c(t)t \, dt \tag{2.8}$$

It happens that the experimental signal shows drifting and/or shifting of the baseline. In Bednar et al. [29] a method is presented to analyze such data without the need to apply a background correction function.

The idea is to use the differentiated UV detector signal for the analysis. This approach has the benefit that a baseline shift cancels immediately and a baseline drift which is linear in time can be simply corrected by shifting the differentiated signal down to the base line. Additionally it is useful to employ a time weighting factor to smooth the signal, particularly for small times. Thus the value of the vertical shift can be determined more precisely.

First of all the rearranged eq. 2.8 has to be partially differentiated.

$$\partial_t(\mu_1\mu_0) = 0 = \int_0^\infty \partial_t(c(t)t) \, dt. \tag{2.9}$$

Because μ_1 and μ_0 are constants, the result of eq. 2.9 is zero. By taking the right side of this equation and expanding it, the following relation is achieved

$$\int_0^\infty c(t) \, dt = -\int_0^\infty c'(t)t \, dt. \tag{2.10}$$

By replacing $c(t)$ with the Dirac delta function and taking the absolute value of both sides the relation used in [29] $|\delta(t)| = |-t\partial_t\delta(t)|$ results. This relation is mathematically meaningful solely if an integral is applied to it.

In order to calculate the integral of the first raw moment, $c(t)$ in eq. 2.10 has to be replaced by $c(t)t$, then by partial integration

$$\mu_1\mu_0 = \int_0^\infty c(t)t \, dt = -\frac{1}{2}\int_0^\infty c'(t)t^2 \, dt \tag{2.11}$$

is obtained.

The maximum of a relation can be determined by its partial differentiation, by doing so, the result of the left side of the equation is zero because μ_0 and μ_1 are constants, as already

shown in eq. 2.9. Therefore also the right hand side has to vanish.

$$-\frac{1}{2}\partial_t \int_0^\infty c'(t)t^2 dt \equiv 0 \tag{2.12}$$

The differentiation and the integral cancel each other out. The resulting equation is

$$c'(t)t^2 = 0. \tag{2.13}$$

The trivial solution of eq. 2.13 is $t = 0$, the non-trivial solution, which is the one of interest, is $c'(t) = 0$. That means that the zero crossing point of the differentiated signal represents the value of the first raw moment, which is associated with the retention time t_R. An additional time weighting of the signal does not influence this result, so the differentiated, time weighted UV detector signal, shifted to the baseline, is used to determine the retention times.

The retention factors are calculated by

$$k' = \frac{t_R - t_0}{t_0} \tag{2.14}$$

with dead time $t_0 = (D_o - D_i)/(2u)$ and by using the following parameters: the outer diameter D_o, the inner diameter D_i and the chromatographic velocity u, which is in turn calculated, according to [29], by

$$u = \nu \frac{1}{L\pi\epsilon} \frac{\log D_o - \log D_i}{D_o - D_i}. \tag{2.15}$$

Here ν stands for the volumetric velocity, ϵ is the porosity and L symbolizes the column length.

2.1.3. Calculation of the surface energies

In eq. 2.4 the Gibbs free energy is linked to the surface energies and via eq. 2.5 these are related to the retention factor.

By setting up a system of equations according to $\Delta G_{ijk} = \mathbf{m'} \cdot \mathbf{b}$, the elements of the vector $\mathbf{b} = \{\gamma_k^{LW}, \gamma_k^+, \gamma_k^-\}$ can be determined. If the porosity is set to a particular value, three unknown parameters, the elements of $\mathbf{b}$, are to be calculated. The system is completely determined by using three molecular probes.

If an exact value for the porosity cannot be inserted, a mathematical move has to be applied to calculate the contributions of the surface energy. For all conventional chromatography columns, the system of four equations was reduced to a system of three equations by subtracting equations from each other. By doing so the porosity (which is assumed to be similar for each molecular probe) cancels out.

For the monoliths, an enhanced method was applied to calculate the surface energy contributions. Each equation was subtracted with another, resulting in six equations to calculate three parameters. The solution to such an overdetermined system is to apply a least squares minimization. Eq. 2.4 is written as a vector product

$$\Delta G_{ijk} = \mathbf{m'}_i \cdot \mathbf{b} \tag{2.16}$$

with $\mathbf{b} = \left\{ \gamma_k^{LW}, \gamma_k^+, \gamma_k^- \right\}$. Then pairwise subtraction was carried out:

$$\Delta G_{ijk} - \Delta G_{i'jk} = (\mathbf{m'}_i - \mathbf{m'}_{i'}) \cdot \mathbf{b}. \tag{2.17}$$

By applying the pseudoinverse matrix $(\mathbf{m'}_i - \mathbf{m'}_{i'})^{-1}$ from the left, the overdetermined system is solved by minimizing the Euclidean length of the residual vector

$$r = \Delta G_{ijk} - \Delta G_{i'jk} - (\mathbf{m'}_i - \mathbf{m'}_{i'}) \cdot \mathbf{b}. \tag{2.18}$$

The system gets even stronger overdetermined if more molecular probes are used, but it is still possible to nd a solution [22].

2.1.4. Relation between contact angle and surface energy contributions

By using Young s equation, wetting can be quantitatively described. The contact angle ϑ_{lk} is related to the interfacial surface energy of the liquid and the solid, γ_{lk} as well as to the surface free energies of the solid γ_k and the liquid γ_l.

$$\gamma_{lk} = \gamma_k - \gamma_l \cos \vartheta_{lk} \tag{2.19}$$

The right hand side of eq. 2.19 does not change if indices are exchanged ($\gamma_{lk} = \gamma_{kl}$). The contact angle is related to the Gibbs free energy via the Young-Dupré equation

$$\Delta G_{lk} = -\gamma_l \left(\cos \vartheta_{lk} \right). \tag{2.20}$$

The Gibbs free energy of two substances can be given in terms of the contributions to the surface energies

$$\Delta G_{lk} = -2\sqrt{\gamma_l^{LW} \gamma_k^{LW}} - 2\sqrt{\gamma_l^+ \gamma_k^-} - 2\sqrt{\gamma_l^- \gamma_k^+}. \tag{2.21}$$

Thereby it is possible to relate the surface free energy contributions to the contact angle.

$$-\gamma_l \left(\cos \vartheta_{lk} \right) = -2\sqrt{\gamma_l^{LW} \gamma_k^{LW}} - 2\sqrt{\gamma_l^+ \gamma_k^-} - 2\sqrt{\gamma_l^- \gamma_k^+}. \tag{2.22}$$

2.1.5. Calculation of the surface energies

Again, by using different liquids a matrix equation can be set up $\mathbf{a} = \widehat{\mathbf{m}} \cdot \mathbf{b}$. Herein vector $\mathbf{a}$ includes the contact angles and vector $\mathbf{b}$ has the surface energy contributions as vector components. The matrix $\widehat{\mathbf{m}}$ comprises the surface energy contributions of the molecular probes. To solve this equation, $\widehat{\mathbf{m}}^{-1}$, the pseudoinverse matrix of $\widehat{\mathbf{m}}$, has to be multiplied from left: $\mathbf{b} = \widehat{\mathbf{m}}^{-1} \cdot \mathbf{a}$. To solve the matrix equation contact angles and surface energy contributions of at least three different liquids have to be known.

2.2. Peak distribution in axial and radial chromatography

Gritti and Guiochon [30] pointed out that serious systematic errors occur when approximate methods were used to measure peak moments of retention data. They investigated pulse experiments with asymmetries differing from exponentially modified Gaussian (EMG) distributions. Peak moments determined by numerical integration were compared with moments obtained via fit parameters of the EMG function and large deviations were found. Although these peaks originated from axial chromatography, this conclusion will also hold for asymmetrical peaks obtained by radial chromatography and diverging from the EMG function. Monoliths show peak tailing very often (regardless if the flow is directed in axial or radial direction) and the EMG function is usually used to fit these peaks although the retention is neither described well by this distribution nor is it physically reasonable. For monoliths with radial flow a fit function describing protein retention better than the EMG distribution

function was found. Furthermore it is physically motivated (see appendix C).

Based on Bednar et al. [28], where an ILC method is established to determine the surface energy of chromatography media with axial flow, this principle has been extended to chromatography media with radial flow geometry. The mass balance equation is formulated in cylindrical coordinates, because the mass transport through the monolithic tubes occurs in radial direction. Furthermore the mass transport through the chromatography media is uniformly distributed along the circumference, therefore it is independent from the azimuth angle φ.

The same constraints to the mobile phase properties and similar constraints to the monolithic tube material as for axial problems are assumed (see [28]). Like its counterpart in axial chromatography, the radial dispersion coefficient is assumed to be constant and independent of the solute concentration.

These assumptions simplify the mass balance equation in cylindrical coordinates to a linear differential equation in r (radial distance)

$$\frac{\partial c}{\partial t} + \frac{(1-\varepsilon)}{\varepsilon}\frac{\partial q}{\partial t} + u\frac{\partial c}{\partial r} = D\frac{1}{r}\frac{\partial}{\partial r}\left(r\frac{\partial c}{\partial r}\right) \tag{2.23}$$

The concentration of the mobile phase $c = c(r,t)$ and the solid loading $q = q(r,t)$ are dependent on time and radial dimension r. D, here the radial dispersion coefficient, combines all peak broadening effects in a single parameter. The total porosity is represented by ε. The (radial) velocity u of the transported mass, is assumed to be independent from the radius and constant over time. With the implicit relation

$$\lim_{c \to 0}\partial_t q = \underbrace{\partial_c q}_{H}\,\partial_t c, \tag{2.24}$$

taking into account that the experimental parameters meet the linear region of the isotherm (Henry region), the linear differential equation is obtained by

$$(1+k')\frac{\partial c}{\partial \tau} + u\frac{\partial}{\partial r}c = D\frac{1}{r}\frac{\partial}{\partial r}\left(r\frac{\partial c}{\partial r}\right). \tag{2.25}$$

The retention factor k' is related to the Henry constant H by $k' = H(1-\varepsilon)/\varepsilon$.

By introducing moving coordinates (analogous to the transformation in Cartesian coordinates) $\xi = r - \dfrac{ut}{1+k'}$ and $\tau = t$ and using the abbreviation $\dfrac{1+k'}{D} = \dfrac{1}{\alpha}$, eq. 2.25 can be

2. Theory

written in a simpli ed form:

$$\frac{1}{\alpha}\partial_\tau c = \frac{1}{\xi}\partial_\xi\left(\xi\partial_\xi c\right). \tag{2.26}$$

Greens approach is used to sort out this problem. Generally, for a homogeneous di erential equation like

$$\mathscr{L}c(\xi,t) = 0 \tag{2.27}$$

where $\mathscr{L}$ is a linear di erential operator in ξ (an arbitrary coordinate) and $c(\xi)$ represents the solution of the di erential equation. For the inhomogeneous case the inhomogeneity the equation gives $f(\xi)$:

$$\mathscr{L}c(\xi,t) = f(\xi) \tag{2.28}$$

The so called Greens function $G(\xi)$ satisfys the equation $\mathscr{L}G(\xi) = \delta(\xi)$.
With the initial condition at time t_0,

$$c(\xi,t_0) = F(\xi,t_0), \tag{2.29}$$

the inhomogeneous equation is solved by

$$c(\xi,t) = \int G(\xi,t|\xi',t_0)F(\xi,t_0)dx', \tag{2.30}$$

where the relevant Green function has to be inserted.

According to [31], the radial Green function for this case is de ned as

$$G(\xi,\tau|\xi',\tau') = \frac{1}{4\pi\alpha(\tau-\tau')}\exp\left[-\frac{\xi^2+\xi'^2}{4\alpha(\tau-\tau')}\right]I_0\left[\frac{\xi\xi'}{2\alpha(\tau-\tau')}\right]. \tag{2.31}$$

Together with initial conditions the problem can be described completely.
Applying a transient concentration pulse to the outer surface (radial distance r_o) of a chromatography material with the shape of a hollow cylinder and radial ow from the outer surface to the inner surface, the initial condition at time τ in moving coordinates is expressed by

$$F(\xi',\tau') = c'\delta(\xi-\xi_2)\delta(\tau'). \tag{2.32}$$

At time $\tau' < \tau_0$ (respectively $t < t_0$) the concentration within the chromatography material is zero. The concentration pulse is localized at the radial distance of r_o (respectively $\xi = \xi_2 = r_o - ut_0$) and occurs at time $t_0 = 0$. Here a constant radial velocity, u, is assumed.

14

By inserting eq. 2.31 and 2.32 into eq. 2.30 the solution of eq. 2.26 is obtained:

$$c(r,t) = \frac{c_0}{4\pi\alpha(t-\tau_0)}\exp\left[-\frac{(r_o-ut)^2+r_i^2}{4\alpha(t-\tau_0)}\right]I_0\left[\frac{(r_o-ut)r_i}{2\alpha(t-\tau_0)}\right]. \tag{2.33}$$

I_0 represents Bessel s function of the rst kind, order zero.

Eq. 2.33 is similar to the Rice distribution in probability theory.

To convey this result to the previously obtained solution function for axial problems [28], eq. 2.31 has to be evaluated at $\xi = r(t)$ and $\xi' = r_i = 0$. So the concentration distribution of a lled cylinder is described. At $r_i = 0$, Bessel s function I_0 becomes $I_0[0] = 1$ and the concentration distribution is then expressed by

$$c(r,t) = \frac{c_0}{4\pi\alpha(t-\tau_0)}\exp\left[-\frac{r(t)^2}{4\alpha(t-\tau_0)}\right] \tag{2.34}$$

If imaginary, in nitesimal, radial slides were cut from this cylinder, rearranged to a cuboid and this cuboid is rolled up to a cylinder, with the mass ow pointing in axial direction, this ends up in a cylinder with axial ow. For a mathematical description of this conversion instead of the radial distance r in eq. 2.34, an axial distance, z, respectively $r(t) \to z - u\frac{t}{1+k'}$ has to be used and the injection time has to be set to $\tau_0 = 0$. Therefore the term $(t-\tau_0)$ in eq. 2.34 is simpli ed to $(t-\tau_0) \to t$. So a function similar to the solution we presented in [28] is obtained:

$$c(r,t) = c_0\frac{1}{2\sqrt{D\pi(t/1+k')}}\exp\left(-\frac{(z-u(t/1+k'))^2}{4D(t/1+k')}\right). \tag{2.35}$$

This shows that the equations for axial and radial distribution can be transferred from one to the other, although their appearance is very di erent. One has to keep in mind that the Rice-like function is an approximation, because the radial velocity is taken as constant, which is, in fact, not true.

3. Hydrophobic chromatographic media

Chromatographic media consists of a porous base material. For cleaning and sanitation, its chemical stability is mandatory. Furthermore it should provide mechanical strength, and its surface should be suitable to be chemically modified for certain applications, e.g. for HIC. This functionalization is realized as ligands which are immobilized to the sorbent surface. In some cases (monoliths) the chromatography material is copolymerized, so the second polymer, inducing a modification, is distributed all over the bulk material and is also present on the surface, but not solely.

3.1. Beaded media

Although conventional chromatography media can be spherically or irregular shaped, the term beaded media is used in both cases. These beaded media are packed in a glass cylinder, due to their inherent material porosity and the packing it can be discriminated between intra- and extra- particle porosity. Chromatography beads are compressible media and have to be handled with care to avoid changes in the column packing.
The following base materials are used: (highly) cross-linked agarose, agarose, cellulose, silica (for HPLC use), (crosslinked) polystyrene/divinyl benzene, methacrylate and other synthetic copolymers. As ligands usually short alkyl/aryl chains like phenyl, (n-)butyl, (n-)octyl, propyl, neopentyl, ether, isopropyl and methyl are employed [32, 15].

3.2. Monoliths

Contrary to beaded media, monoliths are a continuous, porous block of material which was cast into a chromatographic column. The polymeric material features large through-pores without dead ends. This has certain consequences. The solute transport through the monolith is based on convection, else as in beaded media where diffusion takes place generally.

16

Regarding the porosity, a discrimination between intra- and extra- particle porosity is not suitable. The shape and size of monoliths can be adapted as required. Especially for large scales, monoliths are operated in radial direction [15, 33].

Commercial available monoliths for HIC are based on polymethacrylates, polystyrene/divinylbenzene copolymers, polyacrylamide, cellulose as well as on silica, which is used for the puri cation of small molecules. Monoliths are produced by polymerization and therefore customizing via immobilization of ligands or copolymerization to achieve certain surface properties, like hydrophobicity, can be realized. The ligands for HIC monoliths are similar to beaded media, e.g. butyl and phenyl are often used [29, 33, 34].

3.3. Applications of HIC

HIC is implemented in monoclonal antibody (mAb) puri cation processes, it is applied for the separation of aggregates, host cell and recombinant proteins. Also for the removal of nucleic acids and endotoxins from proteins HIC is suitable. Furthermore, HIC is very e ective in separating isoenzymes and other, very similar analytes [35, 32, 36].

3.4. Advantages and disadvantages of HIC

3.4.1. Advantages

HIC is operated under gentle or even physiological conditions, causing less protein denaturation and is therefore able to achieve higher yields than other kinds of chromatography. Besides, HIC is very economically in all scales, several environmentally friendly salts are known to be applicable. Contrary to IEC, the binding mechanism of HIC is not a ected by a high salt concentration and therefore the integration of HIC into a separation scheme can be realized easily [35, 32, 36].

3.4.2. Disadvantages

It was observed that strong hydrophobic ligands may induce a reduced recovery of some biological active proteins. Also unspeci c binding and irreversible unfolding of some proteins occur. To avoid this, weakly hydrophobic media are used, but here the hydrophobicity of the proteins have to be strong enough to enable binding [32].

4. Methods to measure surface free energy

Two methods to determine the surface free energy were accomplished. An Inverse Liquid Chromatography method was developed, in a rst attempt for beaded chromatography materials, in a second step for monoliths. Contact angle measurements were conducted on non-porous monolithic sheets, speci cally produced for this purpose. For both measurement methods the following carbonaceous liquids were used as molecular probes: glycerol (GLY), ethylene glycol (EG), formamide (FORM), dimethyl sulfoxide (DMSO) and methyl ethyl ketone (MEK). The substances were chosen because their contributions to the surface energy (Lifshitz-van der Waals and Lewis acid and base contributions) were known from literature. These parameters were determined by van Oss and coworkers and are determined relative to the according values for water. These parameters are mandatory to determine the surface energy contributions of the chromatography materials by contact angle measurements as well as by Inverse Liquid Chromatography [18, 37, 38].

4.1. Contact angle measurements

The surface energy of materials is usually determined by contact angle measurements. For beaded chromatography media some di culties occur: If the beads would be stacked to build a 2-D layer, this surface would feature a certain surface roughness, depending on the size of the beads. Deviation in the surface roughness leads to di erences in the spreading of the drop applied and to discrepancies in the determination of the contact angle [39]. Beyond that, an application of contact angles on porous materials is di cult due to soaking e ects [40]. By producing monoliths as non-porous sheets these troubles could be avoided and so it has been possible to analyze these materials also by contact angle measurements.
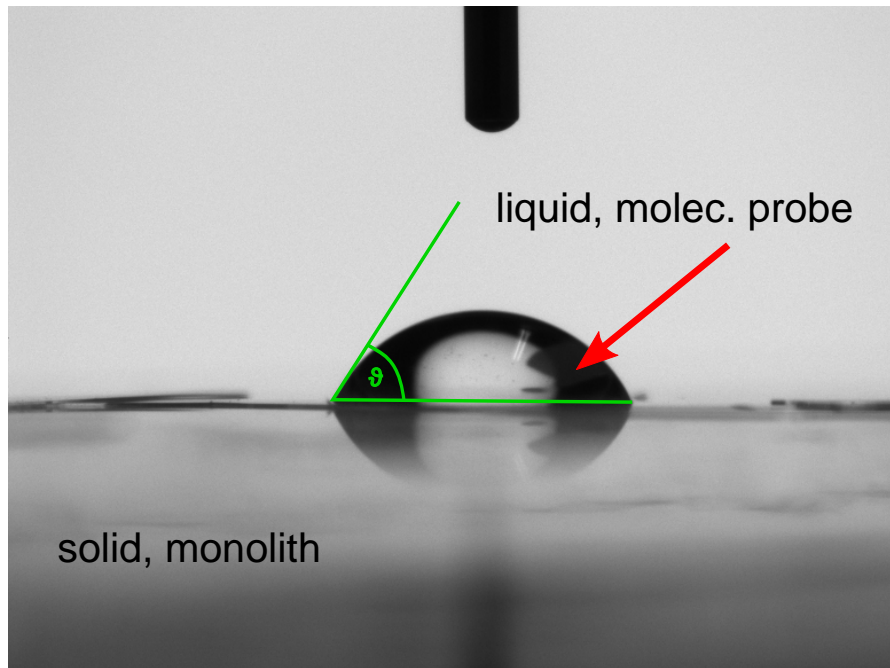
18

Figure 4.1.: A HQ-water drop (indicated with a red arrow) was placed on a monolithic surface. The contact angle ϑ is drawn in in green. At the top of the picture the cannula used to place the drop on the surface is visible.

4.1.1. Experimental method

The dehumidi ed monolithic sheets were placed on a silicon wafer. Most often the sheets bent up, so they were cautious planed by placing a second silicon wafer and on top a small weight. After a while, typically half an hour, the weight and the silicon wafer could be removed and the sheets remained at on the surface. Drops of the molecular probes and water were placed on the sheets and analyzed by an Easy Drop DSA15 drop shape analyzer manufactured by Krüss (Hamburg, Germany). A typical drop and how the contact angle is measured can be seen in g. 4.1.1. The drop shape was automatically analyzed by using the tangential method no. 1, which is also known as conic section method.

4.2. Inverse Liquid Chromatography

Usually, ILC measurements are conducted by pulse response experiments. To determine the surface energy, pulse experiments with the molecular probes, diluted with HQ-water, were undertaken. This Section focuses on the experimental and methodological realization, the underlying theory is outlined in section 2.

4.2.1. Experimental method

Preconditions and technical requirements

As outlined in [28, 29] all chromatographic experiments were conducted by using a conventional HPLC system with an UV detector. The continuously monitored UV extinction increased when the molecular probes were detected. The extinction of the molecular probes were monitored at different wavelengths by an UV detector. The wavelengths were selected by means of their extinction spectra, determined by a Cary 50 UV-VIS spectrophotometer (Varian, Palo Alto, CA, USA).

As shown in fig. 4.2-4.3, glucose dissolved in 5% (v/v) methanol (GLU), GLY and EG were detected at a wavelength of $\lambda =$205 nm, MEK was monitored at a λ of 210 nm in each case with a bandwidth of 4 nm; DMSO and FORM were detected at a wavelength of 250 nm with a bandwidth of 30 nm. The reference wavelength was 400 nm with a bandwidth of 4 nm.

If the particle size is smaller than the radiation wavelength λ, Rayleigh diffraction occurs and the extinction is proportional to λ^{-4}. Although all obtained extinction spectra increase at smaller wavelengths, especially the spectra of DMSO, MEK and FORM (see fig. 4.3) are far more complex than just a λ^{-4} dependence. This leads to the assumption that diffraction effects are combined with absorption.

The wavelengths were selected based on certain considerations:
UV radiation below 200 nm (therefore often called vacuum UV) is absorbed by most substances, including oxygen in the air [41]. A detection of wavelengths below 200 nm should be avoided, because of the larger noise and the error that might be produced due to air pressure, humidity or dispersible dust fluctuations.
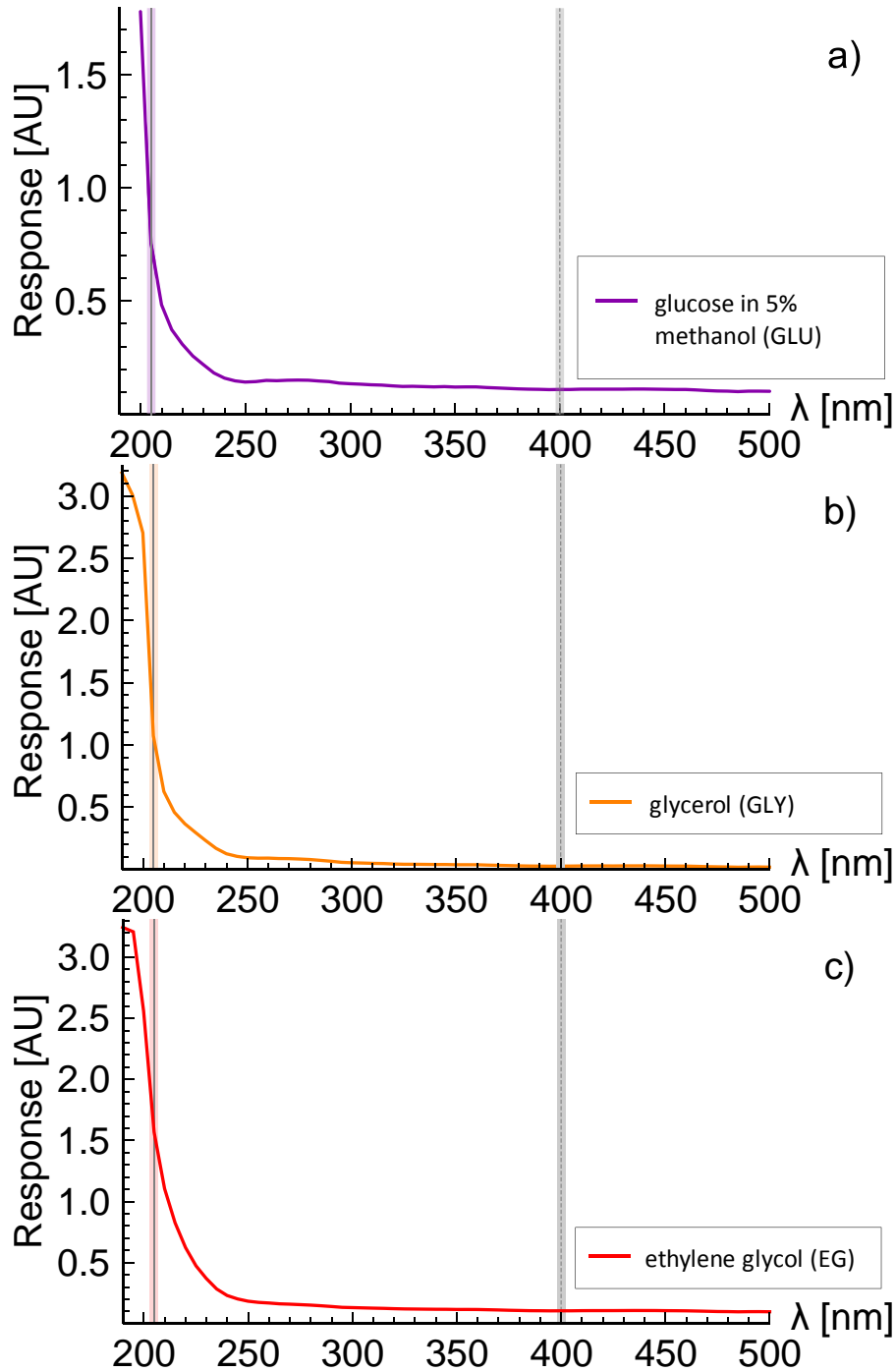
Figure 4.2.: The wavelength dependent extinction spectra of a) glucose (0.35 M) dissolved in 5% (v/v) methanol is plotted in purple, b) pure glycerol is plotted in orange and c) pure ethylene glycol is plotted in red. The spectra are shown from 190 nm to 500 nm. The wavelength selected for the extinction measurement (205 nm) is shown in every spectrum as gray vertical line with a bandwidth of 4 nm in the corresponding color. The reference wavelength of 400 nm is shown as gray, dashed, vertical line with a bandwidth of 4 nm in light gray in every plot.
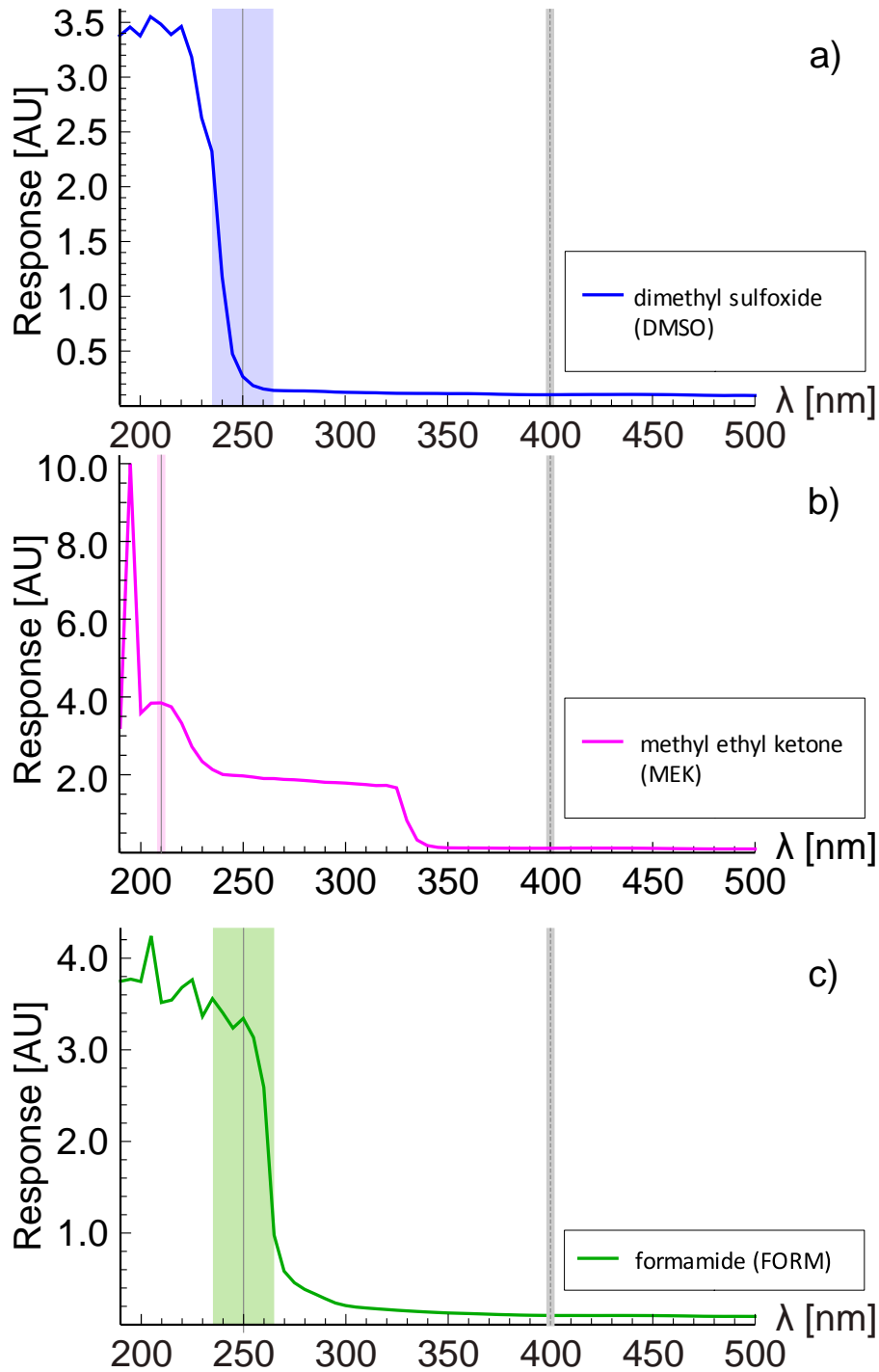
Figure 4.3.: The wavelength dependent extinction spectra of a) pure dimethyl sulfoxide is plotted in blue, b) pure methyl ethyl ketone is plotted in magenta and c) pure formamide is plotted in green. The spectra are shown from 190 nm to 500 nm. The wavelength selected for the extinction measurement are for a) and b) 250 nm with a bandwidth of 30 nm and are colored in light blue and light green. For c) the wavelength selected for the extinction measurement is 210 nm, with a bandwith of 4 nm, colored in light magenta. The reference wavelength of 400 nm is shown as gray, dashed, vertical line with a bandwidth of 4 nm in light gray in every plot.

Additionally, in case of GLU, the lowest possible wavelength was selected to meet the requirement that methanol in a cuvette should not be detected below 203 nm [42]. The detection wavelength of 205 nm with a bandwidth of 4 nm complies this condition. This choice was also suitable to detect GLY and EG. A distinct extinction maximum was observed for MEK at 210 nm and therefore chosen as detection wavelength (with a bandwidth of 4 nm).

For DMSO the detection wavelength was selected at 250 nm, although the extinction height is low. Thus, a larger bandwidth was chosen to increase the number of photons extinguished. When injecting a sample into a column, the signal gets broaden and the peak height decreases compared to a bypass experiment. To achieve reasonable signal to noise ratios for all chromatography columns the bandwidth was adjusted to 30 nm.
A further restriction was applied initially, namely that the detection wavelength plus its bandwidth has to be selected within a region of a steady extinction signal. An aspect which turned out to be irrelevant and therefore the extinction wavelength of FORM was also chosen at 250 nm with a bandwidth of 30 nm.

Linearity test

Contrary to UV-absorption e ects known from proteins, the detected extinction of the molecular probes showed that a doubling of the injection volume, respectively the doubling of molecular probe concentration, did not result in a doubling of the peak height or peak area of the extinction signal. Nevertheless, as long as the extinction is a linear function of the molecular probe concentration, the measurement is meaningful. Since both Rayleigh di raction and absorbency are linear functions of the concentration, the sum of both e ects should be linear as well.

To verify if the extinction at the selected wavelengths are linear functions of the concentration, a HPLC detector test was developed and conducted. The maximum concentrations based on the particular injection volumes, the dilutions of the individual molecular probes and column volumes were calculated. Further concentrations were selected to cover the complete concentration range down to a concentration of zero. The extinction signals of the HPLC detector for the relevant concentration ranges of all molecular probes were conducted, thereby the column was bypassed.

To avoid any influence of the injector the relevant concentrations were prepared as mobile phase, rather than performing pulse response experiments, and the HPLC detector responses were recorded.

For a correct measurement it is required that the flow rate of the HPLC is constant because the height of the extinction signal increases with the flow rate. This is plausible because at a higher flow rate more molecules are present in the optical path during a given time interval. Then more extinction events occur which cause an increased extinction signal. The calibration results are shown in fig. 4.4-4.5 and exhibit linear relationships between concentration and detector response for all molecular probes. That proves that the detector response is a linear function of the concentration and can be correlated.

Pulse experiments

The molecular probes were diluted before injected into the chromatography column to ensure a homogeneous dispersion and an adequate signal response. Glucose was dissolved in 5% (v/v) methanol to a concentration of 0.35 M.
All other molecular probes were diluted 1:2 in HQ-water. Solely for MEK the dilution was 1:6, because of the restricted solubility of MEK in water [43]. If the mixture ratio of MEK and water is too large a two-phase system evolves. This should be avoided because the mixing and also retention behavior of the two phases will be different and might cause unfeasible results.

The pulse experiments were conducted on conventional chromatography materials as well as on monoliths. For conventional chromatography columns good packing quality is essential because the subsequent analysis determines the variations from the perfect symmetry. Prepacked MediaScout MiniChrom columns with a column volume of 10 ml were used to ensure that the symmetry is adequate.

Also the flow rate of the HPLC pump has to be absolutely stable, otherwise a deformation of the resulting peaks caused by a non-constant flow rate will occur. This peak deformation will overlay with the peak tailing caused by the retention and will cause wrong results. The flow rate can be audited by measuring the volume (or mass) per time of HQ-water flowing through the HPLC.

Figure 4.4.: The experimentally determined calibration points (colored diamonds) obtained by recording the detector responses of several concentrations and their linear regression (black line) are shown. The concentrations used are for a) glucose in 5% methanol (purple diamonds) 0M, 0.07M, 0.14M, 0.21M, 0.28M, 0.35M and for both b) glycerol in H_2O (orange diamonds) and c) ethylene glycol in H_2O (red diamonds) 0%, 0.02%, 0.06%, 0.08% and 0.1%.
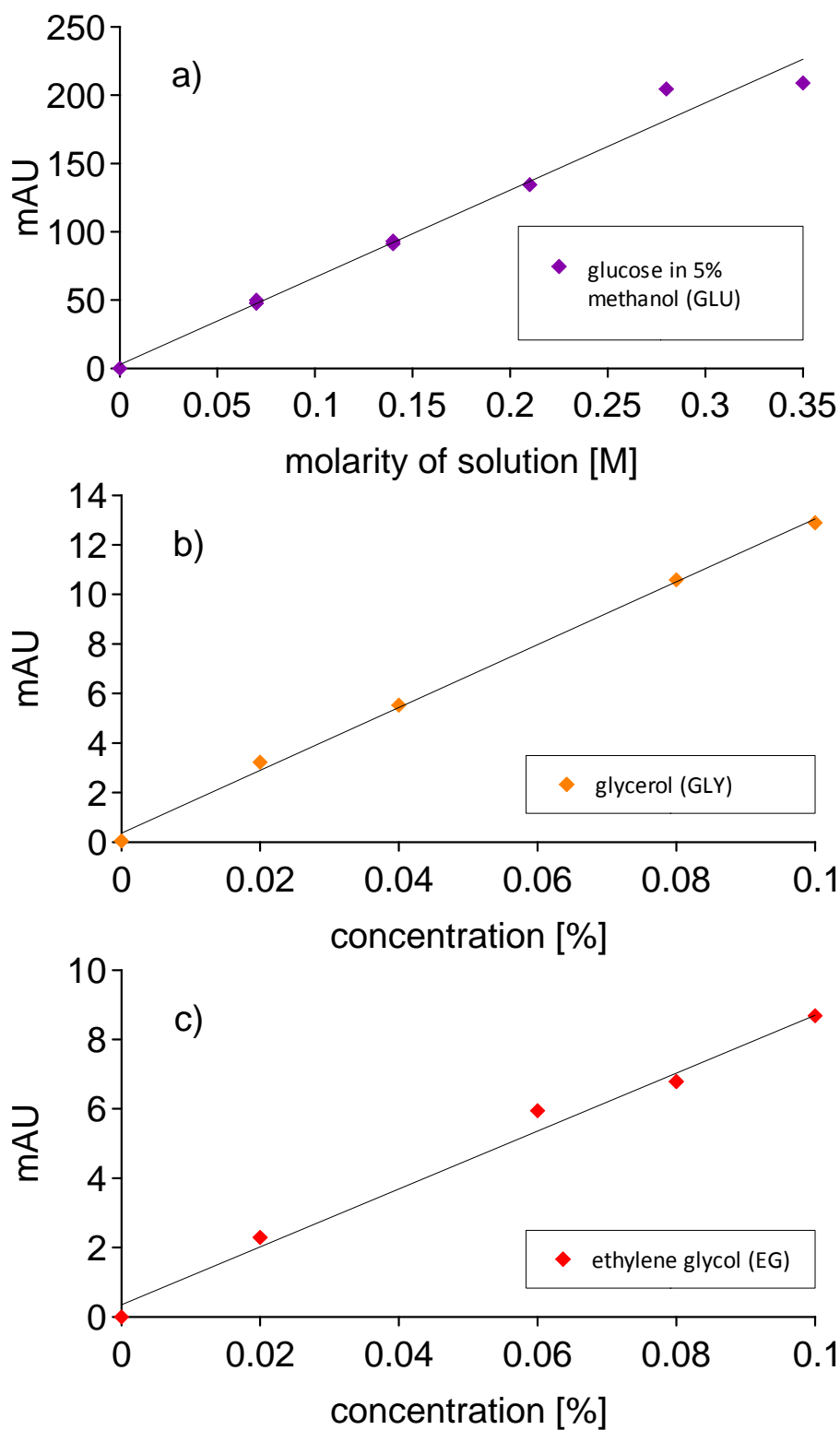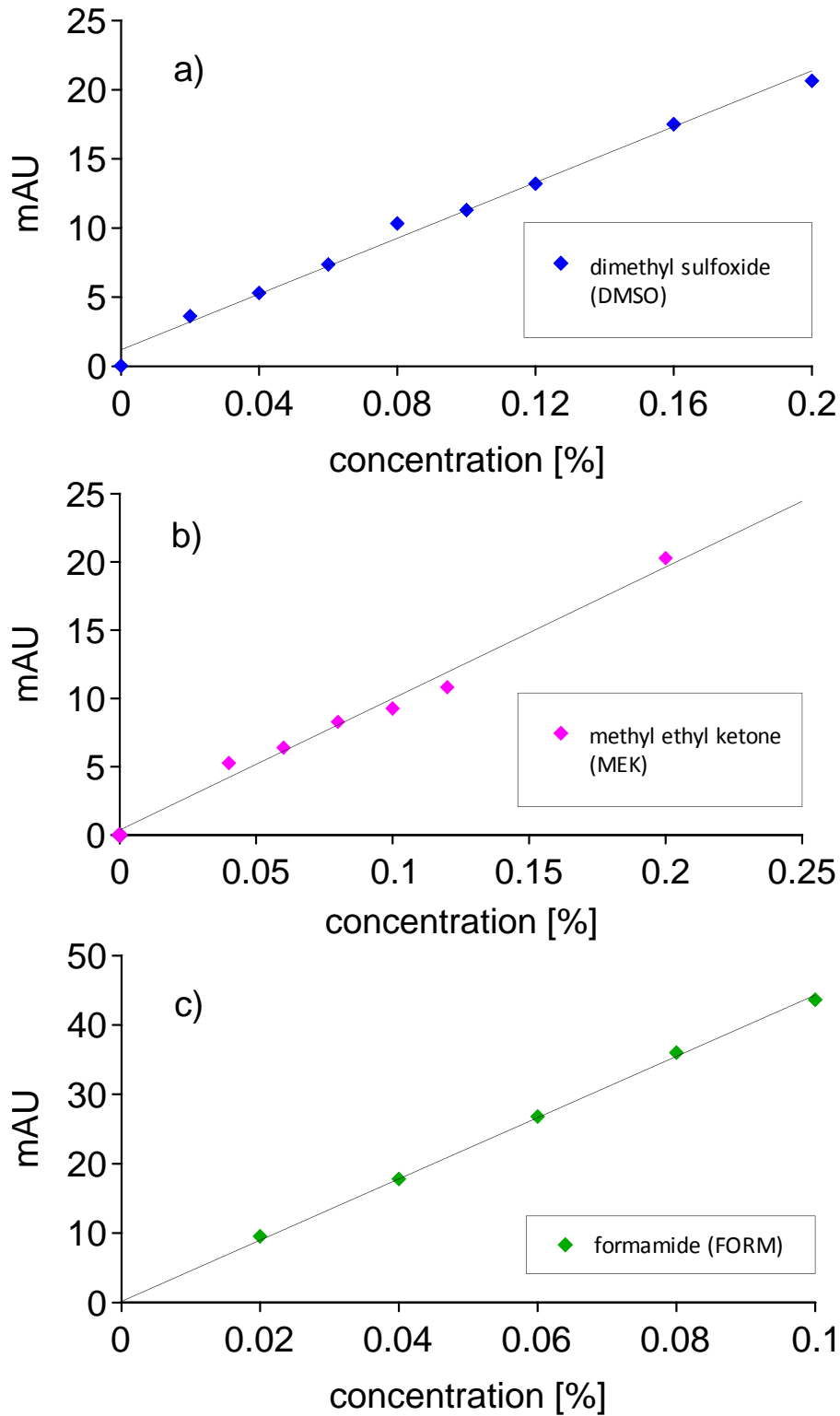
Figure 4.5.: The experimentally determined calibration points (colored diamonds) obtained by recording the detector responses of several concentrations and their linear regression (black line) are shown. The concentrations used are for a) dimethyl sulfoxide in H$_2$O (blue diamonds) 0%, 0.02%, 0.04%, 0.06%, 0.08%, 0.1%, 0.12%, 0.16% and 0.2%, b) methyl ethyl ketone in H$_2$O (magenta diamonds) 0%, 0.04%, 0.06%, 0.08%, 0.1%, 0.12% and 0.2% and c) ethylene glycol in H$_2$O (green diamonds) 0%, 0.02%, 0.04%, 0.06%, 0.08% and 0.1%.

The pulse experiments were conducted by a conventional HPLC equipped with an UV detector. The probes were injected automatically following a programmed agenda. Three pulses of GLU with 5% (v/v) methanol as mobile phase were injected to check if the column had been packed properly. To ensure that the peak symmetry, being an important property of the chromatography column, is stable over time, the glucose experiments were repeated at the end of every measurement sequence to detect packing deterioration before and after the measurements. The glucose measurements were used to determine the chromatographic velocity for the conventional columns as well. The glucose experiments on monoliths were not used for the analysis because the evaluation of the pulse experiments conducted is di erent.

The mobile phase for the pulse experiments with all other molecular probes had been HQ-water. At every switch of the mobile phase a purging step was conducted to equilibrate the column. The injection volumes for the conventional chromatography columns as well as for the monoliths are listed in Table 4.1.

Table 4.1.: Injection volumes of molecular probes for pulse experiments.

molecular probe	conventional columns	monoliths
GLU	50 μl	50 μl
GLY	10 μl, 20 μl	10 μl
EG	10 μl, 20 μl	10 μl
DMSO	10 μl, 40 μl	10 μl
MEK	50 μl	-
FORM	-	10 μl

The recorded UV detector responses over time were readout and further processed with Mathematica.

4.2.2. Revised results and discussion

Synthetic polymer-based media (Tosoh Toyopearl media) and natural polymer based media (GE Healthcare, Sepharose media) were analyzed in [28]. In [29] the corrected formula to calculate the theoretical area of an adsorbed molecule was published. Regarding to this, the surface energies were revised and are listed in Table 4.2.

Table 4.2.: The Lifshitz-van der Waals (γ^{LW}), Lewis acid (γ^+) and Lewis base (γ^-) contributions to the surface energies of conventional beaded HIC media deduced from ILC experiments are given (revised results). In the last column the total surface energies (γ) are listed. All values are given in mJ/m^2.

	γ^{LW}	γ^+	γ^-	γ
Butyl Sepharose 4 FF	39.5	21.3	27.4	87.8
Phenyl Sepharose HP	103	6.4	29.1	130
Phenyl Sepharose 6 FF (ls)	44.6	11.1	31.5	82.0
Toyopearl Butyl-650M	93.8	21.7	43.7	155
Toyopearl Phenyl-650M	82.8	23.5	42.8	146
Toyopearl HW 65	100	25.1	36.9	161

Tosoh materials exhibit an up to two times larger Lifshitz-van der Waals contribution to the surface energy than the materials produced by GE Healthcare. The different backbone chemistry, which can be reached by the molecular probe molecules due to their smallness might be the reason for this difference. The larger surface energy for the ligand free Tosoh material Toyopearl HW 65 reinforces this concept. Interestingly, GE Phenyl Sepharose HP, a material with high ligand density exhibit values within the same range as the Tosoh materials.

Ujimoto and Kurihara [44] found that agarose-based media exhibit a lower hydrophobicity than poly(methyl acrylate)-based ones. This corresponds with the results of this work because the surface energy is related to the hydrophobicity as described in section 5.

Contrary, the surface energies for poly(methyl methacrylate) material found in literature are in the range of 40 mJ/m² [45] to 92.6 mJ/m² [46], which were obtained via contact angle measurements. These values are up to four times lower than those obtained with the ILC method for Tosoh materials, although the materials are similar. The surface energies of monoliths (see Table 4.3) are (by elimination of the porosity) all within that range, but are located at the upper boundary.

Table 4.3.: The Lifshitz-van der Waals (γ^{LW}), Lewis acid (γ^+) and Lewis base (γ^-) contributions to surface energies of monolithic materials deduced from ILC experiments are listed. The monoliths with varying ligand densities of butyl and phenyl as well as the monolith with hydroxyl ligands and the ligand free monolith, Epoxy, were custom made by BIA Separations and kindly provided. Results obtained by elimination of the porosity are added in parentheses. In the last column the total surface energies are listed. All values are given in mJ/m^2.

	γ^{LW}	γ^+	γ^-	γ
Epoxy	14.0 (4.2)	25.6 (25.0)	13.9 (19.5)	51.7 (48.4)
Hydroxy	29.0 (14.8)	24.7 (24.0)	16.8 (22.9)	69.7 (61.7)
25% Butyl	29.4 (14.2)	27.0 (26.6)	16.4 (22.5)	71.5 (63.1)
25% Phenyl	30.7 (15.1)	25.8 (25.1)	17.4 (24.4)	73.1 (64.7)
50% Butyl	37.8 (19.2)	24.7 (23.7)	17.8 (26.0)	79.7 (68.9)
50% Phenyl	45.9 (26.2)	24.2 (23.0)	19.3 (28.9)	89.1 (77.8)
75% Butyl	30.7 (15.1)	25.8 (25.1)	17.4 (24.4)	73.1 (64.7)
75% Phenyl	33.0 (20.1)	23.6 (23.3)	20.2 (26.3)	76.7 (69.7)
100% Phenyl	68.6 (39.5)	20.4 (17.0)	20.8 (40.4)	109.8 (91.9)

In Bednar et al. [29] the surface energies obtained by ILC and by contact angle measurements of the monoliths presented in table 4.3 were compared, except the Epoxy and Hydroxy material. The Epoxy monolith is the backbone material with epoxy connectors immobilized. The Hydroxy material features additionally short hydroxy ligands, as the name indicates. These additional results match with the precognition that the surface energies decrease with the ligand length and density [26]. Possible reasons for the lower values for the surface energies obtained by contact angle measurements were discussed in Bednar et al. [29]. Finally it was argued that these variations are to be found in the different experimental setup, which also holds for the two additional monoliths.

The method introduced may be used to evaluate new materials in terms of their surface energy and compare them to existing media. A determination of the porosity is not necessary. Batch to batch variations of chromatography media may be investigated as well as the influence of aging and fouling. This knowledge is valuable for designing new materials and to predict the (residual) column lifetime.

4.3. Other methods

In DIN ISO 8296:2008 a method to determine the wetting tension of surfaces of plastic lms and sheetings is described. First of all, several test liquids have to be prepared. These are certain mixtures of 2-ethoxyethanol, formamide, methanol and water and feature di erent surface energies. These liquids are applied on the test specimen by a puller, cotton bud or a brush so that a thin lm is generated on its surface. After a certain time any lm breaks open. The surface tension of the mixture which is able to wet the surface for 2 seconds is to be identi ed as the wetting tension of the test specimen [47].

Also a pen test according to ISO 8296 is available. [1] The test liquids are ready made and brought into the pen. So they do not have to be prepared by oneself. The lm is applied like coloring a paper with a pen. The determination of the wetting tension of the test specimen is as described above.

---

[1]Dyne Testing Ltd, Newton House, 5 Parkside Court, Greenhough Road, Lichfield; Staffordshire, WS13 7FE United Kingdom, http://www.dynetesting.com/surface-energy-measurement/dyne-pens/, respectively.

5. The hydrophobic effect and hydrophobicity

5.1. What is the hydrophobic effect?

Molecules which exhibit restricted solubility in water, such as hydrocarbons do, are hydrophobic. The hydrophobic effect is known as the effect which causes aggregation of such nonpolar species in water, e.g. the micellization of hydrocarbon chains.

A process is thermodynamically favorable, once the change of Gibbs free energy

$$\Delta G = \Delta H - T\Delta S \tag{5.1}$$

is negative. The change of Gibbs free energy consists of a change in enthalpy, ΔH, and the change in entropy ΔS multiplied with the Temperature in Kelvin, T.

So the aggregation can be driven by a decrease in enthalpy change or an increase in entropy change. The hydrophobic effect is explained by water molecules forming cages or cavities around these aggregates. The water molecules are by that highly ordered and so the entropy of the water molecules as a bulk decreases, the change in entropy is positive. Simultaneously, by aggregation or adsorption on hydrophobic media the surface of the hydrophobic molecules adjoining water molecules decreases. Thereby the hydrocarbon-water interfacial area is reduced, which is stated to be the second driving force of hydrophobic interaction [15, 21, 48, 49].

5.2. What is hydrophobicity?

Zaslavsky and Masimov pointed out that hydrophobicity and hydrophilicity are special cases of lyophobicity and lyophilicity. Hydrophobicity and hydrophilicity describe molecular interactions of a solute or a solid surface with water in dispersed systems while the dispersing medium is water. They state that the free energy of hydration (respectively solvation) specifies hy-

drophilicity. Hydrophobicity is associated to small values of the free energy of hydration [50]. According to this, the hydrophobicity of chromatographic materials can be identi ed as the free energy of interaction between the chromatographic material and water. This allows to compare the hydrophobicity of di erent chromatography media and even columns with di erent sizes and ow directions.

According to Dupré, this is calculated via

$$\Delta G_{lk} = \gamma_{lk} - \gamma_k - \gamma_l \qquad (5.2)$$

while

$$\gamma_{lk} = \left(\sqrt{\gamma_l^{LW}} - \sqrt{\gamma_k^{LW}}\right)^2 + 2(\sqrt{\gamma_l^+} - \sqrt{\gamma_k^+})(\sqrt{\gamma_l^-} - \sqrt{\gamma_k^-}). \qquad (5.3)$$

The index k represents the chromatographic medium, the index l stands for the liquid, in this case water.

5.3. Results and discussion

In table 5.1 chromatographic media, beaded media as well as monoliths, are ranked according to their hydrophobicity, which is identi ed as the free energy of interaction of the chromatography media with water. The smaller the (negative) value of the free energy of interaction, the larger the hydrophobicity is. This is consistent with considerations regarding the entropy by comparison of two di erent surfaces surrounded by water. If water molecules are neighbouring a hydrophobic surface, they arrange to a cage. Such a system features a higher degree of order than a system with water molecules surrounding a more hydrophilic surface. The (positive) change in entropy of the former, referring to the two single states of water molecules and hydrophobic surface not interacting, is larger than the latter. This leads to a change in Gibbs free energy beeing more negative for the hydrophobic surface, if the entropy is positive in both cases. The negative algebraic sign represents that the chemical reaction proceeds spontaneously [17].

The Tosoh materials exhibit the largest hydrophobicity, headed up by the ligand free material, HW-65. The GE Healthcare materials show broader variety in hydrophobicity, where the Phenyl Sepharose HP material are about 10% to 14% larger than the hydrophobicity of Butyl Sepharose 4 FF and Phenyl Sepharose 6 FF (ls). The hydrophobicity of the monolithic materials are lower than the GE Healthcare materials, apart from 100% Phenyl, which is within this range. The hydrophobicity of monolithic materials is higher for ligands with

Table 5.1.: The free energies of interaction (in mJ/m^2) of the column material with water, as a measure for the hydrophobicity of chromatographic media, are listed. Conventional beaded HIC media, from Tosoh (Toyopearl media) and GE Healthcare (Sepharose media) as well as monoliths (custom made by BIA Separations) with varying ligand densities of Butyl and Phenyl as well as the Epoxy and Hydroxy monolith.

material	ΔG_{ls}
beaded media (axial ow):	
Toyopearl HW-65	-205.3
Toyopearl Butyl-650M	-204.3
Toyopearl Phenyl-650M	-199.9
Phenyl Sepharose HP	-174.8
Butyl Sepharose 4 FF	-158.1
Phenyl Sepharose 6 FF (ls)	-152.6
monoliths (radial ow):	
100% Phenyl	-164.5
50% Phenyl	-150.5
75% Phenyl	-142.5
50% Butyl	-141.7
25% Phenyl	-136.9
75% Butyl	-136.9
25% Butyl	-135.2
Hydroxy	-133.8
Epoxy	-114.3

larger polymer chain length. The exception to this rule is 50% Butyl, having a hydrophobicity between 75% and 25% Phenyl. Interestingly, the hydrophobicity does not directly increase with increasing ligand density. The hydrophobicity of monoliths with ligand densities of 50% are larger than the ones with 75%, regardless if butyl or phenyl ligands are used.

A comparison with literature shows that others found similar results. Ghose et al. [36] determined linear retention data of Lysozyme on several HIC resins by linear gradient experiments using pulse injection. They found that Toyopearl Phenyl-650M is less hydrophobic than Toyopearl Butyl-650M, and Butyl Sepharose 4 FF is less hydrophobic than the former materials. Regarding the two Tosoh materials this is in accordance with the information Tosoh publishes on their website, but the ligand free material, Toyopearl HW-65 is not discussed there [51].

5. The hydrophobic effect and hydrophobicity

The result that the ligand free material exhibits the largest hydrophobicity is surprising at first sight, because in [52] Toyopearl HW-65 is described as hydrophilic resin. The results in table 5.1 reveal that the differences in free energy of interaction betweeen Toyopearl HW-65, Butyl-650M and Phenyl-650M are rather small. This corresponds with results of Rowe et al. [53]. They determined changes in the Gibbs free energy of these resins with different amino acids (serine, alanine, valine leucine and phenylalanine) in ammonium sulfate and found very similar changes of Gibbs energies of these solutes with the resins, especially for Toyopearl HW-65 and Phenyl-650M.

Noticable is that a ranking of the resins according to the change in Gibbs free energy vary with the different amino acids. For simpler molecules, like alanine and serine, but also for valine, Toyopearl Phenyl-650M shows the most positive ΔG, followed by Toyopearl HW-65 and Butyl-650M. The more branched, respectively ring-structured amino acids leucine and phenylalanine have the largest values of changes in ΔG for Toyopearl HW-65, followed by Toyopearl Phenyl-650M and Butyl-650M. Interestingly, the values in ΔG for the three resins are closest to each other for serine, which is the most hydrophilic of all five solutes [54].

The questions arise if a stronger interaction of a hdyrophobic solute with a resin can be interpreted as beeing the resin more hydrophobic as well, as done by Machold et al. [26]. Does a stronger interaction of a resin with a hydrophilic solute lead to the result that the resin is more hydrophilic? In the first case the results of Rowe et al. give that Toyopearl HW-65 could be interpreted as the most hydrophobic resin followed by Phenyl-650M and Butyl-650M, in the latter case Toyopearl Butyl-650M as the most hydrophobic, followed by HW-65 and Phenyl-650M.

For the GE Healthcare materials, the ranking found by the ILC method (see table 5.1) corresponds with the information GE Healthcare give according the hydrophobicity of their HIC materials [55]. Ujimoto and Kurihara [44] found that polymethacrylate based chromatography media (e.g. Toyopearl media) exhibit a stronger hydrophobicity than agarose based media (e.g. GE Healthcare Sepharose materials). Rowe et al. [53] precised that differences in interaction enthalpy, leading to differences in Gibbs energy of interaction, between Toyopearl and Sepharose resins arouse due to larger dispersion (London Van der Waals) forces in Toyopearl resins. This is consistent with the results presented within this work, except for Phenyl Sepharose HP. Additionally, the Lewis acid base contributions to the surface energy of the Toyopearl resins found are larger than those of the Sepharose materials (see table 4.2), particularly the Lewis base part. This also contributes to a larger free energy of interaction of the Toyopearl materials.

34

BIA separations published a poster at their Monolith Summer School and Symposium 2014 [56] regarding the hydrophobicity of several hydrophobic monoliths. They investigated the retention behavior of a protein mixture, namely Lysozyme and α-chymotrypsinogen. They indicated the retention time as measure of hydrophobicity, but some monoliths adsorbed the proteins completely in HIC mode. Proteins adsorbed by these monoliths were eluted by a reversed phase chromatography (RPC) step. The RPC step was also applied to the monolith with 50 % Phenyl ligands. Unfortunately it is not entirely clear according to which criteria the ranking is actually done. The ranking according to the retention time of Lysozyme in RPC mode give different results than they declare on their poster, deviations occur especially for the monoliths with phenyl ligands. The retention times of Lysozyme in the RPC mode would suggest the following ranking, starting with the largest hydrophobicity at 100% Phenyl which equals to that of 50% Phenyl, followed by 75% Phenyl. This corresponds with the findings of the ILC method which gives a larger hydrophobicity for 50% Phenyl than 75% Phenyl. Additionally, the question arises how to arrange retention times achieved by RPC according to retention times by HIC, because different elution methods mostly have an impact on the retention time [15].

The ranking according to hydrophobicity by the ILC method presented in table 5.1 is mostly identical to the ones given by the chromatography media manufacturers. The results of the ligand free monolith, Epoxy and the one with hydroxyl ligands, Hydroxy, indicate that the immobilization of ligands on monoliths do increase the hydrophobicity, whereas for Tosoh materials the ligand free material features the largest hydrophobicity. Furthermore, for the first time it is possible to compare the hydrophobicity of different chromatographic materials with different column volumes and different flow directions. The concept presented within this work identifies hydrophobicity with the free energy of interaction with water. To develop this thought out, the free energy of interaction between a molecule and a chromatography material can give information about the lyophilicity of certain molecules regarding the chromatography resin. This information might facilitate the process of selecting a suitable chromatography material for purification processes.

6. Prediction of protein retention with hydrophobic chromatographic media

Practitioners are interested in the prediction of retention of certain proteins by a column respectively a chromatographic material. There are attempts to estimate the dimensionless retention time (DRT) of proteins, according to their surface hydrophobicity and operating conditions [57]. Another question is still unsolved: How to decide which chromatography media should be used for a chromatography step of this new protein or molecule? Up to now chromatography media were selected based on retention of model proteins and according to expert knowledge and intuition. Also try and error attempts take place [26, 58]. So the following questions arise: How can the ILC method to determine surface free energy be used to predict protein retention? With ILC axial chromatography beaded media and radial monoliths with different column volumes can be compared regarding their hydrophobicity, as already shown. Anyway, how can one come to a decision based on facts regarding which column will be the best for protein purification or separation?

With ILC the contributions to the surface energy of chromatography media can be determined. By conducting ILC experiments with a protein and at least three chromatography columns the three surface energy contributions of the protein can be determined. This result is of course strongly dependent on the accuracy and the actual value of the surface energy contributions of the columns. Therefore an independent method would be preferable.

Once the surface energy contributions of the columns and the proteins are known, the difference in free energy of interaction (ΔG) of the protein with the column can be calculated. The smaller the (negative) value of ΔG, the stronger the interaction will be. By that the combination with the strongest interaction can be found. Also the selectivity of two proteins might be predictable, by finding the column providing the largest difference of free energy of interaction between the proteins of interest and the column. The selectivity can be enhanced later on by adjusting chromatographic parameters like the mobile phase composition [59] and the pH of the mobile phase but ILC should be able to provide at least a first insight.

36

7. Conclusion

As outlined in section 1.3 several aims had to be achieved within this work. An ILC method to determine the surface energy of beaded HIC media with axial ow was developed and subsequently published in *Journal of Chromatography A* (see Publication 1, Appendix A). Van Oss approach was used which provides the most detailed information about the surface energy, which is split into Lewis acid and base and Lifshitz-van der Waals contributions. A method to determine the surface energy of porous chromatography materials within their usual working environment was established. This method was adopted to analyze also HIC monoliths, which were operated in radial ow direction. The corresponding part of the work was published in *Langmuir* (see Publication 2, appendix B).

With these results the investigated HIC materials could be ranked due to their (total) surface energy. Additionally, the hydrophobicities of the materials were calculated and so these media, exhibiting a wide variation in size and di erent ow directions, could be directly compared for the very rst time.

Since it is possible to produce non-porous monolithic sheets this provided the opportunity to compare results obtained by the ILC method with the ones from contact angle measurements. By using non-porous monolithic sheets misleading results due to soaking e ects could be avoided. Apart from a shift in their absolute values, the same pattern for increasing ligand density was found for the two measurements. Although several reasons do exist, most probably the fundamental di erences in the experimental design of both methods are responsible for this deviation.

Also a physically motivated model to describe protein retention caused by monoliths with radial ow direction could be found and will be published in *Analytical chemistry* (see Publication 3, appendix C). In summary, all main objectives of this study were ful lled.

An expansion of the method to ion exchange chromatography is conceivable. This will require a smart choice of new molecular probes, which have to exhibit ionic charges. Furthermore a change of the experimental setup, primarily an (additional) conductivity detector will be necessary. Also the chromatographic conditions have to be selected accordingly to achieve appropriate results.

References

[1] E. Lugscheider and K. Bobzin, The influence on surface free energy of PVD-coatings, *Surface and Coatings Technology*, vol. 142-144, pp. 755 760, July 2001.

[2] M. P. Colombini, F. Modugno, M. Giacomelli, and S. Francesconi, Characterisation of proteinaceous binders and drying oils in wall painting samples by gas chromatography-mass spectrometry, *Journal of Chromatography A*, vol. 846, pp. 113 124, June 1999.

[3] M. P. Colombini, F. Modugno, and A. Giacomelli, Two procedures for suppressing interference from inorganic pigments in the analysis by gas chromatography-mass spectrometry of proteinaceous binders in paintings, *Journal of Chromatography A*, vol. 846, pp. 101 111, June 1999.

[4] Lexikon-Institut Bertelsmann, *Die Grosse Bertelsmann Lexikothek, Bertelsmann Lexikon in 15 Bänden, Band 9, L-Mazo.* Gütersloh: Verlagsgruppe Bertelsmann GmbH, 1988.

[5] F. Awaja, M. Gilbert, G. Kelly, B. Fox, and P. J. Pigram, Adhesion of polymers, *Progress in Polymer Science*, vol. 34, pp. 948 968, Sept. 2009.

[6] P. A. Sørensen, S. Kiil, K. Dam-Johansen, and C. E. Weinell, Anticorrosive coatings: a review, *Journal of Coatings Technology and Research*, vol. 6, pp. 135 176, June 2009.

[7] P. Pospiech, All-ceramic crowns: bonding or cementing?, *Clinical Oral Investigations*, vol. 6, pp. 189 197, Dec. 2002.

[8] L. Graziani, E. Quagliarini, A. Osimani, L. Aquilanti, F. Clementi, C. Yéprémian, V. Lariccia, S. Amoroso, and M. D Orazio, Evaluation of inhibitory effect of TiO_2 nanocoatings against microalgal growth on clay brick façades under weak UV exposure conditions, *Building and Environment*, vol. 64, pp. 38 45, June 2013.

[9] J. Radulovic, J. MacMullen, Z. Zhang, H. N. Dhakal, S. Hannant, L. Daniels, J. Elford, C. Herodotou, M. Totomis, and N. Bennett, Biofouling resistance and practical constraints of titanium dioxide nanoparticulate silane/siloxane exterior facade treatments, *Building and Environment*, vol. 68, pp. 150 158, Oct. 2013.

[10] Q. Zhao, Y. Liu, and C. Wang, Development and evaluation of electroless Ag-PTFE composite coatings with anti-microbial and anti-corrosion properties, *Applied Surface Science*, vol. 252, pp. 1620 1627, Dec. 2005.

[11] Q. Zhao, E ect of surface free energy of graded NI-P-PTFE coatings on bacterial adhesion, *Surface and Coatings Technology*, vol. 185, no. 2-3, pp. 199 204, 2004.

[12] J. Kim, W. Qian, and Z. Y. Al-Saigh, Measurements of water sorption enthalpy on polymer surfaces and its e ect on protein adsorption, *Surface Science*, vol. 605, pp. 419 423, Feb. 2011.

[13] P. Thevenot, W. Hu, and L. Tang, Surface chemistry in uences implant biocompatibility, *Current Topics in Medicinal Chemistry*, vol. 8, no. 4, pp. 270 280, 2008.

[14] D. Williams, On the mechanisms of biocompatibility, *Biomaterials*, vol. 29, no. 20, pp. 2941 2953, 2008.

[15] G. Carta and A. Jungbauer, *Protein Chromatography: Process Development and Scale-Up*. New York: John Wiley & Sons, 1st ed., 2010.

[16] E. Heftmann, *Chromatography: Fundamentals and Applications of Chromatography and Related Di erential Migration Methods*. Elsevier Science & Technology Books, Apr. 2004.

[17] P. W. Atkins and J. De Paula, *Physical chemistry for the life sciences*. Oxford, U.K.: Oxford UnivPress, 2nd ed., 2011.

[18] C. J. van Oss, *Interfacial Forces in Aqueous Media*. Boca Raton, FL: CRC Press, 2nd ed., 2006.

[19] F. M. Fowkes, D. O. Tischler, J. A. Wolfe, L. A. Lannigan, C. M. Ademu-John, and M. J. Halliwell, Acid-base complexes of polymers, *Journal of Polymer Science: Polymer Chemistry Edition*, vol. 22, pp. 547 566, Mar. 1984.

[20] W. Barthlott, Z. Cerman, and A. K. Stosch, Der Lotus-E ekt: Selbstreinigende Ober-ächen und ihre Übertragung in die Technik, *Biologie in unserer Zeit*, vol. 34, pp. 290 296, Sept. 2004.

[21] H.-J. Butt, *Physics and Chemistry of Interfaces*. Weinheim, Germany: Wiley-VCH Verlag GmbH & Co. KGaA, 3rd ed., Mar. 2013.

REFERENCES

[22] M. Gindl, G. Sinn, W. Gindl, A. Reiterer, and S. Tschegg, A comparison of di erent methods to calculate the surface free energy of wood using contact angle measurements, *Colloids and Surfaces A: Physicochemical and Engineering Aspects*, vol. 181, pp. 279 287, June 2001.

[23] Y. Yao and A. M. Lenho , Determination of pore size distributions of porous chromatographic adsorbents by inverse size-exclusion chromatography, *Journal of Chromatography A*, vol. 1037, pp. 273 282, May 2004.

[24] B. A. Grimes, R. Skudas, K. K. Unger, and D. Lubda, Pore structural characterization of monolithic silica columns by inverse size-exclusion chromatography, *Journal of Chromatography A*, vol. 1144, pp. 14 29, Mar. 2007.

[25] M. Al-Bokari, D. Cherrak, and G. Guiochon, Determination of the porosities of monolithic columns by inverse size-exclusion chromatography, *Journal of Chromatography A*, vol. 975, pp. 275 284, Nov. 2002.

[26] C. Machold, K. Deinhofer, R. Hahn, and A. Jungbauer, Hydrophobic interaction chromatography of proteins: I. comparison of selectivity, *Journal of Chromatography A*, vol. 972, pp. 3 19, Sept. 2002.

[27] C. J. Van Oss, M. K. Chaudhury, and R. J. Good, Interfacial lifshitz-van der waals and polar interactions in macroscopic systems, *Chemical Reviews*, vol. 88, pp. 927 941, Sept. 1988.

[28] I. Bednar, R. Tschelie nig, E. Berger, A. Podgornik, and A. Jungbauer, Surface energies of hydrophobic interaction chromatography media by inverse liquid chromatography, *Journal of Chromatography A*, vol. 1220, pp. 115 121, Jan. 2012.

[29] I. Bednar, E. Berger, N. L. Krajnc, J. Vidi , A. Podgornik, A. Jungbauer, and R. Tscheliessnig, Surfaces energies of monoliths by inverse liquid chromatography and contact angles, *Langmuir*, vol. 30, pp. 5435 5440, May 2014.

[30] F. Gritti and G. Guiochon, Accurate measurements of peak variances: Importance of this accuracy in the determination of the true corrected plate heights of chromatographic columns, *Journal of Chromatography A*, vol. 1218, pp. 4452 4461, July 2011.

[31] J. V. Beck, *Heat conduction using Green s functions*. London; Washington, DC: Hemisphere Pub. Corp., 1992.

[32] L. R. Jacob, Chapter 4 Hydrophobic Interaction Chromatography, in *Journal of Chromatography Library* (Michael Kastner, ed.), vol. 61 of *Protein Liquid Chromatography*, pp. 235 269, Elsevier, 1999.

[33] A. Jungbauer and C. Machold, Chapter 16 Chromatography of proteins, in *Journal of Chromatography Library* (E. Heftmann, ed.), vol. 69, Part B of *Chromatography 6th Edition Fundamentals and Applications of Chromatography and Related Di erential Migration Methods*, pp. 669 737, Elsevier, 2004.

[34] H. Sklená ová, P. Chocholou , P. Koblová, L. Zahálka, D. ' atínský, L. Matysová, and P. Solich, High-resolution monolithic columns - a new tool for e ective and quick separation, *Analytical and Bioanalytical Chemistry*, vol. 405, pp. 2255 2263, Mar. 2013.

[35] T. W. Perkins, D. S. Mak, T. W. Root, and E. N. Lightfoot, Protein retention in hydrophobic interaction chromatography: modeling variation with bu er ionic strength and column hydrophobicity, *Journal of Chromatography A*, vol. 766, pp. 1 14, Apr. 1997.

[36] S. Ghose, Y. Tao, L. Conley, and D. Cecchini, Puri cation of monoclonal antibodies by hydrophobic interaction chromatography under no-salt conditions, *mAbs*, vol. 5, pp. 795 800, Sept. 2013.

[37] C. J. van Oss, Use of the combined Lifshitz-van der Waals and Lewis acid-base approaches in determining the apolar and polar contributions to surface and interfacial tensions and free energies, *Journal of Adhesion Science and Technology*, vol. 16, no. 6, pp. 669 677, 2002.

[38] C. J. van Oss and R. J. Good, Surface tension and the solubility of polymers and biopolymers: The role of polar and apolar interfacial free energies, *Journal of Macromolecular Science, Part A*, vol. 26, no. 8, pp. 1183 1203, 1989.

[39] N. A. Patankar, On the modeling of hydrophobic contact angles on rough surfaces, *Langmuir*, vol. 19, pp. 1249 1253, Feb. 2003.

[40] V. M. Starov, A. N. Tyatyushkin, M. G. Velarde, and S. A. Zhdanov, Spreading of non-newtonian liquids over solid substrates, *Journal of Colloid and Interface Science*, vol. 257, pp. 284 290, Jan. 2003.

REFERENCES

[41] Encyclopædia Britannica Online, vacuum-ultraviolet radiation. `http://www.britannica.com/EBchecked/topic/621412/vacuum-ultraviolet-radiation`, July 2014.

[42] A. E. Berger, Arbeitsbuch für analytische Chemie und das analytisch chemische Laboratorium, Band 2 Quantitative Methoden. Approbiert vom BM. f. U. K. u. Sp. Schulbuch-Nr. 6289, 1988.

[43] W. Neier and G. Strehlke, 2-butanone, in *Ullmann s Encyclopedia of Industrial Chemistry*, Wiley-VCH Verlag GmbH & Co. KGaA, 2000.

[44] K. Ujimoto and H. Kurihara, Evaluation of hydrophobicity of gels by use of some 1-alkanols as pilot solutes, *Journal of Chromatography A*, vol. 301, pp. 57 64, 1984.

[45] C. J. van Oss, R. J. Good, and M. K. Chaudhury, Additive and nonadditive surface tension components and the interpretation of contact angles, *Langmuir*, vol. 4, pp. 884 891, July 1988.

[46] F. M. Fowkes, M. B. Kaczinski, and D. W. Dwight, Characterization of polymer surface sites with contact angles of test solutions. 1. Phenol and iodine adsorption from methylene iodide onto PMMA lms, *Langmuir*, vol. 7, pp. 2464 2470, Nov. 1991.

[47] Deutsche Norm DIN ISO 8296:2008, *Kunststo e - Folien und Bahnen - Bestimmung der Benetzungsspannung (ISO 8296:2003)*. DIN Deutsches Institut für Normung e.V., 2008.

[48] R. Breslow, Hydrophobic e ects on simple organic reactions in water, *Accounts of Chemical Research*, vol. 24, pp. 159 164, June 1991.

[49] B. Widom, P. Bhimalapuram, and K. Koga, The hydrophobic e ect, *Physical Chemistry Chemical Physics*, vol. 5, pp. 3085 3093, July 2003.

[50] B. Y. Zaslavsky and E. A. Masimov, Methods of analysis of the relative hydrophobicity of biological solutes, in *Physical Organic Chemistry*, no. 146 in Topics in Current Chemistry, pp. 171 202, Springer Berlin Heidelberg, Jan. 1988.

[51] Tosoh Bioscience GmbH, Toyopearl orientation sheet. `http://www.separations.eu.tosohbioscience.com/NR/rdonlyres/A288E183-92F3-429C-8A32-208F24CDCA6B/0/P09P24A_ToyopearlOrientationSheet.pdf`, 2014.

42

[52] R. Carbonell, S. Menegatti, and A. Naik, Alkaline-stable chromatographic resins. http://www.google.com/patents/US20130165539, June 27 2013. US Patent App. 13/724,245.

[53] G. E. Rowe, H. Aomari, T. Chevaldina, M. Lafrance, and S. St-Arnaud, Thermodynamics of hydrophobic interaction chromatography of acetyl amino acid methyl esters, *Journal of Chromatography A*, vol. 1177, pp. 243 253, Jan. 2008.

[54] L. Stryer, *Biochemie*. Heidelberg ua: Spektrum, AkadVerl, 4. au ., 1. korr. nachdr. ed., 1999.

[55] General Electric Company, Hydrophobic interaction chromatography (HIC) selection guide. `http://www.gelifesciences.com/gehcls_images/GELS/Related\ %20Content/Files/1349939730181/litdoc29022223_20130925000229.pdf`, June 2012.

[56] U. Simoni , M.and ernigoj, N. Lendero Krajnc, and A. ' trancar, Characterization of chromatographic monolithic columns with di erent hydrophobicity. `http: //www.biaseparations.com/education/publications/technology/product/ 774-Characterization-of-Chromatographic-Monolithic-Columns-with-\ \Different-Hydrophobicity`, June 2014.

[57] M. E. Lienqueo, A. Mahn, J. C. Salgado, and J. A. Asenjo, Current insights on protein behaviour in hydrophobic interaction chromatography, *Journal of Chromatography B*, vol. 849, pp. 53 68, Apr. 2007.

[58] K. Valkó, Chapter 2 Retention prediction of pharmaceutical compounds, in *Journal of Chromatography Library* (Roger M. Smith, ed.), vol. 57 of *Retention and Selectivity in Liquid Chromatography Prediction, Standardisation and Phase Comparisons*, pp. 47 92, Elsevier, 1995.

[59] A. Mahn, M. E. Lienqueo, and J. A. Asenjo, Optimal operation conditions for protein separation in hydrophobic interaction chromatography, *Journal of Chromatography B*, vol. 849, pp. 236 242, Apr. 2007.

A. Publication 1

Surface energies of hydrophobic interaction chromatography media by inverse liquid chromatography☆

Ingeborg Bednar[a], Rupert Tscheließnig[a], Eva Berger[a], Aleš Podgornik[b], Alois Jungbauer[a,c]

[a] Austrian Centre of Industrial Biotechnology, Muthgasse 11, 1190 Vienna, Austria
[b] BIA Separations, Ljubljana, Slovenia
[c] Department of Biotechnology, University of Natural Resources and Life Sciences Vienna, Muthgasse 18, Vienna, Austria

ARTICLE INFO

ABSTRACT

Hydrophobicity of hydrophobic interaction chromatography media is currently ranked according to retention of reference proteins. A new method, suitable for porous media, is presented here to determine the surface energy and its Lifshitz–van-der-Waals, Lewis acid and Lewis base contributions. The theory of van Oss has been adapted for data obtained by inverse liquid chromatography. Furthermore, this method is characterized by the independence of the determination of the phase ratio. The retention of probes with different molecular properties was used to calculate the surface energy and the Lifshitz–van-der-Waals as well as Lewis acid and Lewis base contributions to the surface energy. The media with polymethacrylate backbone had a higher surface energy ($\gamma \approx 200$ mJ/m^2) and Lifshitz–van-der-Waals contribution ($\gamma^{LW} \approx 140$ mJ/m^2) than the agarose-based media ($\gamma \approx 90$–180 mJ/m^2 and $\gamma^{LW} \approx 50$–160 mJ/m^2).

1. Introduction

Surface energy is the general property describing the adsorption strength of surfaces and this concept can be extended to chromatography. For hydrophobic interaction chromatography (HIC) media, this property allows a quantitative description of the surface and provides a ranking according to a physical quantity, i.e., the surface energy expressed in mJ/m^2. Current methods have characterized media on an empirical basis, which has only allowed ranking in a relative manner. The retention of reference proteins in isocratic or gradient elution has been used for this purpose [1,2]. Retention has been also predicted by docking experiments [1,3,4]. Alternatively, quantitative structure property relationship (QSPR) models have provided an indirect insight into hydrophobicity [5,6]. However, none of these methods are able to predict surface energy.

Claessens et al. [7] have classified reversed phase liquid chromatography (RPLC) media with respect to hydrophobicity by various tests as suggested by Engelhardt [8,9], Walters [10], Tanaka [11] and Galushko [12]. In these tests, the hydrophobicitiy was assessed by the hydrophobic selectivity of the chromatographic media for each of two molecular probes. Unfortunately, these assessments proved to be poor descriptors for hydrophobicity.

These investigators developed these analyses by using absolute values of retention factors and observed a better correlation by using the logarithm of the retention factor k' as a measure of hydrophobicity rather than from using hydrophobic selectivity. Hydrophobicity is not a definite quantitative physical property because the hydrophobicity is always specific for a certain column and therefore it is dependent on the surface area as well as on the ligand size [13].

Herein, we describe a new method to evaluate hydrophobicity that also uses absolute values of k'. This method compares different surfaces on a rational basis in terms of physical quantities, independent of column dimensions.

Chromatography media for protein separation on the preparative scale are porous beads in the range of 10–300 μm, with pore sizes ranging from 10 nm to 1300 nm. The selection of the best medium with an adequate combination of these dimensions depends on the application for which the media will be used [14]. Chromatography beads are compressible and the extraparticle and therefore also the total porosity depends on the packing density [15]. Generally, natural polymer-based media are more compressible than synthetic polymer-based media.

The determination of surface energies is conventionally done via contact angle measurements [16]. The contact angle measurements of porous media are often erroneous due to soaking effects of the media [17], as well as discrepancies in the determination of the surface angle on non-planar surfaces. For this reason contact angle measurements are rarely applied for this purpose. Reports

have shown different values of the contact angle with advancing and retracting drops when HIC media were investigated [18]. Thus, a method to determine the surface energy independent of the packing density is needed. Furthermore, the test samples (molecular probes) and the chromatography media must be compatible.

We have developed a method based on inverse liquid chromatography (ILC) in which the retention of the molecular probes serves as a measure for the strength of interaction. The concept of van Oss [19] was adapted for ILC and has been modified to calculate surface energies (see theory Section 3) without requiring the determination of porosity. The chromatographic experiments have shown that the retention time of different molecular probes as defined by the peak maximum is not a suitable measure to describe the different interactions between the molecular probes and the HIC media. As a distinctive criterion, the shape of the peaks was used to gain information about the interaction of each molecular probe with the different column media. By fitting the data with a suitable function, we obtained the parameters required for calculating the surface energies according to the concept of van Oss were obtained.

2. Experimental

Five molecular probes were selected and used to determine the surface energy of three natural polymer-based and two synthetic polymer-based chromatography media.

2.1. Stationary phases

The natural polymer-based media used included Butyl Sepharose 4 Fast Flow (FF), Phenyl Sepharose 6 FF (low sub), and Phenyl Sepharose High Performance (HP) from GE Healthcare (Uppsala, Sweden). We also used the synthetic polymer-based media Toyopearl Butyl-650M, Toyopearl Phenyl-650M and Toyopearl HW-65 from Tosoh Bioscience (Stuttgart, Germany). All media were packed by Atoll (Weingarten, Germany) in MediaScout MiniChrom columns with a column volume of 10 ml.

2.2. Mobile phases and molecular probes

We used glycerin ($MW_{GLY} = 92.09$ g/mol), ethylene glycol ($MW_{EG} = 62.07$ g/mol), dimethyl sulfoxide ($MW_{DMSO} = 78.13$ g/mol) and methyl ethyl ketone ($MW_{MEK} = 72.11$ g/mol), all analytical grade, as the molecular probes. The dilution was 1:2 in HQ-water, except for MEK, where the dilution was 1:6. As mobile phase HQ-water was used. We also performed studies with glucose (0.35M) in a 5% methanol solution.

2.3. Instrumentation and data handles

The columns were connected to a HPLC workstation (Agilent Series 1100 LC, Santa Clara, CA, United States) which was connected to a PC and controlled by Chem Station for LC 3D systems Rev. B. 04.03 (Agilent Technologies, Inc. 1994–2007, 2008). The UV detector response was transferred to the program where the files were exported in CSV format for further handling with Mathematica (Wolfram Research, Inc., Mathematica, Version 8.0, Champaign, IL (2010)).

2.4. Chromatography experiments

The pulse experiments were completed individually for each molecular probe. An aliquot (50 μl of glucose solution; 10 and 20 μl of GLY; 10 and 20 μl of EG; 10 and 40 μl of DMSO and 60 μl of MEK) of the molecular probe was injected into the column. The flow rate for all experiments was 1 ml/min. The continuously detected UV

absorption (the glucose solution, GLY and EG were monitored at a λ of 205 nm, MEK was monitored at a λ of 210 nm in each case with a bandwidth of 4 nm; DMSO was monitored at a λ of 250 nm with a bandwidth of 30 nm, the reference wavelength was 400 nm with a bandwidth of 4 nm), increased when the molecular probes reached the detector. The retention behaviors were interpreted as discussed in Section 3.

3. Theory

3.1. The exact solution for the infinite diluted system

We formulated the mass balance for the column, assuming that: the column media is homogeneous, the compressibility of the mobile phase is negligible; the axial dispersion coefficient is constant and independent of the solute concentration; the density and velocity of the mobile phase are constant along the column; the partial molar volumes are the same in both phases; no thermal effects occur; the influence of the heat of adsorption on the band profile is negligible; the experimental parameters fall within the linear region of the isotherm (Henry region); and the mass transfer kinetics are fast (but not infinitely fast) [20].

$$\partial_t c + \frac{1 - \epsilon}{\epsilon} \partial_t q_{vol} + u\, \partial_z c - D\, \partial_z^2 c = 0 \qquad (1)$$

The solid loading q_{vol} (equilibrium concentration of a component in the stationary phase) and the concentration in the mobile phase c are dependent on time t and on a spatial dimension z in the direction of the column. A single axial dispersion coefficient, D takes into account various contributions to peak broadening. The parameter u is conventionally the interstitial velocity; here it represents the chromatographic velocity and was obtained by using the retention time t_R (peak maximum) of glucose: $u = L/t_R$, with L, the column length. Next we adapted Eq. (1), and we introduced the implicit relation:

$$\lim_{c \to 0} \partial_t q = \underbrace{\partial_c q}_{H}\, \partial_t c \qquad (2)$$

Therein, H gives the Henry constant. We introduce a parameter $k' = (1 - \varepsilon/\varepsilon)H$ with ε identifying the total porosity. It describes the ratio between the volume of the mobile phase and the column volume.

To give Eq. (1) in a more compact form, we follow [21] and introduce new coordinates: $\xi = z - ut$ and $\tau = t$. Then the mass balance equation can be rewritten:

$$\partial_\tau c = \frac{D}{1 + k'} \partial_\xi^2 c \qquad (3)$$

A general solution is

$$c = \left(2\sqrt{D\pi \frac{\tau}{1 + k'}} \right)^{-1} \int_{-\infty}^{\infty} \phi(\beta') \exp\left(-\frac{(\xi - \beta')^2}{4D(\tau/1 + k')} \right) d\beta' \qquad (4)$$

where $\phi(\beta)$ represents an initial condition. We insert $\phi(\beta') = \delta(\beta')$ and obtain for the original coordinates:

$$c_{k'} = c_0 \frac{1}{2\sqrt{D\pi(t/1 + k')}} \exp\left(-\frac{(z - u(t/1 + k'))^2}{4D(t/1 + k')} \right) \qquad (5)$$

Finally, if we assume the response is a superposition of those part of the molecular probes that have interacted, and thus were retarded ($k' > 0$), and the remaining part of these probes that had not interacted with the surface ($k' = 0$), then:

$$c_{k'} = \int_0^{\infty} (\delta(k'') + \delta(k'' - k'))c_{k''} dk'' \qquad (6)$$

At which δ represents the Dirac delta function.

3.2. Surface energy contributions

van Oss postulated that interactions in condensed media may be divided into apolar interactions (Lifshitz–van-der-Waals, LW) and polar interactions [19]. The polar interactions are defined as comprising all electron-acceptor (Lewis acid) and electron-donor (Lewis base) interactions, denoted by AB. The polar and apolar components of the free energies of interfacial interaction are additive:

$$\Delta G = \Delta G^{LW} + \Delta G^{AB} \tag{7}$$

with

$$\gamma_i = -\frac{1}{2}\Delta G_{ii} \tag{8}$$

The surface energy is partitioned in the same way:

$$\gamma_i = \gamma_i^{LW} + \gamma_i^{AB} \tag{9}$$

The polar contribution to the surface energy is defined as:

$$\gamma_i^{AB} = 2\sqrt{\gamma_i^+ \gamma_i^-} \tag{10}$$

with γ_i^+ representing the electron acceptor (Lewis acid) parameter of phase i, while γ_i^- represents the electron donor (Lewis base) parameter of phase i.

The Dupré equation describes the work between solid (S) and liquid (L) components as:

$$-\Delta G_{SL} = \gamma_{SL} - \gamma_S - \gamma_L \tag{11}$$

By expanding this concept to a description of interactions between two media (1 and 2) which are immersed in a liquid (3) the free energy of interaction is then:

$$\Delta G_{132} = \gamma_{12} - \gamma_{13} - \gamma_{23} \tag{12}$$

where γ_{lm} describes the interfacial tension between two phases l and m. Also the interfacial tension can be divided into polar and apolar contributions:

$$\gamma_{lm}^{LW} = \left(\sqrt{\gamma_l^{LW}} - \sqrt{\gamma_m^{LW}}\right)^2 \tag{13}$$

$$\gamma_{lm}^{AB} = 2\left(\sqrt{\gamma_l^+} - \sqrt{\gamma_m^+}\right)\left(\sqrt{\gamma_l^-} - \sqrt{\gamma_m^-}\right) \tag{14}$$

If both contributions to surface tension are present, polar and apolar, the surface energy Eq. (12) calculates to:

$$\Delta G_{ijk} = -2\gamma_j^{LW} + 2\sqrt{\gamma_i^{LW}\gamma_j^{LW}} + 2\sqrt{\gamma_k^{LW}\gamma_j^{LW}} - 2\sqrt{\gamma_i^{LW}\gamma_k^{LW}}$$
$$+ 2\sqrt{\gamma_j^+}\left(\sqrt{\gamma_i^-} + \sqrt{\gamma_k^-} - \sqrt{\gamma_j^-}\right) + 2\sqrt{\gamma_j^-}\left(\sqrt{\gamma_i^+}\right.$$
$$\left. + \sqrt{\gamma_k^+} - \sqrt{\gamma_j^+}\right) - 2\sqrt{\gamma_i^+\gamma_k^-} - 2\sqrt{\gamma_i^-\gamma_k^+} = \{\gamma_{i,j,k}^{\{LW,+,-\}}\} \tag{15}$$

The difference of the free energy of adsorption is proportional to the logarithm of the equilibrium binding constant K_{eq} [22]:

$$\Delta G_{ijk} = -\frac{k_B T}{A_i}\ln K_{ijk} \tag{16}$$

where k_B is Boltzmann's constant, A_i is the theoretical area an adsorbed molecule of substance i covers on the surface, the values for all molecular probes (listed in Table 1) were calculated by Eq. (17), as described in Ref. [23].

$$A_i = \sqrt[3]{\pi}\left(3\frac{MW_i}{4\rho_i N_A}\right)^{2/3} \tag{17}$$

For weak concentrations, the distribution coefficient of adsorption K_{ijk} equals the Henry coefficient, H_{ijk}, and therefore the Henry

Table 1
The theoretical area an adsorbed molecule of substance i covers on the surface; values are given in m².

	A_i
GLY	2.962×10^{-19}
DMSO	2.907×10^{-19}
EG	2.474×10^{-19}
MEK	3.394×10^{-19}

coefficient of a substance can be written as a function of the polar and apolar contributions to the surface energies of the substance itself as well as the media which adsorbs the substance and a third substance, the liquid in which the two other substances are immersed:

$$-\frac{k_B T}{A_i}\ln H_{ijk} = \{\gamma_{i,j,k}^{\{LW,+,-\}}\} \tag{18}$$

To calculate the three contributions of the substance k: γ_k^{LW}, γ_k^+ and γ_k^- (the media absorbing a substance i) a set of three equations are necessary (therefore one substance has to be varied), then a linear set of three equations allows the calculation of the three parameters of interest.

3.2.1. Adaption of the van Oss concept

From fitting the experimental data, we obtained the parameter k' which is linked to the Henry coefficient H by the following equation:

$$H_{ijk} = k'_{ijk}\frac{\varepsilon}{1-\varepsilon} \tag{19}$$

Due to the relation described in Eq. (19) the estimation of the Henry coefficient from k'_{ijk} (and vice versa) depends strongly on the flawless and accurate determination of the porosity. To eliminate the influence of the porosity and the accuracy of determination of the porosity, the concept of van Oss was developed further. Another set of equations is set up by a linear combination of four equations of this form:

The linear combination of two equations (with different molecular probes 1 and 2) is:

$$\ln H_{1jk} - \ln H_{2jk} = \ln\frac{H_{1jk}}{H_{2jk}} = \ln\frac{k'_{1jk}}{k'_{2jk}} + \underbrace{\ln\frac{\varepsilon_1(1-\varepsilon_2)}{\varepsilon_2(1-\varepsilon_1)}}_{\text{for } \varepsilon_1 \approx \varepsilon_2 \to 0} = \ln\frac{k'_{1jk}}{k'_{2jk}}$$

$$= \frac{1}{k_B T}(A_1\{\gamma_{1,j,k}^{\{LW,+,-\}}\} - A_2\{\gamma_{2,j,k}^{\{LW,+,-\}}\}) \tag{20}$$

Using k'_{ijk} instead of H_{ijk} has the advantage that there is no need to determine the porosity by an extra measurement. This requires that the ratio of H_{1jk} to H_{2jk} is the same as the ratio of k'_{1jk} to k'_{2jk}, which determines the values of the porosity for different molecular probes to be almost equal, so that the term $\ln(\varepsilon_1(1-\varepsilon_2))/(\varepsilon_2(1-\varepsilon_1))$ can be neglected. From fitting the experimental data, we gain k'_{ijk} directly.

Once the three contributions to the surface energy of a chromatography media are obtained, the Henry coefficient can be calculated by using Eq. (18). As a next step, the porosity can be determined by using the relation between H, k' and ε as described in Eq. (19).

4. Results and discussion

First the molecular probes have been injected to the respective chromatography columns. The retention data of the molecular probes with the media investigated are plotted in Figs. 1a–2c. In
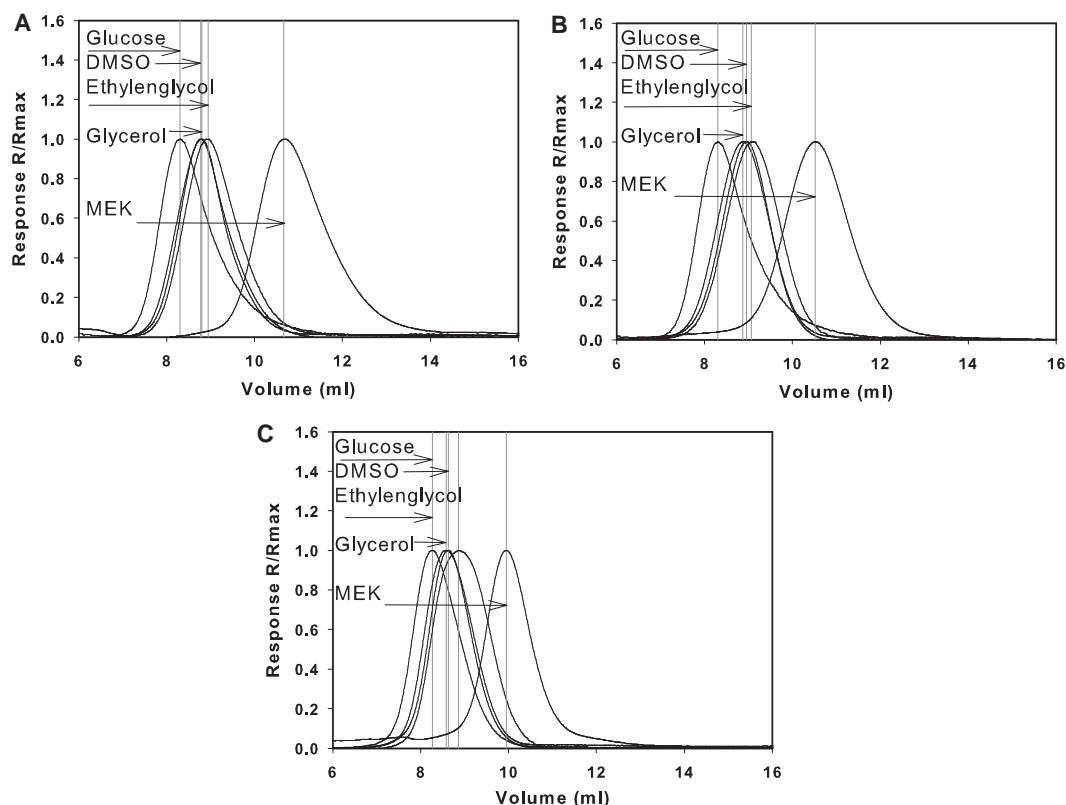
Fig. 1. UV-absorbance over time, normalized to the maximum response. (a) Tosoh Butyl-650M, (b) Tosoh Phenyl 650-M and (c) Tosoh HW 65.

Table 2
Arithmetical mean of k' values for GLY and DMSO with the standard deviation σ; values have to be multiplied by a factor of 10^{-3}.

	k'_{GLY}	k'_{DMSO}
GE Butyl Seph. 4 FF	35 ± 3	29 ± 9
GE Phenyl Seph. HP	51.6 ± 0.3	16.8 ± 0.4
GE Phenyl Seph. 6 FF (ls)	106 ± 13	56.4 ± 0.7
Tosoh Butyl-650M	64.6 ± 0.2	70.2 ± 0.1
Tosoh Phenyl-650M	51 ± 1	59.48 ± 0.09
Tosoh HW 65	45.7 ± 0.3	49.5 ± 0.6

Table 4
The LW-, Lewis acid (+) and Lewis base (−) contributions to the surface energy γ for the chromatography media investigated; values are given in mJ/m².

	γ^{LW}	γ^{+}	γ^{-}	γ
GE Butyl Seph. 4 FF	49.4	19.5	28.3	96.4
GE Phenyl Seph. HP	161	1.86	30.9	176
GE Phenyl Seph. 6 FF (ls)	57.9	6.37	34.4	87.5
Tosoh Butyl-650M	144	20.1	53.8	210
Tosoh Phenyl-650M	124	22.5	52.3	193
Tosoh HW 65	156	24.6	42.9	221

Fig. 3, the fit of the retention behavior of DMSO with GE Healthcare Phenyl Sepharose HP media is shown as an example.

The parameter k' (see Tables 2 and 3) is obtained by taking the average value of all measurements of a molecular probe. This was done for the investigated chromatography media. The contributions to the surface energies for the chromatography media were calculated by using the system of equations (see Eq. (20)) and listed in Table 4. γ is calculated by using Eq. (9).

Table 3
Arithmetical mean of k' values for EG and MEK with the standard deviation σ; values have to be multiplied by a factor of 10^{-3}.

	k'_{EG}	k'_{MEK}
GE Butyl Seph. 4 FF	35 ± 2	41 ± 5
GE Phenyl Seph. HP	30.4 ± 0.3	38.9 ± 0.3
GE Phenyl Seph. 6 FF (ls)	58.7 ± 0.9	77.4 ± 0.3
Tosoh Butyl-650M	89 ± 3	312.1 ± 0.3
Tosoh Phenyl-650M	71.6 ± 0.3	235.6 ± 0.1
Tosoh HW 65	80.1 ± 0.6	209 ± 0.4

The synthetic polymer-based media (Tosoh Toyopearl media) exhibited an approximately 2–3 times larger Lifshitz–van-der-Waals contribution to the surface energy than the natural polymer based media (GE Healthcare Sepharose media), except GE Phenyl Sepharose HP which has a Lifshitz–van-der-Waals contribution of the same order of magnitude than the polymer-based media (Table 4). Considering the small size of the molecular probes, one would expect that the molecular probes can enter the space between the ligands attached to the gel surface and come in contact with the backbone media. This would explain the larger surface energy values of the synthetic polymer-based backbone media.

The determination of the surface energy of the ligand free backbone material for the Tosoh materials, Tosoh HW 65 supports this theory. Tosoh HW 65 exhibits a surface energy of about 110% of the surface energy of Tosoh material with ligands, which corresponds with the theoretical concept.

On the other hand, surface energies for polymethacrylate material have been determined and are in the range of 40 mJ/m² [24,25]. This value is about five times lower than the values we obtained for the synthetic media (see Table 4, Tosoh materials).
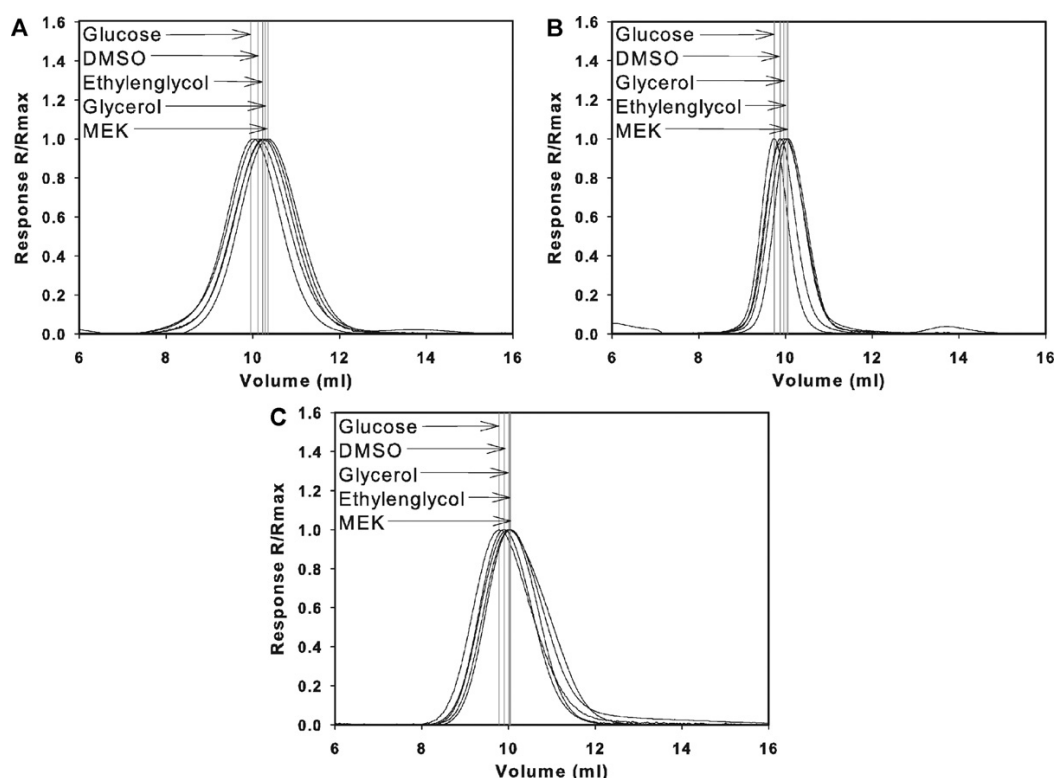
Fig. 2. UV-absorbance over time, normalized to the maximum response. (a) GE Butyl Seph. 4 FF, (b) GE Phenyl Seph. HP and (c) GE Phenyl Seph. 6 FF (low sub).

The most common method for determination of surface energies of planar surfaces is contact angle measurement. Gindl et al. [30] showed that the outcome is dependent on the selected algorithm. The data must be interpreted with care and an absolute value of surface energy is definitely not obtained by either contact angle or inverse chromatography.

Ujimoto and Kurihara [26] used 1-alkanols for determination of hydrophobicity of chromatography material without ligands. They found a lower hydrophobicity for agarose-based media than polymethacrylate-based ones. Furthermore, our method can be used to determine batch to batch variations of chromatography media. Riske et al. [27] suggested that the retention of lysozyme

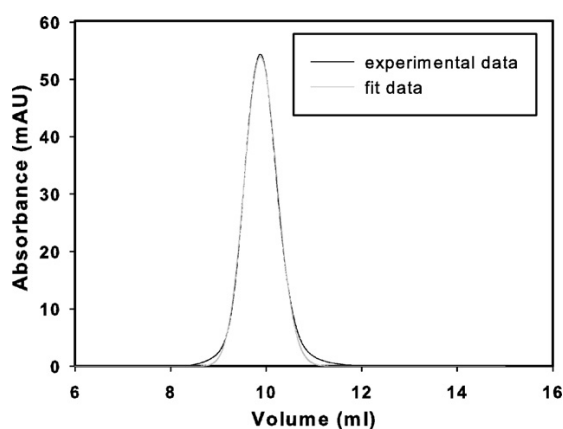**Fig. 3.** Comparison of experimental data with data of the fit for the combination DMSO with GE Phenyl Sepharose HP media.

Table 5
The Henry coefficients of the molecular probes used (GLY, DMSO, EG, MEK) for the chromatography media investigated.

	H_{GLY}	H_{DMSO}	H_{EG}	H_{MEK}
GE Butyl Seph. 4 FF	0.96	0.80	0.94	1.1
GE Phenyl Seph. HP	1.3	0.41	0.74	0.95
GE Phenyl Seph. 6 FF (ls)	2.2	1.2	1.2	1.6
Tosoh Butyl-650M	0.99	1.1	1.4	4.8
Tosoh Phenyl-650M	0.99	1.2	1.4	4.6
Tosoh HW 65	0.53	0.58	0.93	2.4

depends on the source of material and packing quality of the column as well as the extra column volume and injection profile. Our method is independent of the packing density and thus our method is, in principle, easily transferable to other labs.

Jennissen [28,29] has proposed a critical hydrophobicity for purification of proteins. This approach is limited to actual HIC media and is confined to a certain protein purification problem. Knowledge of the surface energy makes our theory generally applicable.

The results of calculating the Henry coefficients based on Eq. (18) by using the values of Table 4 are listed in Table 5.

Table 6
The total porosity calculated for all resins.

	ε
GE Butyl Seph. 4 FF	0.96
GE Phenyl Seph. HP	0.96
GE Phenyl Seph. 6 FF (ls)	0.95
Tosoh Butyl-650M	0.94
Tosoh Phenyl-650M	0.95
Tosoh HW 65	0.92

49

Table 7
Arithmetical mean of k' values for GLY and DMSO with the standard deviation σ, determined by using the Retention volume via momentum, and via peak maximum; values have to be multiplied by 10^{-3}.

	k'_{GLY}		k'_{DMSO}	
	Moment.	Peak max.	Moment.	Peak max.
GE Butyl Seph. 4 FF	26	26 ± 3	17	17 ± 3
GE Phenyl Seph. HP	21	24.7 ± 0.8	9.9	15.6 ± 0.4
GE Phenyl Seph. 6 FF (ls)	74	26 ± 6	38	10.8 ± 0.7
Tosoh Butyl-650M	18	60 ± 1	37	57.8 ± 0.7
Tosoh Phenyl-650M	3.9	39 ± 1	4	47.7 ± 0.3
Tosoh HW 65	60	38 ± 1	28	44 ± 0.6

The results of calculating the porosity based on Eq. (19) by using the values of Tables 4 and 5 are listed in Table 6.

The synthetic polymer based media exhibit marginal lower porosities, compared to Sepharose based media.

5. Determination of k' via Retention volume, surface energies, Henry constants and porosities with this method

The conversion from a volumetric interpretation to the surface is through the relation ship shown in Eq. (18). k' and the Henry constant are dimensionless numbers in our case.

The term A (see Eq. (17)) is the link between volume and surface because it describes the theoretical area/footprint of an adsorbed molecule and thus the retention data can be converted into a surface energy. The outcome is based on the assumption of the area which interacts with the surface. We used always the same algorithm for the calculations of the A value. Slightly different values are found in literature. This maybe a source of error, but this is not only valid for our method, it has also an impact on contact angle measurement and is often neglected.

It is not clear if the molecular probe partitions between the liquid phase and the layer of ligands and to which extent the backbone is involved in the retention of the probe. Only a molecular model would help, but then we cannot expect an average value of the surface energy anymore.

We have used three different methods to evaluate the retention data one by deconvoluting the peak using Eq. (6) the others by simply measuring the first moment respectively the peak maximum. All methods give similar results. So this indicates that the algorithm itself is stable. As control experiments we have calculated the porosities from surface energies via Henry constant and compared to experimental data. We found good agreement. The molecular probes were selected by the criterion of solubility in water, this makes them suitable for investigation of HIC media.

Tables 7–11

6. Conclusion

With the described procedure, the Lifshitz–van-der-Waals and the Lewis acid and Lewis base contributions to the surface

Table 8
Arithmetical mean of k' values for EG and MEK with the standard deviation σ, determined by using the Retention volume via momentum and via peak maximum; values have to be multiplied by 10^{-3}.

	k'_{EG}		k'_{MEK}	
	Moment.	Peak max.	Moment.	Peak max.
GE Butyl Seph. 4 FF	12	25 ± 2	49	33 ± 4
GE Phenyl Seph. HP	21	30 ± 1	31	33.9 ± 0.4
GE Phenyl Seph. 6 FF (ls)	53	24.1 ± 0.4	96	26.9 ± 0.8
Tosoh Butyl-650M	210	78 ± 5	280	288 ± 1
Tosoh Phenyl-650M	16	61 ± 2	230	230.4 ± 0.8
Tosoh HW 65	50	76 ± 5	270	203.5 ± 0.8

Table 9
The LW-, Lewis acid (+) and Lewis base (−) contributions to the surface energy γ for the chromatography media investigated, determined by using the Retention volume via momentum (left column) and via peak maximum (right column); values are given in mJ/m².

	γ^{LW}		γ^+		γ^-		γ	
GE Butyl Seph. 4 FF	81.1	93.7	3.59	13.5	72.3	30.4	113	135
GE Phenyl Seph. HP	188	123	7.42	15.6	31.5	24.7	219	162
GE Phenyl Seph. 6 FF (ls)	131	169	5.82	6.96	39.3	25	161	195
Tosoh Butyl-650M	308	168	88	16.2	14.3	56	379	228
Tosoh Phenyl-650M	32.9	148	98.1	23.3	103	55.2	234	220
Tosoh HW 65	338	168	1.75	27.8	69.3	42.5	360	237

Table 10
The total porosity calculated for all resins, initially k' was determined by pulse shape method (identical Table 6), via momentum and via peak maximum.

	ε		
	Pulse shape meth.	Moment.	Peak max.
GE Butyl Seph. 4 FF	0.96	0.97	0.97
GE Phenyl Seph. HP	0.96	0.98	0.95
GE Phenyl Seph. 6 FF (ls)	0.95	0.93	0.96
Tosoh Butyl-650M	0.94	0.88	0.95
Tosoh Phenyl-650M	0.95	0.94	0.96
Tosoh HW 65	0.92	0.96	0.92

Table 11
The total porosity calculated for all resins, determined by the retention volumes of glucose in methanol ($\varepsilon = (V_R - V_0)/V$); where V_R is the retention volume and V_0 the bypass volume, obtained with via momentum and via peak maximum.

	ε	
	Moment.	Peak max.
GE Butyl Seph. 4 FF	0.99	0.99
GE Phenyl Seph. HP	0.97	0.96
GE Phenyl Seph. 6 FF (ls)	0.95	0.97
Tosoh Butyl-650M	0.86	0.82
Tosoh Phenyl-650M	0.88	0.85
Tosoh HW 65	0.84	0.82

energy according to van Oss' theory can be obtained for porous beads. Therefore the hydrophobicity, expressed in terms of the Lifshitz–van-der-Waals contributions to the surface energy can be quantified. The Lifshitz–van-der-Waals contribution to the surface energy of synthetic polymer-based media (Tosoh Toyopearl) is, as obtained by the method described, 2–3 times larger than the same contribution of natural polymer based media (GE Healthcare Sepharose media), except GE Healthcare Phenyl Sepharose HP media, which Lifshitz–van-der-Waals contribution is in the same range as the synthetic polymer-based media. Beside the convenience of having a fast and independent procedure for the determination of the phase ratio, this method has the advantage of being suitable for porous media.

Acknowledgements

References

[1] A. Mahn, M.E. Lienqueo, J.C. Salgado, J. Chromatogr. A 1216 (2009) 1838.
[2] C. Machold, K. Deinhofer, R. Hahn, A. Jungbauer, J. Chromatogr. A 972 (2002) 3.

[3] V.P. Shanbhag, Estimation of surface hydrophobicity of proteins by partitioning, in: G.J. Harry Walter (Ed.), Aqueous Two-Phase Systems, Methods in Enzymology, vol. 228, Academic Press, 1994, p. 254 (Chapter 23).
[4] A. Mahn, G. Zapata-Torres, J. Asenjo, J. Chromatogr. A 1066 (2005) 81.
[5] J. Chen, T. Yang, S.M. Cramer, J. Chromatogr. A 1177 (2008) 207, 5th Hydrophobic Interaction Chromatography/Reversed-Phase Liquid Chromatography Bioseparation Conference.
[6] A. Ladiwala, F. Xia, Q. Luo, C.M. Breneman, S.M. Cramer, Biotechnol. Bioeng. 93 (2006) 836.
[7] H. Claessens, M. Van Straten, C. Cramers, B. Jezierska, M. Buszewski, J. Chromatogr. A 826 (1998) 135.
[8] H. Engelhardt, M. Jungheim, Chromatographia 29 (1990) 59.
[9] H. Engelhardt, M. Arangio, T. Lobert, LC–GC 15 (1997) 856.
[10] M.J. Walters, J. Assoc. Off. Anal. Chem. 70 (1987) 465.
[11] K. Kimata, K. Iwaguchi, S. Onishi, K. Jinno, R. Eksteen, K. Hosoya, M. Araki, N. Tanaka, J. Chromatogr. Sci. 27 (1989) 721.
[12] S.V. Galushko, Chromatographia 36 (1993) 39.
[13] Á Sándi, Á Bede, L. Szepesy, G. Rippel, Chromatographia 45 (1997) 206.
[14] A. Jungbauer, J. Chromatogr. A 1065 (2005) 3, 1st Monolith Summer School.
[15] G. Carta, A. Jungbauer, Protein Chromatography: Process Development and Scale-Up, Wiley-VCH, 2010.
[16] A.W. Adamson, Physical Chemistry of Surfaces, Wiley, 1990.
[17] V.M. Starov, S.A. Zhdanov, S.R. Kosvintsev, V.D. Sobolev, M.G. Velarde, Adv. Colloid Interface Sci. 104 (2003) 123.
[18] J.D. Andrade (Ed.), Surface and interfacial aspects of biomedical polymers, Plenum Press, 1985.
[19] C.J. van Oss, Interfacial Forces in Aqueous Media, Taylor & Francis Group, LLC, 2006.
[20] G. Guiochon, S. Shirazi, A. Katti, Fundamentals of Nonlinear and Preparative Chromatography, 1994.
[21] S.J. Farlow, Partial Differential Equations for Scientists and Engineers, Dover Pubns, 1993.
[22] R. Bonomo, L. Minim, J. Coimbra, R. Fontan, L.M. da Silva, V. Minim, J. Chromatogr. B: Anal. Technol. Biomed. Life Sci. 844 (2006) 6.
[23] M. Millitzer, Zur Ad- und Desorption von Proteinen an hydrophoben Adsorbentien. Ph.D. Thesis. Universität Erlangen-Nürnberg, Erlangen, 2007.
[24] M. Wulf, P. Uhlmann, S. Michel, K. Grundke, Prog. Org. Coat. 38 (2000) 59.
[25] C.J. van Oss, R.J. Good, M.K. Chaudhury, Langmuir 4 (1988) 884.
[26] K. Ujimoto, H. Kurihara, J. Chromatogr. 301 (1984) 57.
[27] F.J. Riske, M.A. Smith, C. Zhang, K.H. White, Biotechnol. Appl. Biochem. 54 (2009) 157.
[28] H. Jennissen, A. Demiroglou, J. Chromatogr. A 1109 (2006) 197.
[29] H. Jennissen, Int. J. Bio-Chromatogr. 5 (2000) 131.
[30] M. Gindl, G. Sinn, W. Gindl, A. Reiterer, S. Tschegg, J. Colloids Surf. A 181 (2001) 279.

51

B. Publication 2

Langmuir

Surfaces Energies of Monoliths by Inverse Liquid Chromatography and Contact Angles

Ingeborg Bednar,[†,‡] Eva Berger,[‡] Nika Lendero Krajnc,[§] Jana Vidič,[§] Aleš Podgornik,[§] Alois Jungbauer,[†,‡] and Rupert Tscheliessnig*[,‡]

[†]University of Natural Resources and Life Sciences, Vienna, Austria

[‡]Austrian Centre for Industrial Biotechnology, Vienna, Austria

[§]BIA Separations, Ajdovščina, Slovenia

Ⓢ *Supporting Information*

ABSTRACT: Seven porous chromatographic columns, termed monoliths, and seven nonporous sheets were produced from polymethacrylates. Their surfaces were activated by different densities of butyl and phenyl ligands. We determined the retention times of highly dilute molecular probes in monoliths and accessed contact angles of pure molecular probes of sheets. We calculated surface energies for both systems. We applied theories of Young, Dupré, and van Oss and compared the results of both types of experiments with respect to Lifshitz−van der Waals and Lewis acid and Lewis base contributions and find agreement but an additive constant.
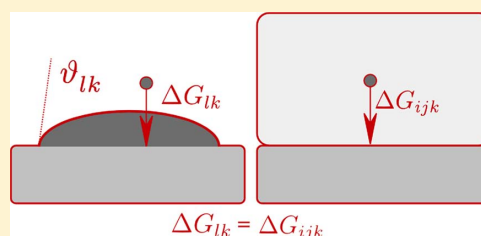
■ INTRODUCTION

A key invention in separation sciences have been monoliths as stationary phases in liquid chromatography. Monoliths are porous polymers. Their porosity is caused by porogenic solvents, which lead to precipitation during polymerization. The interlaced network forms large surface areas which are accessible to solvents and solutes. The characteristic channel diameters vary from 100 nm to several μm.[1] On one hand, channel widths discriminate biomolecules such as peptides, proteins, viruses, and viruslike particles[2] of different sizes. On the other hand, particular surface modifications trigger the solutes' retention times and thus determine the units' separation performance. In this work, we analyze polymethacrylate-based monoliths. Their surfaces have been additionally functionalized to enable hydrophobic interactions. In particular, we are interested in surfaces energies as a function of the different functionalization of the monoliths. But how do we access the surfaces energies of a porous material? A straightforward experimental method was to deduce surface energies from contact angle measurements.[3] And indeed the surfaces energies of the outer surfaces of monoliths are easily accessible. It is different if we consider the monoliths' pores. These volumes of interest, in particular their surfaces, are buried deep in the monolith. A destructive way to access these surfaces is to cleave the monolith. However, the cleavage will cause additional dangling bonds, and these will shift contact angles and result in surface energies that have less in common with the energy landscape as a molecular probe for samples on its trajectory through the intact monolith. Beside the additional dangling bonds and their impact on the surface energies, we challenge soaking effects. The media are porous, and part of the

liquid drops may be soaked into the monolithic media. Soaking consequently makes true contact angles inaccessible. In this work, we follow the concepts of Young,[4] Dupré,[5] and van Oss[3] and discriminate between apolar Lifshitz−van der Waals and polar Lewis acid and base (AB) intraactions and interactions. For comparison with other works, we performed contact angle measurements. In order to avoid any possible soaking effect, we produced flat sheets, which we functionalized. We sampled these sheets by five molecular probes including water. The contact angles are considered to be references only. With respect to contact angle measurements, we introduce an orthogonal approach to accessing Lifshitz−van der Waals and AB forces to which we refer: inverse liquid chromatography. Pulses of highly diluted molecular probes were injected. Due to the particular interactions of the molecular probes with the surfaces or the absence of interactions, the pulses were distorted. From the distortions of the pulses, the Henry coefficients were accessed.[6] The method is very accurate but computationally challenging. In the present work, we adapt the method and calculate the Henry coefficient from the zero point of the differentiated and time-weighted pulses. The article is organized as follows: We briefly summarize the experimental methods in the theoretical part, we introduce the mathematical methods on which basis we analyze the pulse responses, and we discriminate the monoliths according to their different surface energies.

A

EXPERIMENTAL SECTION

Production of Flat Sheets and Monoliths. We produced nonporous sheets and porous chromatographic columns, called monoliths. While sheets were used for contact angle measurements, monoliths were used for the inverse liquid chromatography experiments.

Materials used for the production of either were monomers glycidyl methacrylate (GMA, 97%), butyl methacrylate (BuMA, 99%), and benzyl methacrylate (BeMA, 96%), cross-linker ethylene glycol dimethacrylate (EDMA, 98%), and porogens dodecanol (98%), cyclohexanol (99%), butanol (≥99%), 1,4-butandiol (99%), propanol (≥99%), octanol (≥99%), and toluene (99.8%). These were purchased from Sigma-Aldrich (St. Louis, MO, USA). Initiator benzoyl peroxide (BPO, 75%) was obtained from Tokyo Chemical Industry (Tokyo, Japan), and ethanol was from Kefo (Ljubljana, Slovenia).

Monoliths with different ligand densities but the same pore size were prepared: methacrylate monoliths were polymerized from the monomer mixtures consisting of monomers, cross-linker agent, porogens, and initiator. In all cases, the same amounts of cross-linker EDMA and initiator BPO were used. For butyl monoliths, GMA and BuMA were used as monomers, and for phenyl monoliths, GMA and BeMA were used as monomers. To obtain the same pore size for all monoliths, various mixtures of porogenic solvents were used; mixtures of alkyl alcohols were used to prepare butyl monoliths, while toluene was also used for phenyl monoliths. The monomer mixture was poured into a closed mold, which was placed into a water bath. The polymerization was performed at elevated temperature (60 °C ± 5 °C) overnight. Once the polymerization was completed, the monoliths were washed extensively with ethanol to remove porogenic solvents. All monolithic columns had an inner diameter of 6.7 mm and an outer diameter 18.6 mm and a length of 4.2 mm. The total volume was 1 mL, and the average pore size was 2 μm.

For the preparation of flat sheets with different ligand densities, we used the same monomeric mixture and the same ratio of monomers, cross-linker, and initiator but without porogenic solvents. The solution was polymerized in a stainless steel mold in a water bath at elevated temperature. At the end, the polymer was washed with ethanol.

Molecular Probes. All in all, seven monolithic materials, listed in section 1, were probed by four organic solvents and HQ water. The molecular probes purchased were (a) glycerol (GLY, 92.09 g/mol, Fisher Scientific, analytical reagent grade, G/0650/17, 2.5 l); (b) ethylene glycol (EG, 62.07 g/mol, Merck, p. a., 9621.5000, 5 l); (c) formamide (FORM, 45.04 g/mol, Carl Roth, >99.5% RNase/DNase free, P040.1, 250 mL); and (d) dimethyl sulfoxide (DMSO, 78.13 g/mol, Sigma-Aldrich, Chromasolv, 34869, 1 l).

Contact Angles. For all contact angle experiments, we used HQ-water drops and drops of four pure molecular probes: glycerol, ethylene glycol, formamide, and dimethyl sulfoxide. Literature data of the contributions to the surface energy (Lifshitz−van der Waals (LW), Lewis acid (+), and Lewis base (−) energies of five liquids) are given in the Supporting Information. Contact angles were accessed with an Easy Drop DSA15 drop-shape analyzer from Krüss (Hamburg, Germany). Drops of pure liquids were placed on flat nonporous monolithic surfaces. Pictures of drops were taken and analyzed by the corresponding analysis software. In detail, we fitted the drop shape by the tangential method (no. 1). Hereby we refer to a method by which the drop shape is fitted with a general conic section equation and the contact angle is measured between the tangent of this curve at the three-phase contact point and the baseline. The method is also known as the conic section method.

Inverse Liquid Chromatography. Retention times of the molecular probes were determined by inverse liquid chromatography experiments. The monolithic tubes were connected to a high-performance liquid chromatography workstation (Agilent Series 1100 LC, Santa Clara, CA, USA). Experiments were controlled by the use of Agilent ChemStation software, Rev. B. 04.03(16), for LC 3D systems. The monolithic materials were functionalized either by butyl or phenyl ligands. The different concentrations ranged from 25

to 100% ligand density (section 1). HQ deionized water was used as the mobile phase. Four molecular probes—GLY, EG, DMSO, FORM—were diluted in HQ-water to a ratio of 1:2. Aliquots of 10 μL were injected and eluted by isocratic elution with HQ-water. The flow rate was kept at 1 mL/min. The UV adsorption was continuously monitored at 205 nm for GLY and EG with bandwidths of 4 and 250 nm (bandwidth 30 nm) for DMSO and FORM. In each case, the reference wavelength was 400 nm with a bandwidth of 4 nm.

THEORIES

Van Oss and Dupré Theory. We follow Young,[4] Dupré,[5] and van Oss[3] and discriminate between apolar Lifshitz−van der Waals forces and polar or Lewis acid or base intraaction and interactions. Lifshitz−van der Waals forces are long-range, their decay length equals approximately 10 nm, they are electrodynamic by nature, and they allude to van der Waals−Keeson (dipole−dipole attraction), van der Waals−Debye (interactions between molecules with permanent dipoles and molecules where the dipole is induced), and van der Waals−London (temporary dipoles) interactions. Complements to van der Waals and electrostatic forces are Lewis acid and base (AB) intraactions and interactions. In this work, forces of hydrophic characteristics and their repulsive counterpart, hydrophobic pressure, are polar forces which are of neither electrodynamic nor electrostatic origin. They are termed AB interactions. These are short-ranged with decay lengths of approximately 1 nm. The concept of Van Oss is to split interactions in apolar (Lifshitz−van der Waals, LW) and polar (AB) interactions and intraactions.[3] The polar and apolar contributions to the Gibbs free energy, ΔG, are additive:

$$\Delta G = \Delta G^{LW} + \Delta G^{AB} \tag{1}$$

For two substances, the molecular probe here shall be indexed by l and the surface shall be indicated by the index k, where the Gibbs free energy of the system equals

$$\Delta G_{lk} = \Delta G_{lk}^{LW} + \Delta G_{lk}^{AB} \tag{2}$$

In the case in which we consider intraactions only, the latter equation simplifies to $\Delta G_{kk} = \Delta G_{kk}^{LW} + \Delta G_{kk}^{AB}$. If we split a monolith, then we created two surfaces and the amount of energy necessary for the cleavage were equivalent to the surface energy, γ_k:

$$\Delta G_{kk} = -2_{\gamma k} \tag{3}$$

The total surface energy is, analogous to the Gibbs free energy, the sum of the polar and apolar contributions

$$\gamma_k = \gamma_k^{LW} + \gamma_k^{AB} \tag{4}$$

The polar contribution to the Gibbs free energy includes both electron-acceptor (Lewis acid, +) and electron-donor (Lewis base, −) interactions because γ is a linear function of the Gibbs free energy; this holds for the surface energy as well. According to van Oss, the polar contribution to the surface energy is defined as

$$\gamma_k^{AB} = 2\sqrt{\gamma_k^+ \gamma_k^-} \tag{5}$$

With respect to interactions for a system of medium k immersed in a liquid l, Dupré's equation links ΔG_{lk} to the interfacial surface energies of both compounds, γ_{lk}, and the separate surface energies of the medium, γ_k, and the liquid, γ_l:

$$\Delta G_{lk} = \lambda_{lk} - \lambda_k - \lambda_l \tag{6}$$

54

The (total) interfacial surface energy is the sum of both polar and apolar contributions:

$$\gamma_{lk} = \gamma_{lk}^{LW} + \gamma_{lk}^{AB} \tag{7}$$

These contributions to the interfacial surface energy of two components introduced as in refs 7 and 8 or as found in van Oss[3] are given as

$$\gamma_{lk}^{LW} = (\sqrt{\gamma_l^{LW}} - \sqrt{\gamma_k^{LW}})^2$$

$$\gamma_{lk}^{AB} = 2(\sqrt{\gamma_l^+} - \sqrt{\gamma_k^+})(\sqrt{\gamma_l^-} - \sqrt{\gamma_k^-}) \tag{8}$$

Contact-Angle Theory. Young's equation, eq 9, describes the relationship between the interfacial surface energy of a liquid and a solid, γ_{jk}, taking into account the contact angle ϑ_{lk} between them in a gaseous environment. Two phases are distinguished. The substance of the drop is indexed by l and the surface by k:

$$\gamma_{lk} = \gamma_k - \gamma_l \cos\vartheta_{lk} \tag{9}$$

Here $\gamma_{lk} = \gamma_{kl}$ is imperative.

Combining Young's equation, eq 9' with the Dupré equation, eq 6, we obtain the so-called Young–Dupré equation, which relates the free energy of interaction of a liquid l and a solid k with the surface energy of the liquid and the contact angle between the liquid and solid:

$$\Delta G_{lk} = -\gamma_l(1 + \cos\vartheta_{lk}) \tag{10}$$

The free energy of interaction ΔG_{lk} can be expanded in terms of the contributions to the surface energy by inserting eqs 4, 5, 7, 8 into eq 6, leading to

$$\Delta G_{lk} = -2\sqrt{\gamma_l^{LW}\gamma_k^{LW}} - 2\sqrt{\gamma_l^+\gamma_k^-} - 2\sqrt{\gamma_l^-\gamma_k^+} \tag{11}$$

By substituting the free energy of interaction into eq 11 with eq 10, the Young–Dupré equation can be rewritten as

$$-\gamma_l(1 + \cos\vartheta_{lk}) = -(2\sqrt{\gamma_l^{LW}\gamma_k^{LW}} + 2\sqrt{\gamma_l^+\gamma_k^-} + 2\sqrt{\gamma_l^-\gamma_k^+}) \tag{12}$$

If a surface is probed by different molecules based on the latter equation, then we may formulate a simple matrix equation $\mathbf{a} = \hat{\mathbf{m}}\cdot\mathbf{b}$. Herein, $\mathbf{a}$ is a vector with components that reflect the different contact angles. These values may be experimentally acquired. The matrix $\hat{\mathbf{m}}$ holds the characteristic parameters of the molecular probes, whereas $\mathbf{b}$ is a vector with the characteristic surface energy contributions as components. The solution of the equation is simple: the pseudoinverse of the matrix is calculated; consequently, the surface energies can be assessed by $\mathbf{b} = \hat{\mathbf{m}}^{-1}\cdot\mathbf{a}$.[9]

Inverse Liquid Chromatography Theory. The Dupré equation links the free energy of interaction for a system of a molecular probe, i immersed in a liquid, with j next to a surface k. The change in the free energy ΔG_{ijk} can be expressed as a sum of the individual contributions of the molecular probe with the surface γ_{ik}, the molecular probe with the solution γ_{ij}, and the solution with the surface γ_{jk}:

$$\Delta G_{ijk} = \gamma_{ik} - \gamma_{ij} - \gamma_{jk} \tag{13}$$

By inserting eqs 7 and 8 and analogous relations for γ_{ij} and γ_{ik} into eq 13, the free energy of interaction among three interaction partners can be expressed as

$$\frac{\Delta G_{ijk}}{2} = -\gamma_j^{LW} + \sqrt{(\gamma_i^{LW}\gamma_j^{LW})} + \sqrt{(\gamma_j^{LW}\gamma_k^{LW})} - \sqrt{(\gamma_i^{LW}\gamma_k^{LW})}$$
$$+ \sqrt{\gamma_j^+}(\sqrt{\gamma_i^-} - \sqrt{\gamma_j^-} + \sqrt{\gamma_k^-}) + \sqrt{\gamma_j^-}(\sqrt{\gamma_i^+} - \sqrt{\gamma_j^+} + \sqrt{\gamma_k^+})$$
$$- \sqrt{\gamma_i^+\gamma_k^-} - \sqrt{\gamma_i^-\gamma_k^+}$$

or more mathematically compact

$$\Delta G_{ijk} = \mathbf{m}'\cdot\mathbf{b} \tag{14}$$

As with the contact angles mentioned above, we can formulate a complex equation as a simple vector product, and for a set of different molecular probes, we may expand the equation to matrix notation. In a chromatographic experiment, the Henry coefficient describes the linear relationship between the concentration of molecules adsorbed and those not adsorbed to the surface of the chromatography material and the concentration of molecules in the mobile phase. For infinite dilution, the logarithm of the Henry coefficient is proportional to the free energy of interaction

$$\Delta G_{ijk} = -\frac{k_B T}{A_i \ln H_{ijk}} \tag{15}$$

where k_B is Boltzmann's constant, T is the temperature in Kelvin, and A_i is the theoretical area of an adsorbed molecule of substance i covering the surface. The corrected formula, if compared to ref 6, holds: $A_i/(\pi^2)^{3/2} = (3(MW_i)/(4\rho_i N_A))^{2/3}$, and in a previous publication the factor $(\pi)^{3/2}$ was missing. The theoretical areas that molecular probes cover are $A_{GLY} = 4.338$, $A_{EG} = 3.624$, $A_{DMSO} = 4.257$, and $A_{FORM} = 2.897$. The mean theoretical area is $\langle A \rangle = 3.779$. All values are given as multiples of 10^{-19} m^2. For calculations, we used the mean value of all molecular probes to estimate the area the probes cover on the surface, $\langle A \rangle$. The Henry coefficient and the retention factor, k'_{ijk}, can be linked by $H_{ijk} = k'_{ijk}\,\varepsilon/(1 - \varepsilon)$, with the total porosity estimated by $\varepsilon = 0.65$.[1] In this work, we bypass the necessity of an exact knowledge of the total porosity by a mathematical move that we introduced recently:[6]

$$\frac{k_B T}{\langle A \rangle(-\ln k'_{ijk} + \ln k'_{i'jk})} = (\mathbf{m}'_i - \mathbf{m}'_{i'})\cdot b \tag{16}$$

Method of the First Moment. As the pulse that is injected is considered to be a delta function in time, it is related to its derivative by

$$|\delta(t)| = |t\partial_t\delta(t)| \tag{17}$$

This is a powerful relationship, and the identity shall hold if the experimental pulse was a delta function. We can argue the opposite: if we impose the identity above on the experimental data, then we enforce the signal as being a delta function. If we argue this way or the other, both rest on the assumption that we imposed in ref 6: the pulse was a delta function. As the identity shall hold, consequently the maximum on the left-hand side should coincide with the maximum on the right-hand side. The identity has an additional benefit. The background correction of the signal is no longer necessary. Usually the signal is corrected by subtracting an arbitrary function which is linear in time. If we work with the first derivative in time of the signal, then the background correction cancels. In this article, in order to determine the retention factors the UV detector signals were differentiated and time weighted. The retention times t_R were determined by the zero positions of the time-weighted signals. The retention factor was calculated by the

retention time and the dead time t_0, where $k' = (t_R - t_0)/t_0$. We used $t_0 = (D_o - D_i)/(2u)$ and obtained u as the (radial) chromatographic velocity, which was calculated by

$$u = v \frac{1}{L\pi\varepsilon} \frac{(\log D_o - \log D_i)}{(D_o - D_i)} \tag{18}$$

as adapted from ref 10. The outer diameter of the monoliths was $D_o = 18.6$ mm, while the inner diameter was $D_i = 6.7$ mm with velocity $v = 1$ mL/min, porosity $\varepsilon = 0.65$, and column length $L = 4.2$ mm.

■ RESULTS AND DISCUSSION

In Table 2, contact angles on nonporous monolithic surfaces of different ligand densities for four molecular probes are given.

Table 1. Materials Investigated: Monolithic Tubes (1 mL, for Inverse Liquid Chromatography Experiments) and Flat Sheets (for Contact Angle Experiments)

| acronym	ligand densities
25% C4	25% butyl, 75% hydroxyl groups
50% C4	50% butyl, 50% hydroxyl groups
75% C4	75% butyl, 25% hydroxyl groups
25% Ph	25% phenyl, 75% hydroxyl groups
50% Ph	50% phenyl, 50% hydroxyl groups
75% Ph	75% phenyl, 25% hydroxyl groups
100% Ph	100% phenyl groups

Table 2. Mean Values of Contact Angles of Water and Molecular Probes[a]

material	ϑ_{H_2O} (deg)	ϑ_{GLY} (deg)	ϑ_{EG} (deg)	ϑ_{DMSO} (deg)	ϑ_{FORM} (deg)
25% C4	69.1	5.6	46.1		41.9
25% Ph	68.9	64.2	39.9	27.4	42.4
50% C4	73.8	67.9	47.7	27.4	43.5
50% Ph	62.9	61.0	33.3		39.8
75% C4	76.6	67.7	61.6	31.1	53.6
75% Ph	67.8	59.3	40.2		47.4
100% Ph	74.1	69.9	42.5		54.2

[a]A bar indicates the absence of a contact angle due to spreading of the drop. The standard deviations are $H_2O = \pm1.9°$, GLY $= \pm2.3°$, EG $= \pm2.8°$, and DMSO $= \pm2.2°$. All values are given in degrees.

We synthesized flat sheets in the absence of a porogenic solvent and thus hindered precipitation during polymerization. Starov et al.[11] observed the spreading of drops on dry porous layers. They examined a decrease in the contact angles as the wetted areas of the porous surfaces expanded over time, after the drops had been deposited. Experimental data were modeled to account for the shrinkage of the drop while the liquid soaked into the porous layer and the radius of the wetted region grew.[12] The model of Alleborn et al.[13] provided an even more detailed picture of the wetting phenomena. Although the authors constrained their work to theoretical considerations, they observed agreement with the presented model, which is based on lubrication theory, in context with the experimental data of others, e.g., Starov et al.[12] The flat sheets were nonporous, and soaking effects were less problematic. Some of the contact angles of DMSO were not accessible at all, as drops spread and covered the surfaces. This may hint at metastable drop formation. Values close to 0° or close to 30° seem plausible. We point to the small standard deviation of each

experiment; each measurement has been repeated at least three times. We apply eq 12 and calculate surface energies and discriminate these according to their three contributions. We do find that our results for surface energies, in particular, the small values for γ^+, are comparable to findings published by Correia et al.[14] on poly(methyl methacrylate). For this particular material, the authors published values of $\gamma^{LW} = 43.9$ mJ/m^2, $\gamma^+ = 0.03$ mJ/m^2, and $\gamma^- = 16.2$ mJ/m^2. These were determined from contact angle measurements by the use of eq 12. If we compare the published values to the ones that we obtained from contact angles on surfaces that have been grafted, we may be tempted to argue that the molecular probes sample the matrix of the material only. In particular, the minimal γ^+ contribution favors the argument that the molecular probes do not interact with the ligands at all. The apparently low Lewis acid part of the surface energy is consistent with the findings of Bismarck et al.[15] The latter author doubts the accessibility of this interaction by contact angle measurements. Surface energies were compared to results determined from zeta-potential measurements, and the higher complement contributions were interpreted as being overestimated. At this point, it is probably helpful to refer to Morra et al.,[16] who doubted the general basic properties of solid surfaces found by contact angle measurements, especially if polymers are involved. This statement finds support as the distribution and arrangement of polymer (side) chains have a crucial effect on the chemical−physical properties. Polymers of the same kind may feature different formations of ligands. Additives used during polymerization are another reason for huge variances in surface energies for poly(methyl methacrylate), which were published in the literature: 40.6[17] and 92.6 mJ/m^2.[18] What are the experimental alternatives? In separation sciences, we need to know the surface energies of polymer-based materials, and we need to discriminate the surface energy into its different contributions. We need an orthogonal method. We were the first[6] who proposed the use of chromatography experiments to access retention times of molecular probes and, by the use of the van Oss concept, to discriminate surface energies into apolar Lifshitz−van der Waals and polar Lewis acid and base contributions. While in the latter work we focused on the distortion of the shape of the delta pulse and deduced the solute surface interactions thereof, here we present a shortcut that is less computational demanding. In Figure 1, representative of all other samples, the differentiated and time-weighted UV-detector signals of DMSO for all monolithic materials are
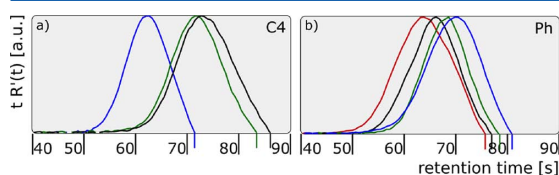

Figure 1. Differentiated normalized and time-weighted detector responses of the isocratic elution of DMSO with HQ-water are plotted for the different monolithic materials as a function of time. Only positive values are shown. The plot starts at 40s because no peaks were detected at shorter times. For (a) the butyl ligand (C4) densities vary from 25−75% and for (b) the phenyl (Ph) ligand densities vary from 25−100%. The different retention times are indicated by vertical lines, and the color code for the different ligand densities is red for 100%, blue for 75%, green for 50%, and black for 25% ligand density.

given. The zero positions of the differentiated and time-weighted signals are associated with the retention times. If the retention times are considered to be a function of ligand densities, then they cope with the contact angles discussed before. High contact angles are found for intermediate ligand densities and can be related to longer retention times. The surface energies obtained by inverse liquid chromatography experiments and contact angle measurements are listed in the Supporting Information. To ease the comparison of the surface energies obtained by the two experimental methods, individual contributions were plotted in Figure 2 and the total surface
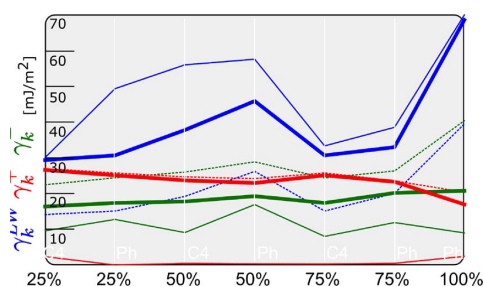

Figure 2. Results of inverse liquid chromatography (full and dashed lines; the dashed lines are the results obtained by the elimination of the porosity) and contact angle (thin full lines) experiments are compared. The color code is read as follows: blue indicates γ^{LW} contributions while red and green lines highlight γ^+ and γ^-.
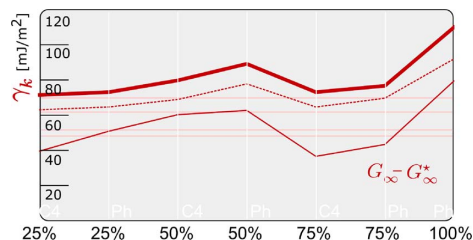
Figure 3. Full and dashed lines (inverse liquid chromatography, the dashed lines are the results obtained by the elimination of the porosity) and a thin full line (contact angle) give the total surface energy as a function of increasing ligand densities for phenyl (Ph) and butyl (C4) monoliths. The pink horizontal lines indicate typical surface energies of the monolith matrix.

energies, in Figure 3. The results of the total surface energies of the monolithic materials for inverse liquid chromatography measurements vary between 71.5 and 109.8 mJ/m^2. In Figure 3, the total surface energy increases with the amount of ligand for both methods. Clearly, because of the lower Lewis acid and base contributions, the total surface energies obtained by contact angle measurements were lower than the inverse liquid chromatography values and range from 29.4 to 68.6 mJ/m^2. Why is there a difference in the absolute values of the surface energies for the two experimental methods? They seem to be shifted by an additive constant. Different reasons are plausible: it may be the system's porosity or the net area of the molecular probe. Both are quantities that shift the surface energy by an additive constant. Additional possible explanations are sketched in Figure 4a,b. If the surface were porous, then the molecular
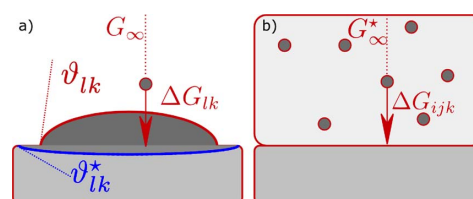
Figure 4. (a) In contact angle experiments, a drop of liquid (dark-gray ellipsoid with a red border) is in contact with an ideal flat surface (light gray). Due to soaking effects, the true contact angle ($\vartheta_{lk} + \vartheta_{lk}*$) differs from the measured one, ϑ_{lk}. (b) In an inverse liquid chromatography experiment, molecular probes (dark-gray circles with red borders) are diluted in water (gray body). The two molecular probes highlighted indicate the different reaction pathways and the work necessary to move it from the remote site toward the surface.

probes would be absorbed and soaked into the solid. Consequently, the apparent contact angle would differ from the actual value. To avoid this in particular, we prepared the nonporous sheets, so the latter argument does not count in the present work. Or, for contact angle measurements, the ligands of the monolithic material may not be actively involved in the wetting process. Perhaps the ligands have collapsed and therefore are spread out on the surface instead of being aligned in a straight-up, active, moveable, brushlike position, which may also distort the contact angle. In fact, the difference in the experimental setup might be even more profound. Consider contact angle measurements. In Figure 4a, when remote from the surface the molecular probe is in equilibrium with the gaseous phase. In Figure 4b, in the inverse liquid chromatography setup the probe is in equilibrium with the solvent. For both systems, we may speculate on the Henry coefficient, which is equivalent to the work necessary to move the hypothetical particle from the remote region to the surface. Apparently the environment for the sample differs in these two models, and thus the pair interactions will differ, giving rise to differences in the Henry coefficient, and serve as a possible explanation for the additive shift.

■ CONCLUSIONS

Inverse liquid chromatography measurements have been introduced as a complementary method to contact angle measurements, where the latter is a standard procedure used to determine the surface energies of different surfaces. The method we introduced is nondestructive, and we may access the energy landscape that is buried deep in monolithic structures. We perform pulse response experiments and calculate from retention times Lifshitz−van der Waals, Lewis acid, and Lewis base contributions to the surface energies of monoliths of different activated surfaces. The surface energies that were determined by the two methods were compared, and their tendencies with increasing ligand density were coincident but an additive constant. We name and discuss different reasons that may account for the additive shift of surface energies. Among all, we favor the one in which both experiments are inherently different in their design.

■ ASSOCIATED CONTENT

ⓢ Supporting Information

and FORM that were determined by inverse liquid chromatography experiments, and the LW, Lewis acid, and Lewis base energies that were deduced from inverse liquid chromatography experiments (ILC) as well as results from contact angle measurements (CA). This material is available free of charge via the Internet at http://pubs.acs.org/.

■ AUTHOR INFORMATION

Corresponding Author

*E-mail: rupert.tscheliessnig@acib.at. Phone: +43 147654 6226. Fax: +43 1 47654 6675.

Notes

The authors declare no competing financial interest.

■ REFERENCES

(1) Merhar, M.; Podgornik, A.; Barut, M.; Žigon, M.; Štrancar, A. Methacrylate monoliths prepared from various hydrophobic and hydrophilic monomers − Structural and chromatographic characteristics. *J. Sep. Sci.* **2003**, *26*, 322−330.

(2) Gerster, P.; Kopecky, E.-M.; Hammerschmidt, N.; Klausberger, M.; Krammer, F.; Grabherr, R.; Mersich, C.; Urbas, L.; Kramberger, P.; Paril, T.; Schreiner, M.; Nöbauer, K.; Razzazi-Fazeli, E.; Jungbauer, A. Purification of infective baculoviruses by monoliths. *J. Chromatogr., A* **2013**, *1290*, 36−45.

(3) van Oss, C. J. *Interfacial Forces in Aqueous Media*, 2nd ed.; CRC Press: Boca Raton, FL, 2006.

(4) Young, T. An Essay on the Cohesion of Fluids. *Philos. Trans. R. Soc. London* **1805**, *95*, 65−87.

(5) Dupré, A.; Dupré, P. *Théorie Mécanique de la Chaleur*; Gauthier-Villars: Paris, 1869.

(6) Bednar, I.; Tscheliessnig, R.; Berger, E.; Podgornik, A.; Jungbauer, A. Surface energies of hydrophobic interaction chromatography media by inverse liquid chromatography. *J. Chromatogr., A* **2012**, *1220*, 115−121.

(7) Good, R. J.; Girifalco, L. A. A theory for estimation of the surface and the interfacial energies. III. Estimation of surface energies of solids from contact angle data. *J. Phys. Chem.* **1960**, *64*, 561−565.

(8) Fowkes, F. M. Additivity of intermolecular forces at interfaces. I. Determination of the contribution to surface and interfacial tensions of dispersion forces in various liquids. *J. Phys. Chem.* **1963**, *67*, 2538−2541.

(9) Gindl, M.; Sinn, G.; Gindl, W.; Reiterer, A.; Tschegg, S. A comparison of different methods to calculate the surface free energy of wood using contact angle measurements. *Colloids Surf., A* **2001**, *181*, 279−287.

(10) Podgornik, A.; Jančar, J.; Merhar, M.; Kozamernik, S.; Glover, D.; Čuček, K.; Barut, M.; Štrancar, A. Large-scale methacrylate monolithic columns: design and properties. *J. Biochem. Biophys. Methods* **2004**, *60*, 179−189.

(11) Starov, V.; Kostvintsev, S.; Sobolev, V.; Velarde, M.; Zhdanov, S. Spreading of Liquid Drops over Dry Porous Layers: Complete Wetting Case. *J. Colloid Interface Sci.* **2002**, *252*, 397−408.

(12) Starov, V.; Zhdanov, S.; Kosvintsev, S.; Sobolev, V.; Velarde, M. Spreading of liquid drops over porous substrates. *Adv. Colloid Interface Sci.* **2003**, *104*, 123−158.

(13) Alleborn, N.; Raszillier, H. Spreading and sorption of a droplet on a porous substrate. *Chem. Eng. Sci.* **2004**, *59*, 2071−2088.

(14) Correia, N. T.; Ramos, J. J.; Saramago, B. J.; Calado, J. C. Estimation of the Surface Tension of a Solid: Application to a Liquid Crystalline Polymer. *J. Colloid Interface Sci.* **1997**, *189*, 361−369.

(15) Bismarck, A.; Kumru, M.; Springer, J. Characterization of Several Polymer Surfaces by Streaming Potential and Wetting Measurements: Some Reflections on Acid-Base Interactions. *J. Colloid Interface Sci.* **1999**, *217*, 377−387.

(16) Morra, M. Some Reflection on the Evaluation of the Lewis Acid-Base Properties of Polymer Surfaces by Wetting Measurements. *J. Colloid Interface Sci.* **1996**, *182*, 312−314.

(17) van Oss, C. J.; Good, R. J.; Chaudhury, M. K. Additive and nonadditive surface tension components and the interpretation of contact angles. *Langmuir* **1988**, *4*, 884−891.

(18) Fowkes, F. M.; Kaczinski, M. B.; Dwight, D. W. Characterization of polymer surface sites with contact angles of test solutions. 1. Phenol and iodine adsorption from methylene iodide onto PMMA films. *Langmuir* **1991**, *7*, 2464−2470.

(19) van Oss, C. J. Use of the combined Lifshitz-van der Waals and Lewis acid-base approaches in determining the apolar and polar contributions to surface and interfacial tensions and free energies. *J. Adhes. Sci. Technol.* **2002**, *16*, 669−677.

(20) van Oss, C. J.; Good, R. J. Surface Tension and the Solubility of Polymers and Biopolymers: The Role of Polar and Apolar Interfacial Free Energies. *J. Macromol. Sci., Part A* **1989**, *26*, 1183−1203.

Supporting Information to: Surfaces energies of monoliths by inverse liquid chromatography and contact angles

Ingeborg Bednar,[†,‡] Eva Berger,[‡] Nika Lendero Krajnc,[¶] Jana Vidič,[¶] Aleš Podgornik,[¶] Alois Jungbauer,[†,‡] and Rupert Tscheliessnig[∗,‡]

University of Natural Resources and Life Sciences, Vienna, Austria, Austrian Centre for Industrial Biotechnology, Vienna, Austria, and BIA Separations, Ajdovščina, Slovenia

E-mail: rupert.tscheliessnig@acib.at

Phone: +43 147654 6226. Fax: +43 1 47654 6675

Supporting information

In Table STable 1 we pool the literature data of the Lifshitz-van der Waals (LW), Lewis Acid ($+$) and Lewis Base ($-$) contributions to the surface energy for water, GLY, EG, DMSO and FORM. The experimental data of k' for GLY, EG, DMSO and FORM, determined from inverse liquid chromatography experiments are listed in Table STable 2. In Table STable 3 the LW-, Lewis acid and Lewis base contributions to the surface energy of monolithic materials, deduced from inverse liquid chromatography experiments (ILC) and from contact angle measurements (CA) are summarized.

[∗]To whom correspondence should be addressed
[†]University of Natural Resources and Life Sciences, Vienna, Austria
[‡]Austrian Centre for Industrial Biotechnology, Vienna, Austria
[¶]BIA Separations, Ajdovščina, Slovenia

Table S1: The Lifshitz van der Waals (LW), Lewis Acid ($+$) and Lewis Base ($-$) contributions to the surface energy of water, glycerol (GLY), ethylene glycol (EG), formamide (FORM) and dimethyl sufoxide (DMSO), are listed. All values are given in J/m^2.

	reference(s)	γ^{LW}	γ^{+}	γ^{-}
H_2O	[1]	0.0218	0.0255	0.0255
GLY	[1–3]	0.034	0.00392	0.0574
EG	[2,3]	0.029	0.003	0.0301
FORM	[1–3]	0.039	0.00228	0.0396
DMSO	[3]	0.036	0.0005	0.032

Table S2: Values of k' for GLY, EG, DMSO and FORM, determined from inverse liquid chromatography experiments. All values are unitless.

	k'_{GLY}	k'_{EG}	k'_{DMSO}	k'_{FORM}
25% C4	1.286	1.324	1.29	1.22
25% Ph	1.137	1.242	1.156	1.153
50% C4	1.204	1.325	1.256	1.284
50% Ph	1.222	1.307	1.259	1.354
75% C4	1.137	1.241	1.156	1.152
75% Ph	0.873	1.003	0.937	0.97
100% Ph	1.24	1.558	1.34	1.737

2

Table S3: The LW-, Lewis acid and Lewis base contributions to surface energies of monolithic materials deduced from inverse liquid chromatography experiments (ILC), results obtained by elimination of the porosity are added in parentheses, and from contact angle measurements (CA) are given. In the last column the total surface energies are listed. All values are given in mJ/m^2.

| | γ^{LW} | | γ^{+} | | γ^{-} | | γ | |
	ILC	CA	ILC	CA	ILC	CA	ILC	CA
25% C4	29.4 (14.2)	30.1	27. (26.6)	2.4	16.4 (22.5)	9.6	71.5 (63.1)	39.7
25% Ph	30.7 (15.1)	49.4	25.8 (25.1)	0.	17.4 (24.4)	12.8	73.1 (64.7)	50.9
50% C4	37.8 (19.2)	56.	24.7 (23.7)	0.5	17.8 (26.)	9.1	79.7 (68.9)	60.3
50% Ph	45.9 (26.2)	57.6	24.2 (23.)	0.4	19.3 (28.9)	16.9	89.1 (77.8)	62.7
75% C4	30.7 (15.1)	33.4	25.8 (25.1)	0.3	17.4 (24.4)	8.	73.1 (64.7)	36.7
75% Ph	33. (20.1)	38.5	23.6 (23.3)	0.5	20.2 (26.3)	11.9	76.7 (69.7)	43.4
100% Ph	68.6 (39.5)	70.	20.4 (17.)	2.5	20.8 (40.4)	9.	109.8 (91.9)	79.4

References

(1) van Oss, C. J. *Journal of Adhesion Science and Technology* **2002**, *16*, 669–677.

(2) van Oss, C. J.; Good, R. J. *Journal of Macromolecular Science, Part A* **1989**, *26*, 1183–1203.

(3) van Oss, C. J. *Interfacial Forces in Aqueous Media*, 2nd ed.; CRC Press: Boca Raton, FL, 2006.

C. Publication 3

Describing the peak distribution in radial chromatography

Ingeborg Bednar,[†,‡] Eva Berger,[†] Nika Lendero Krajnc,[¶] Aleš Podgornik,[¶]

Rupert Tscheließnig,[†] and Alois Jungbauer[*,†,‡]

Austrian Centre of Industrial Biotechnology, Muthgasse 11, 1190 Vienna, Austria, Department of Biotechnology, Department of Biotechnology, University of Natural Resources and Life Sciences Vienna, Muthgasse 18, Vienna, Austria, and BIA Separations, Ajdovščina, Slovenia

E-mail: alois.jungbauer@boku.ac.at

Abstract

The exponentially modified Gaussian (EMG) function is commonly used to describe protein retention by radial monoliths. Neither does a physical justification exist for its usage nor can this function describe the retention behavior properly. We introduce a function consisting of two terms being similar to the Rice distribution (Rice-like function) which allows describing protein retention superior to the EMG function. Furthermore the underlying theory also implies a physical meaning. We compared the performances of the EMG function and also the sum of two EMG terms with the Rice-like function for four model proteins on cation and anion exchangers. The Rice-like function is able to model the fronting behavior, the pronounced peak tailing and the

---

[*]To whom correspondence should be addressed
[†]acib
[‡]boku
[¶]bia

peak height and is therefore the most suitable function to describe protein retention
for radial monoliths.

Introduction

The advantage of radial flow chromatography are the fast flow, high productivity and the
low pressure drop.[1] Monoliths[2] and often very soft media[3,4] are operated under radial chromatography conditions. The current mathematical description of the retention of peaks obtained by radial chromatography is unsatisfying.[5] So far the exponentially modified Gaussian
(EMG) function have been used as approximation also in radial chromatography, although
developed for axial chromatography.[6]

In axial chromatography the flow is directed along the axis of the column, the fluid
velocity does not change along the z-position at the column. Whereas in radial chromatography, where the column is usually realised as an annulus, the velocity increases from the
outer surface to the inner surface along the radial flow direction, because of the reducing
cross-sectional area, as sketched in Fig. 1.

The number of theoretical plates (N) is a measure to define the efficiency of a chromatographic column.[7] N can be calculated by the use of the statistical moments of the
distribution, also other methods e.g. via the width at half peak height exists, but these
methods usually assume a Gaussian distribution.[8] The number of theoretical plates increase
with the column length (in axial chromatography), therefore the HETP (height equivalent to
a theoretical plate) of a column is of interest; it allows comparison between different columns.
If the statistical distribution is known, e.g. the EMG function, the statistical moments are
easy to calculate through the distribution parameters. It is also possible to determine the
statistical moments by numerical integration of the data itself, but this should be avoided
because background effects can cause misleading results very easily.[9]

A more pronounced tailing of peaks has been observed in radial chromatography and
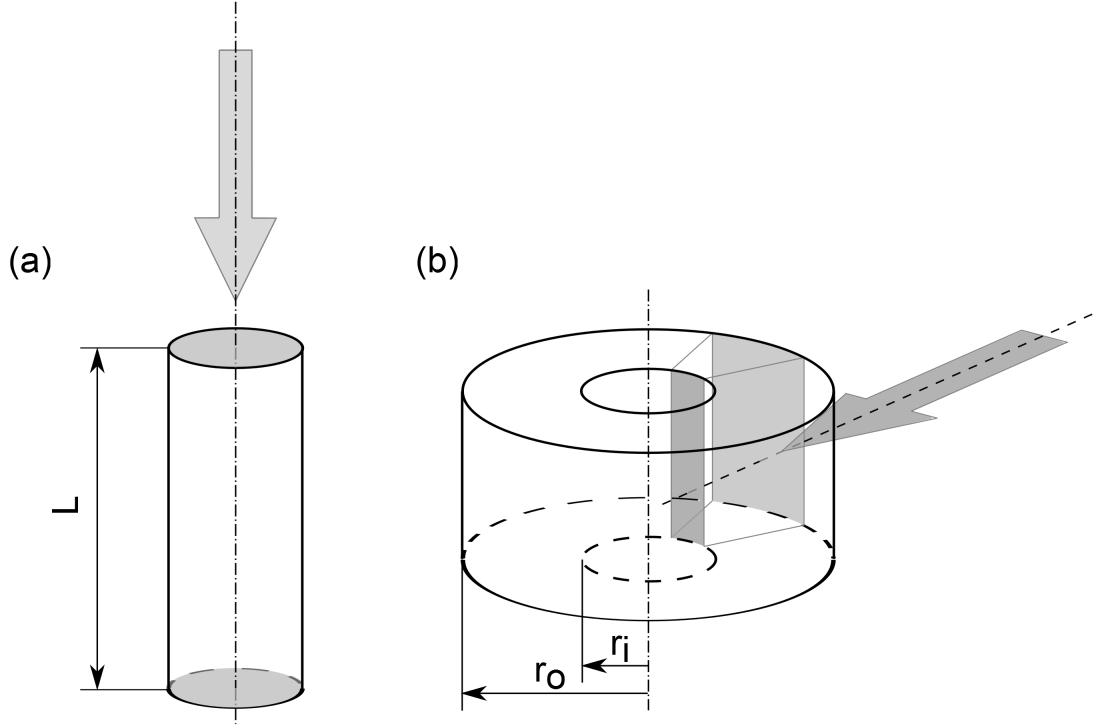
2

Figure 1: (a) A chromatography column with axial flow, the cross-sectional areas at the inlet and the outlet are highlighted in grey and are identical, due to its constant radius. The length of the column is indicated. (b) A tubular column with radial flow is sketched here. The cross-sectional area is reduced with decreasing radial distance from the z-axis. To indicate the different cross-sectional areas a segment of the tubular column is highlighted in grey. The outer radius r_o and the inner radius r_i are indicated.

the tailing could not be fully described by the EMG function. The shortcomings because in radial chromatography the different geometry causes non-constant velocity[2] and therefore a different tailing behavior occurs.

Within this work we show that using the EMG function to describe the retention of protein peaks of several model proteins on tubular monoliths is just a rough estimation, even if we use the sum of two EMG functions. We introduce a new function to describe protein peaks obtained by radial chromatography. EMG curves provide a perfect fit to (axial) chromatography peaks also for linear gradients even under non-linear conditions.[10] Unfortunately the physical meaning of the parameters is lost in these cases.

3

Decades ago, Lapidus and Amundson explored adsorption in beds with radial flow.[11] As they neglect diffusion in radial direction, their fundamental differential equation represents just the homogeneous form of the diffusion equation we used to describe radial chromatography. This, of course, results in a solution different to what we found. We Galilei-transformed the mass balance equation for axial chromatography to obtain the diffusion equation, which we solve by a Greens function approach in cylindrical coordinates. Lapidus and Amundson used boundary conditions to find a solution to their differential equation while we used initial conditions.

The function was applied to describe the retention behavior of certain model proteins with different monoliths, the monoliths were operated as radial columns. From this equation we calculate the first and second peak moment by numerical integration and calculated the HETP from it.

The monolithic materials used are a strong cation exchanger, with SO3-1 (Sulfonyl) ligands, a strong anion exchanger, with QA-1 (quaternary amine) ligands and a weak anion exchanger, with DEAE-1 (Diethylamino) ligands. The model proteins Immunoglobulin G (IgG), Bovine albumin serum (BSA), β-Lactoglobulin and Amyloglucosidase were used for the peak experiments and do vary in shape, compressibility, pI and size.[12–14]

We used three statistical distributions, while the EMG function was used also as sum of two EMG function terms, to describe the pulse response data of several proteins eluted with a gentle salt gradient.

Theory

The exponentially modified Gaussian function

The EMG function is a convolution of a Gaussian curve with an exponential decay and is widely used to describe tailing peaks.[8] Several ways to express the EMG function can be found in the literature, Grushkas[15] formula can be transcribed to

4

$$c(t)^{EMG} = A/(2\tau_G) \exp\left[\left(\frac{\sigma_G}{\tau_G}\right)^2 \frac{1}{2} - \frac{t - t_G}{\tau_G}\right] \text{erfc}\left[\frac{1}{\sqrt{2}}\left(\frac{t_G - t}{\sigma_G} + \frac{\sigma_G}{\tau_G}\right)\right] \tag{1}$$

The parameters t_G and σ_G are the retention time and the standard deviation of the Gaussian function, τ_G is the time constant of the exponential function, A the amplitude.

The HETP can be calculated easily by using two moments of this distribution, these are the mean $\mu_1 = t_G + \tau_G$ and the peak variance $\sigma^2 = \sigma_G^2 + \tau_G^2$

$$HETP = L/N = \frac{\sigma^2 L}{\mu_1^2}, \tag{2}$$

while L usually represents the column length.[8] Here we deal with radial systems, therefore we used, as it is the direct path through the separation medium, the radial thickness of the monolith instead of its length: $L = r_o - r_i$ (compare with Fig. 1).

Additionally, we also used the sum of two EMG function terms:

$$c(t)_{EMG^*} = c_{(1)}(t) + c_{(2)}(t) \tag{3}$$

The single terms and parameters of the sums are indexed with (1) and (2), the index EMG^* denotes that the function is consisting of two terms.

Here we calculated the statistical moments, necessary to determine the HETP, numerically; the first raw moment μ_1 and the variance of the distribution, σ^2 were calculated. The numerical determination of these statistical moments are defined as follows:[8] The first raw moment, the mean is calculated by

$$\mu_1 = \frac{1}{\mu_0} \int_0^\infty c(t) \, t \, dt \tag{4}$$

the second central moment, also called variance is

$$\sigma^2 = \frac{1}{\mu_0} \int_0^\infty c(t) \, (t - \mu_1)^2 dt. \tag{5}$$

5

Both are normalized with the zeroth moment, the peak area

$$\mu_0 = \int_0^\infty c(t)\, dt. \tag{6}$$

These definitions are valid for all statistical distributions. We determined the HETP by inserting these results into Eq. 2.

The exact solution for the infinite diluted system in cylindrical coordinates

In analogy to the heat flow from a cylindrical heat source we formulated the mass balance equation in cylindrical coordinates. With the assumption that the mass transport occurs just in radial direction and is uniformly distributed along the circumference, this equation is independent from its position at the longitudinal axis z and the azimuth angle φ. To transform the equation to moving coordinates a Galilei transform is necessary, then a Greens approach leads to the solution. According to Beck,[16] the radial Green function for radial heat transport in a hollow cylinder, which we identified to be appropriate to describe the analyte concentration in radial chromatography, is defined as

$$G(r,t|r',t') = \frac{1}{4\pi\alpha(t-t')} \exp\left[-\frac{r^2 + r'^2}{4\alpha(t-t')}\right] I_0\left[\frac{rr'}{2\alpha(t-t')}\right]. \tag{7}$$

I_0 represents Bessels function of the first kind, order zero.

The concentration pulse is initiated at the radial distance of r_o (the outer radius of monolith, compare with Fig. 1) and occurs at time $t' = t_0$, so we considered that at a time $t' < t_0$ the analyte concentration within the chromatography material is zero. The position of the pulse shifts with time, so we replaced $r = r_o - ut$. r' can be identified as the inner radius of the monolith, r_i, as indicated in Fig. 1. The parameter α contains the radial dispersion coefficient D and the retention factor k' by the relation $\alpha = D/(1 + k')$. So we obtain the specific solution

6

$$c(r, t) = \frac{1}{4\pi\alpha(t - t_0)} \exp\left[-\frac{(r_o - ut)^2 + r_i^2}{4\alpha(t - t_0)}\right] I_0\left[\frac{r_o r_i}{2\alpha(t - t_0)}\right]. \tag{8}$$

If we allocate Becks[16] result, which was derived for radial heat transport, to radial chromatography, this equation describes the analyte concentration within a hollow cylinder consisting of a single material.[17] To account for the fact that chromatography columns are porous and the void volume is filled with mobile phase as well as that retention of analyte molecules takes place by interaction with the solid phase, we assume a superposition of two solutions, where molecules interacting with the solid ($k' \neq 0$) and molecules being non-retained ($k' = 0$) sum up to the particular response over time.

$$c(r, t) = \int_0^\infty \left(A_{(1)}\delta(k'' - k') + A_{(2)}\delta(k'')\right) c(r, t) dk'' \tag{9}$$

with δ representing the Dirac delta function and $A_{(1)}$ and $A_{(2)}$ the respective amplitudes. We already used such a superposition to describe retention, but in axial chromatography.[18] Eq. 7 is similar to the Rice distribution in probability theory,[19] therefore we named Eq. 9 Rice-like function. The parameters of the two terms of the Rice-like functions are indexed with (1) and (2).

The statistical moments of this distribution were calculated numerically, as defined in Eq. 4 to Eq. 6. Subsequently, the HETP was determined by inserting these results into Eq. 2.

Goodness of fit - the R^2 parameter

The coefficient of determination, R^2, a dimensionless parameter, describes the quality of a model function. We used this parameter to quantify how well the statistical distributions we used describe the data. According to Egert,[20] R^2 is defined as

$$R^2 = 1 - \frac{S^2}{S_Y^2}; \ 0 \leq R^2 \leq 1. \tag{10}$$

7

The residual sum of squares, S^2 is calculated by

$$S^2 = \sum_{j=1}^{k}(y_j - \widehat{y}_j)^2 \tag{11}$$

while y_j indicates the measured quantity of the observed data points and $\widehat{y}_j$ the corresponding values of the model, so the squared differences of all data points and their predicted values are summed up.

S_Y^2, the total sum of squares, is defined as

$$S_Y^2 = \sum_{j=1}^{k}(y_j - \overline{y})^2 \tag{12}$$

while $\overline{y} = \frac{1}{n}\sum_{j=1}^{k} y_j$ is the mean value of the observed data.

Results and Discussion

Several chromatographic experiments have been made with radial columns. Peaks were fitted by EMG functions with one term and two terms, as well as with the Rice-like function (all fit parameters are listed in Table 1 - 3). A good approximation was obtained with all functions although just the Rice-like function is able to describe the fronting behavior, the pronounced peak tailing and also the peak height (see Fig. 2). This can be visually detected, to ease the comparison of the fits with the data; the remaining areas are colored in shades of grey. When the data are plotted in a semi-logarithmic form the difference of the approximations become even more clear (Fig. 3). The EMG function with one summand cuts a major part of the tailing off. This leads to smaller values of variances and so, in contrast to the other model functions, considerably smaller values for the HETP are obtained (compare Table 1, 2 and 3).

In Fig. 3 the remaining areas between the fits and the data are also colored in different shades of grey. Additional, the summands of the EMG fit function with two terms and of

the Rice-like function are plotted separately. By comparison of Fig. 3 - 8 it caches the eye that for all Rice-like fits one summand describes the fronting behavior while the other one describes the tailing behavior. We interpret the former peak to result from molecules which are not interacting with the monolithic surface (remaining in the mobile phase) and the later peak to result from molecules which do interact with the monolithic surface. There is no physical interpretation for the EMG function neither for the one with two summands, but clearly a model with a larger number of parameters to adjust leads to a more accurate description of the data and might have been an alternative to the Rice-like function.

Although in Fig. 3 the fit of the EMG function with two terms seems to be the best to fit the tailing behavior at a first glance, one has to keep in mind that, because of the semi-logarithmic plot, the areas along the ordinate are distorted, so areas near the abscissa seem larger as they actually are. Besides, the fronting behavior of the data is poorly described by both EMG functions, but is exactly reproduced by the Rice-like function. The objective parameter R^2, describing the goodness of the fit, is largest for the Rice-like function (compare Table 1, 2 and 3). The only exception is IgG on the QA monolith, where the R^2 parameter of the EMG function with two summands is slightly larger than of the Rice-like function (compare Table 2 with Table 3). By comparing both fits in Fig. 8, it is evident that the EMG function (with two summands) fails to describe the fronting behavior, while the Rice-like function might not describe the tailing behavior best. That leads to overall R^2 parameters which are almost identical.

In peak fitting and determination of peak areas, variances etc. long tailing always creates a problem and leads to inaccuracy. Either peak width or related peak parameters are over- or underestimated. The Rice-like function is excellently suited to approximate the tailing caused by the geometry of the column. Examples are shown in Fig 3 to 8 and the trend is identical for nearly all of them.
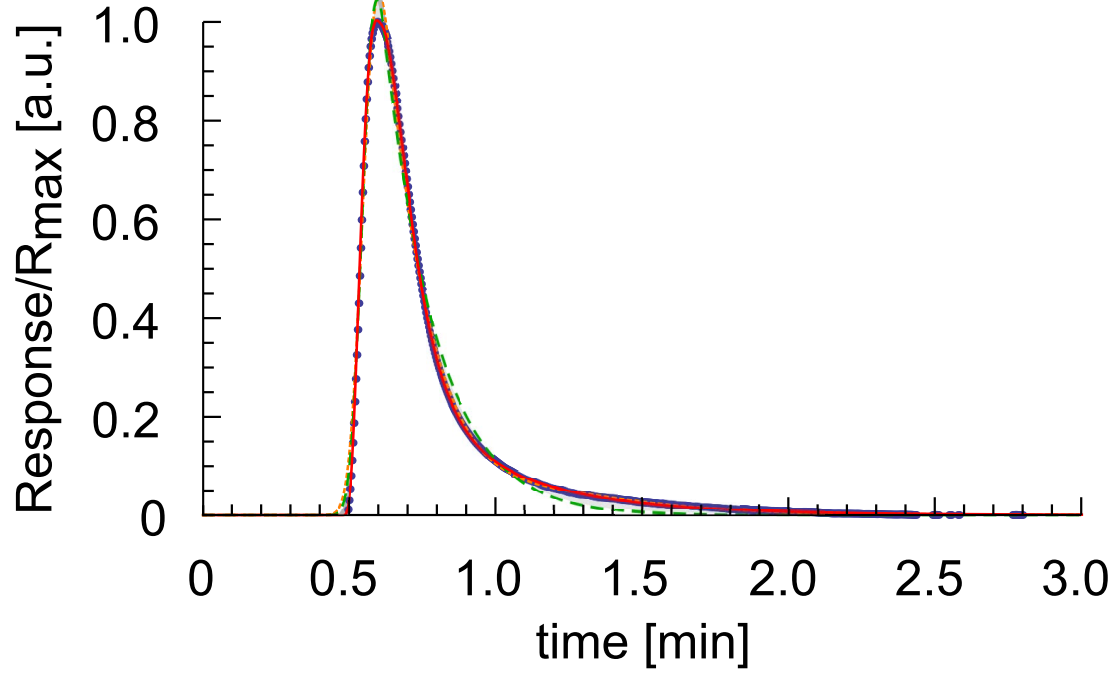
9

Figure 2: The pulse response experiment of β-Lactoglobulin on the SO3-1 monolith and its appendant fits are shown here. The normalized UV-detector response is plotted over time. The data points are plotted as blue dots, the green, dashed line is the fit with the EMG function, while the orange, dotted line represents the fit obtained by two terms of an EMG function. The red, solid line represents the fit with the Rice-like function. To indicate the differences between the fits and the data, the areas between them are colored in shades of grey.
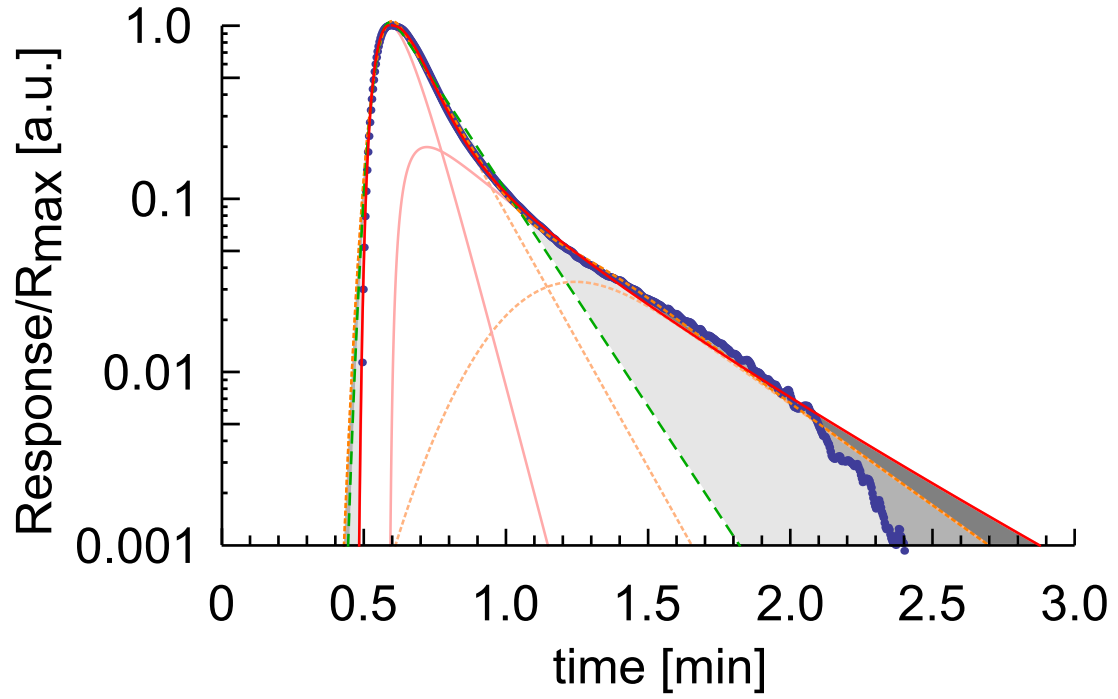
10

Figure 3: The pulse response experiment of β-Lactoglobulin on the SO3-1 monolith and its appendant fits are plotted. The normalized UV-detector response in logarithmic scale is plotted over time. The blue dots represent the measured data and the green, dashed line is the curve obtained by the EMG fit with one term. The orange, dotted line belongs to the EMG fit of two terms; the plots of both single terms are light orange colored and plotted as dotted line. The red, solid line represents the Rice-like function, which is the sum of two terms; the plots of both single terms are plotted as solid lines in light red color. To indicate the differences between the fits with the data respectively among each other, the areas between the curves are colored in shades of grey.
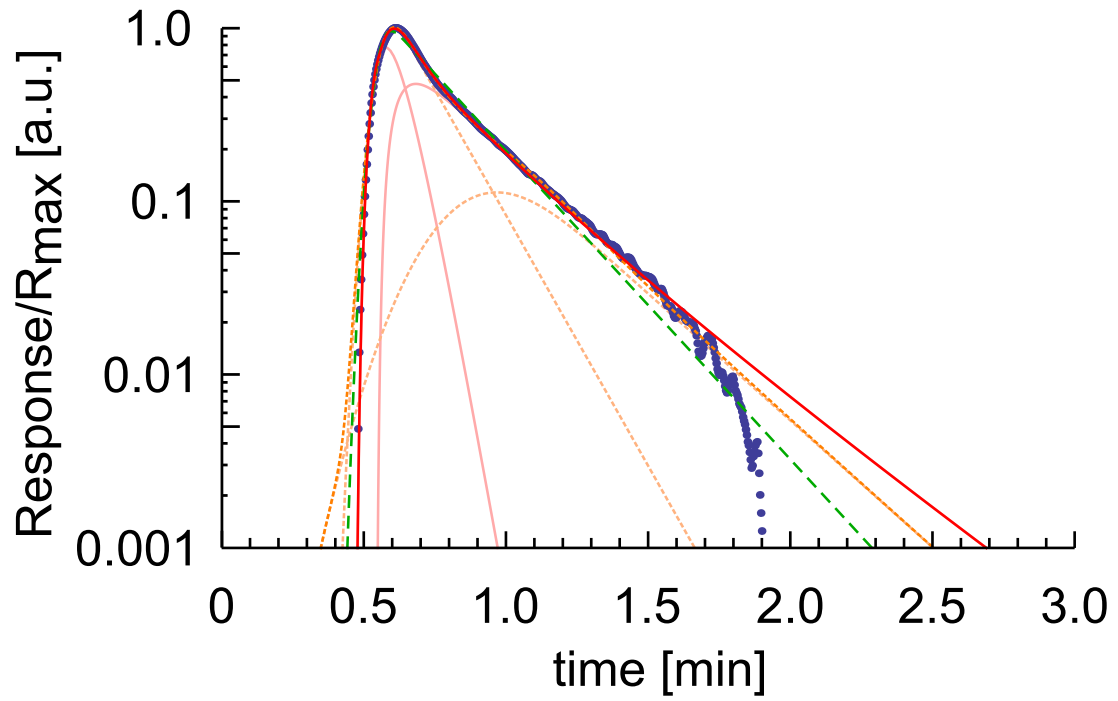
11

Figure 4: The pulse response experiment of BSA on the SO3 monolith and its appendant fits are shown. The normalized UV-detector response in logarithmic scale is plotted over time. The blue curve represents the measured data, the green one is the EMG fit with one term and the orange curve the one obtained by the EMG fit with two terms. The plot of the Rice-like function is colored in red.
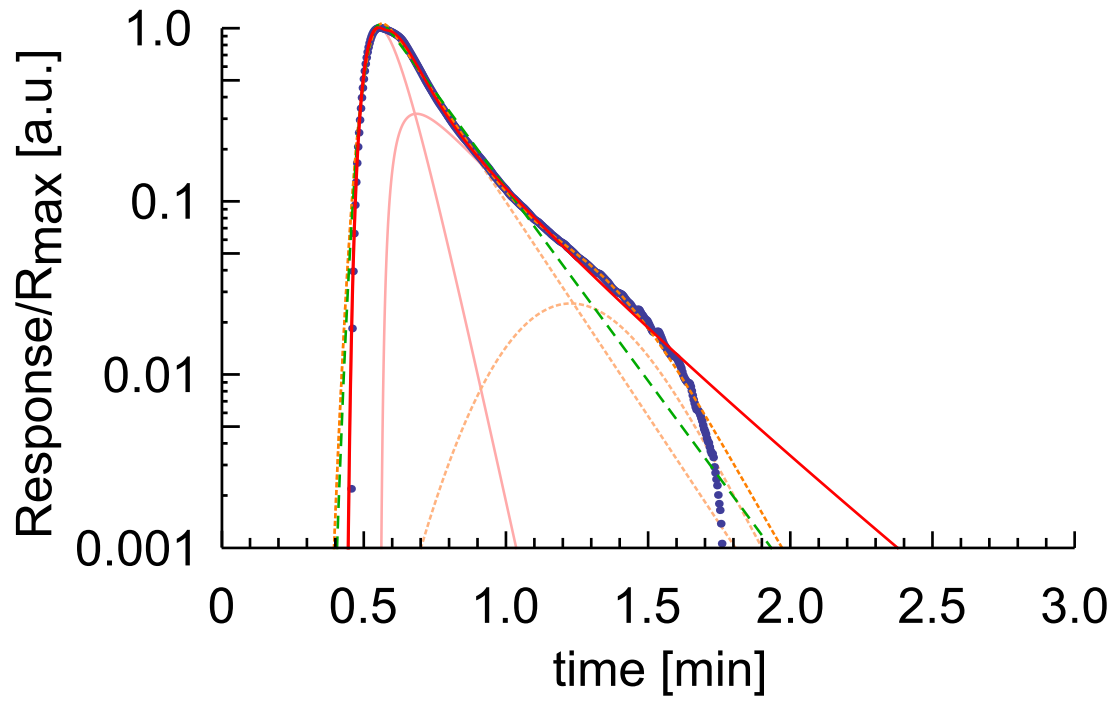
12

Figure 5: The pulse response experiment of Amyloglucosidase on the SO3 monolith and its appendant fits are plotted. The normalized UV-detector response in logarithmic scale is plotted over time. The blue curve represents the measurement data, the green line is the curve obtained by the EMG fit with one term and the orange curve is the EMG fit with two terms. The curve of the Rice-like function is red colored.
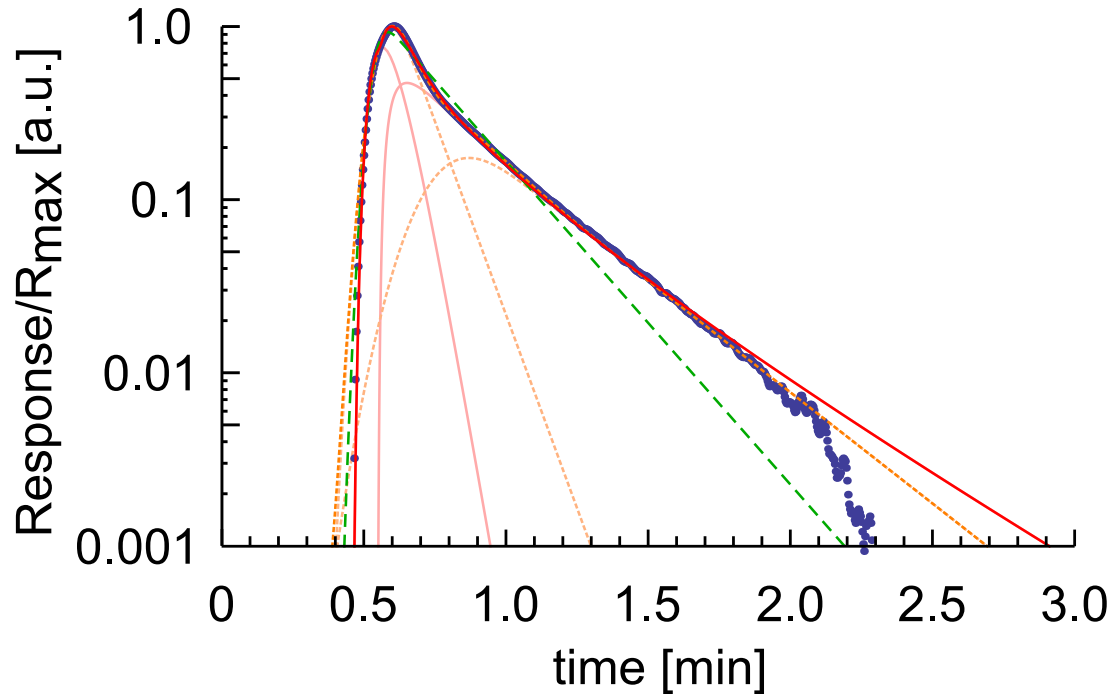
Figure 6: The pulse response experiment of IgG on the SO3 monolith and its fits are plotted here. The difference to Fig. 2 is the ordinate, which shows the normalized UV-detector response in logarithmic scale but also plotted over time. The measurement data is colored in blue, the red line represents the curve obtained by the fit with the Rice-like function. The orange line is the curve obtained by the EMG fit with two terms. The curve of the EMG function with one term is the green one.
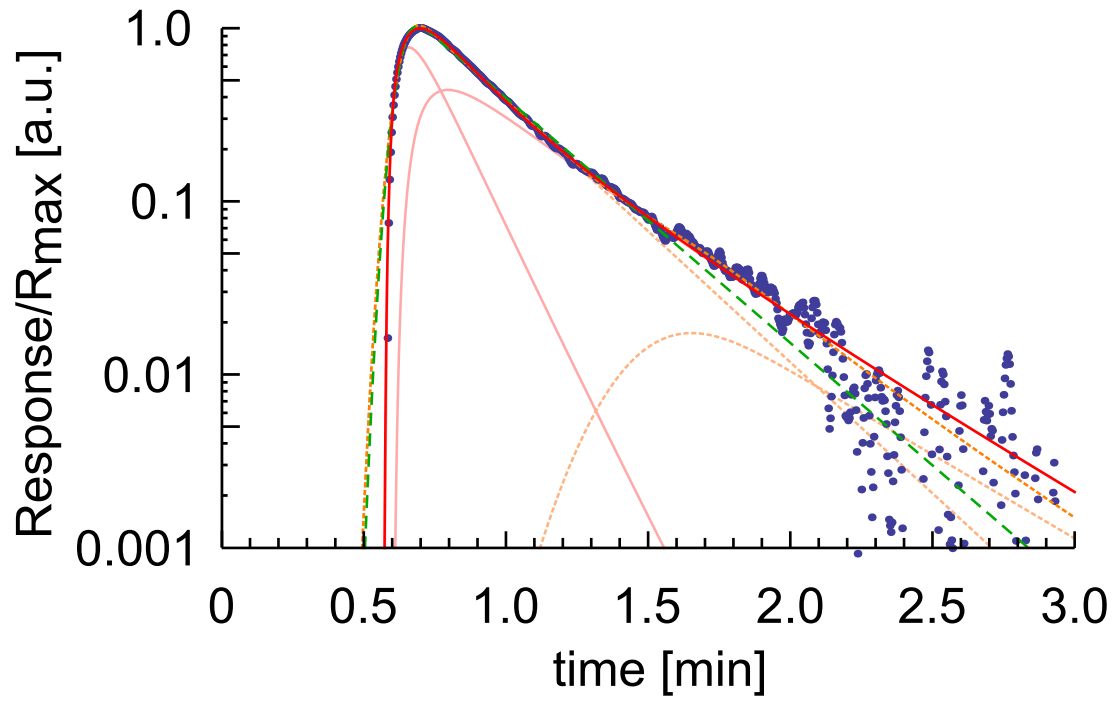
14

Figure 7: The pulse response experiment of IgG on the DEAE monolith and its fits are shown here. The normalized UV-detector response in logarithmic scale is plotted over time. The blue curve represents the data measured, the green curve is obtained by the EMG fit with one term and the orange one by the EMG fit with two terms. The red curve is the plot of the Rice-like function.
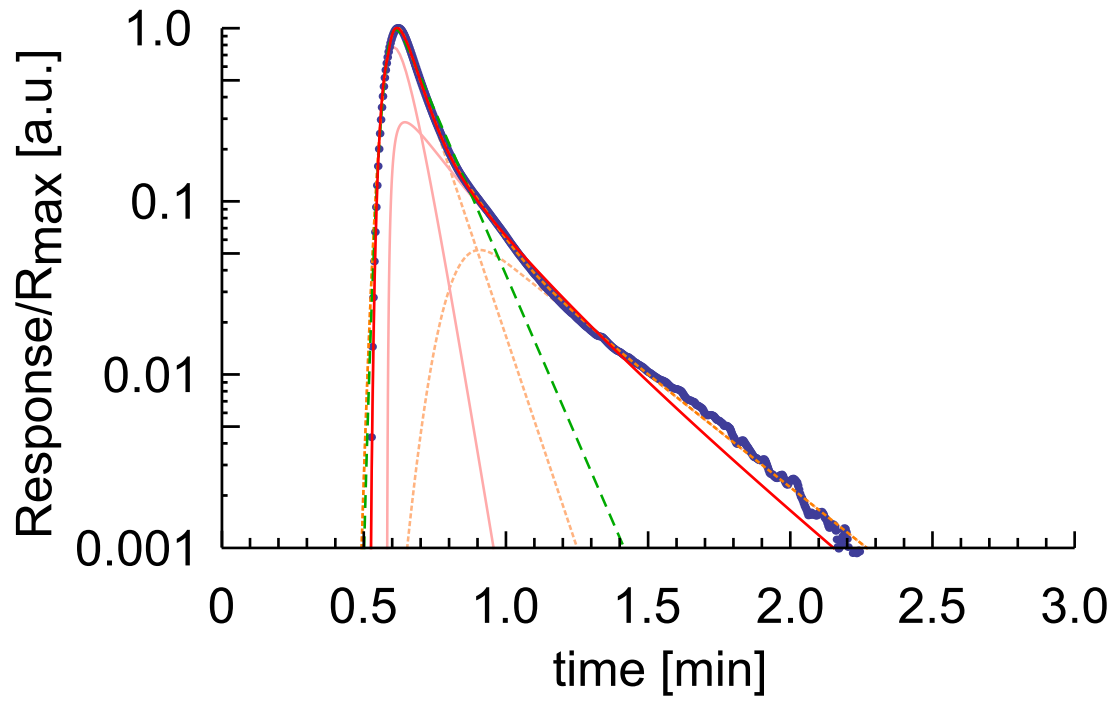
Figure 8: The pulse response experiment of IgG on the QA monolith and its fits are shown here. The normalized UV-detector response in logarithmic scale is plotted over time. The blue curve represents the data measured, the green line is the curve obtained by the EMG fit with one term and the orange curve is obtained by the EMG fit with two terms. The red curve represents the Rice-like function.

16

Table 1: The fit parameters, R^2, the measure of fit quality and the HETP (in mm) of the EMG function (one summand) are listed.

SO3	A	τ_G	t_G	σ_G	R^2	HETP
IgG	0.286	0.233	0.532	0.032	0.985	0.56
BSA	0.307	0.244	0.543	0.032	0.992	0.58
β-Lactoglobulin	0.259	0.174	0.545	0.032	0.993	0.36
Amyloglucosidase	0.284	0.195	0.509	0.032	0.994	0.47
DEAE	A	τ_G	t_G	σ_G	R^2	HETP
IgG	0.407	0.307	0.625	0.038	0.997	0.66
QA	A	τ_G	t_G	σ_G	R^2	HETP
IgG	0.167	0.115	0.578	0.024	0.994	0.17

Table 2: The fit parameters, R^2, the measure of fit quality and the HETP (in mm, numerical determination) of the EMG function (two summands, indexed by (1) and (2)) are listed. β-L. and Amyl. are used as abbreviations for β-Lactoglobulin and Amyloglucosidase.

SO3	$A_{(1)}$	$\tau_{G(1)}$	$t_{G(1)}$	$\sigma_{G(1)}$	$A_{(2)}$	$\tau_{G(2)}$	$t_{G(2)}$	$\sigma_{G(2)}$	R^2	HETP
IgG	0.191	0.097	0.551	0.046	0.105	0.339	0.728	0.119	0.9984	0.87
BSA	0.237	0.15	0.553	0.04	0.077	0.297	0.803	0.175	0.9984	0.71
β-L.	0.246	0.148	0.55	0.037	0.027	0.372	1.045	0.203	0.9966	0.85
Amyl.	0.275	0.176	0.512	0.036	0.015	0.14	1.119	0.191	0.9955	0.57
DEAE	$A_{(1)}$	$\tau_{G(1)}$	$t_{G(1)}$	$\sigma_{G(1)}$	$A_{(2)}$	$\tau_{G(2)}$	$t_{G(2)}$	$\sigma_{G(2)}$	R^2	HETP
IgG	0.399	0.287	0.627	0.042	0.015	0.449	1.449	0.182	0.9972	0.81
QA	$A_{(1)}$	$\tau_{G(1)}$	$t_{G(1)}$	$\sigma_{G(1)}$	$A_{(2)}$	$\tau_{G(2)}$	$t_{G(2)}$	$\sigma_{G(2)}$	R^2	HETP
IgG	0.153	0.089	0.583	0.028	0.026	0.334	0.807	0.07	0.9997	0.56

17

Table 3: The fit parameters, indexed by (1) and (2), because the Rice-like function consists of two terms, the quality of the fit, R^2 and the HETP values (in mm, numerical determination) are listed. For the radii the following values have to be inserted: $r_o = 0.93$ mm and $r_i = 0.335$ mm. β-L. and Amyl. and are used as abbreviations for β-Lactoglobulin and Amyloglucosidase.

SO3	$A_{(1)}$	$\alpha_{(1)}$	$u_{(1)}$	$t0_{(1)}$	$A_{(2)}$	$\alpha_{(2)}$	$u_{(2)}$	$t0_{(2)}$	R^2	HETP
IgG	$945.4 \cdot 10^3$	0.233	4.5	0.43	19.	1.907	3.849	0.541	0.9990	0.99
BSA	$625.2 \cdot 10^3$	0.226	4.342	0.442	53.1	2.008	4.418	0.532	0.9993	0.79
β-L.	$23.7 \cdot 10^3$	0.329	4.275	0.454	14.5	2.385	4.097	0.577	0.9999	0.95
Amyl.	$217.9 \cdot 10^3$	0.38	5.063	0.411	27.9	1.411	3.922	0.545	0.9999	0.69
DEAE	$A_{(1)}$	$\alpha_{(1)}$	$u_{(1)}$	$t0_{(1)}$	$A_{(2)}$	$\alpha_{(2)}$	$u_{(2)}$	$t0_{(2)}$	R^2	HETP
IgG	78	0.329	2.983	0.56	134.1	3.745	5.362	0.584	0.9995	0.86
QA	$A_{(1)}$	$\alpha_{(1)}$	$u_{(1)}$	$t0_{(1)}$	$A_{(2)}$	$\alpha_{(2)}$	$u_{(2)}$	$t0_{(2)}$	R^2	HETP
IgG	$56.2 \cdot 10^3$	0.124	3.331	0.499	4.1	0.779	2.885	0.576	0.9996	0.5

Outline

In this work we pointed out that the usage of the EMG function to describe protein retention in linear gradient mode for monoliths is neither justified by an underlying theory nor an excellent fit. Furthermore we introduced a function to describe the pulse responses. The quality of the fits with this function presented here are usually far better, which can be nailed down by the coefficient of determination, R^2, being a measure of the quality of the fits.

Experimental

Pulse response experiments were performed on a strong cation exchanger, a CIM® SO3-1 (Sulfonyl ligands) Tube Monolithic Column, a strong anion exchanger, a CIM® QA-1 (quaternary amine ligands) Tube Monolithic Column and a weak anion exchanger, CIM® DEAE-1 (Diethylamino ligands) Tube Monolithic Column, all with a channel size of 1.5 μm, kindly provided from BIA separations (Ajdovščina, Slovenia). The dimensions of the monolith are: the inner diameter $D_i = 6.7$ mm, the outer diameter $D_o = 18.6$ mm and the length of the column $L = 4.2$ mm. The model proteins IgG (Octagam 5% was kindly provided from Octapharma) was used for all monolithic columns, BSA (from Sigma, A3912, $\geq 96\%$), β-Lactoglobulin (from Sigma, L0130, $\geq 90\%$) and Amyloglucosidase (from Sigma, 10113, ≈ 120 U/mg) were used for SO3. The puffer systems and pH-values were choosen according to the retention mechanism (anion or cation exchanger) and to the particular pI-values of the proteins. For the SO3 monolith, IgG was diluted and BSA was solved in 50mM MES (2-(N-morpholino)ethanesulfonic acid - buffer A) to reach a concentration of 1.5mg/ml. Before injecting 10μl into the monolithic column the samples were filtered through a 0.22μm (PVDF) syringe filter purchased from Millipore and Whatman. The gradient for elution was from buffer A to 20% B (50mM MES + 100mM NaCl) in 30min for IgG and to 2% B in 15min for BSA. After every run cleaning of the monolithic columns of possible remaining

<div align="center">19</div>

proteins were obtained by using 50mM MES + 1M NaCl. The measurements were performed at a pH of 5.5, at a flow rate of 2ml/min and at room temperature. β-Lactoglobulin and Amyloglucosidase were solved in 50mM Acetic acid (buffer A) to reach a concentration of 0.5mg/ml, for Amyloglucosidase it was observed that not all of the protein was solved in the buffer, these agglomerated proteins were detained by filtering through a 0.22μm (PVDF) syringe filter purchased from Millipore and Whatman, the actual concentration in the sample was less than 0.5mg/ml, although not measured. The injection volume was 30μl and the gradient for elution was from buffer A to 10% B (50mM Acetic acid + 100mM NaCl) in 15min for both proteins. A cleaning run was performed after every measurement by using 50mM Acetic Acid + 1M NaCl. The measurements were performed at a pH of 4.5, at a flow rate of 2ml/min and at room temperature. For the anion exchangers (QA and DEAE) the following buffer system was used: 20mM TRIS (buffer A), 20mM TRIS + 100mM NaCl (buffer B), 20mM TRIS + 300mM NaCl (buffer C) and to clean the monolithic columns 20mM MES + 1M NaCl was used, all buffers at a pH of 7.5. For the use with the QA monolith, IgG was diluted in buffer B (to a concentration of 1.5mg/ml), and eluted with buffer C, the gradient was to reach 100% buffer C in 7.5min. For the use with the DEAE monolith, IgG was diluted in buffer A (to a concentration of 0.5mg/ml) and eluted with buffer B, while the gradient was adjusted so that 10% of buffer B were reached in 15min. The injection volume was 10μl in both cases. All buffers were filtered by a 0.45μm filter before chromatography, degassing was obtained by the HPLC system (Agilent 1200 series, Santa Clara, CA, United States). The HPLC workstation was controlled through a connected PC using Chem Station for LC 3D systems Rev. B. 04.03[16] (Agilent Technologies, Inc. 2001-2010). The UV detector signals were exported into CSV formatted files and further processed with Mathematica (Wolfram Research, Inc. Mathematica 9.0.0.0 Champaign, IL: Wolfram Research, Inc.; 2012).

Supplementary

An alternative way to calculate the statistical moments and furthermore the HETP of a function consisting of two terms, e.g. two EMG functions, is to insert this sum (Eq. 3) into the general expression for the moments (Eq. 4 and 5). By doing that we obtain a general expression for the first moment of the sum of two functions:

$$
\begin{aligned}
\mu_{1,\,EMG^*} &= \left(\int_0^\infty \big(c_{(1)}(t) + c_{(2)}(t) \big)\, dt \right)^{-1} \int_0^\infty \big(c_{(1)}(t) + c_{(2)}(t) \big)\ t\, dt \\
&= \underbrace{\big(\mu_{0,\,(1)} + \mu_{0,\,(2)} \big)}_{\mu_{0,\,EMG^*}}^{-1} \big(\mu_{0,\,(1)}\, \mu_{1,\,(1)} + \mu_{0,\,(2)}\, \mu_{1,\,(2)} \big).
\end{aligned}
\tag{13}
$$

The single terms of the sums are indexed with (1) and (2), the index EMG^* is used for the overall function.

Accordingly, the variance can be expressed as

$$
\begin{aligned}
\sigma^2_{EMG^*} &= \frac{1}{\mu_{0,\,EMG^*}} \int_0^\infty c(t)_{EMG^*} \big(t^2 - 2t\mu_{1,\,EMG^*} + \mu^2_{1,\,EMG^*} \big)\, dt \\
&= \frac{1}{\mu_{0,\,EMG^*}} \int_0^\infty c(t)_{EMG^*}\, t^2\, dt - 2\mu_{1,\,EMG^*} \underbrace{\frac{1}{\mu_{0,\,EMG^*}} \int_0^\infty c(t)_{EMG^*}\, t\, dt}_{\mu_{1,\,EMG^*}} +
\end{aligned}
\tag{14}
$$

$$
\frac{\mu^2_{1,\,EMG^*}}{\mu_{0,\,EMG^*}} \underbrace{\int_0^\infty c(t)_{EMG^*}\, dt}_{\mu_{0,\,EMG^*}}
\tag{15}
$$

and by using the second raw moment $\mu_{2,\,EMG^*} = \frac{1}{\mu_{0,\,EMG^*}} \int_0^\infty c(t)_{EMG^*}\, t^2\, dt$ we obtain

$$
\sigma^2_{EMG^*} = \mu_{2,\,EMG^*} - \mu^2_{1,\,EMG^*}
\tag{16}
$$

as general formula for the variance.

Therefore the HETP can be expressed as:

<div align="center">21</div>

$$HETP_{EMG^*} = \frac{\mu_{2,\,EMG^*}}{\mu_{1,\,EMG^*}^2} - 1. \tag{17}$$

Acknowledgement

References

(1) Huang, S. H.; Lee, W.-C.; Tsao, G. T. Mathematical models of radial chromatography. *The Chemical Engineering Journal* **1988**, *38*, 179–186.

(2) Podgornik, A.; Jančar, J.; Merhar, M.; Kozamernik, S.; Glover, D.; Čuček, K.; Barut, M.; Štrancar, A. Large-scale methacrylate monolithic columns: design and properties. *Journal of Biochemical and Biophysical Methods* **2004**, *60*, 179–189.

(3) Stickel, J. J.; Fotopoulos, A. PressureFlow Relationships for Packed Beds of Compressible Chromatography Media at Laboratory and Production Scale. *Biotechnology Progress* **2001**, *17*, 744–751.

(4) Sofer, G. K.; Nyström, L.-E. *Process chromatography: a practical guide*; Academic Press, 1989.

(5) Di Marco, V. B.; Bombi, G. Mathematical functions for the representation of chromatographic peaks. *Journal of Chromatography A* **2001**, *931*, 1–30.

(6) Hahn, R.; Tscheliessnig, A.; Bauerhansl, P.; Jungbauer, A. Dispersion effects in prepar-

ative polymethacrylate monoliths operated in radial-flow columns. *Journal of Biochemical and Biophysical Methods* **2007**, *70*, 87–94.

(7) Guiochon, G.; Shirazi, S. G.; Katti, A. M. *Fundamentals of preparative and nonlinear chromatography*; Academic Press, 1994.

(8) Carta, G.; Jungbauer, A. *Protein Chromatography: Process Development and Scale-Up*; John Wiley & Sons, 2010.

(9) Miyabe, K. Moment analysis of chromatographic behavior in reversed-phase liquid chromatography. *Journal of Separation Science* **2009**, *32*, 757770.

(10) Jungbauer, A. Insights into the chromatography of proteins provided by mathematical modeling. *Current Opinion in Biotechnology* **1996**, *7*, 210–218.

(11) LAPIDUS, L.; AMUNDSON, N. R. Mathematics of adsorption in beds. III. Radial flow. *The Journal of physical and colloid chemistry* **1950**, *54*, 821–829, PMID: 15422538.

(12) Machold, C.; Deinhofer, K.; Hahn, R.; Jungbauer, A. Hydrophobic interaction chromatography of proteins: I. Comparison of selectivity. *Journal of Chromatography A* **2002**, *972*, 3–19.

(13) Vandersall, A. S.; Cameron, R. G.; Nairn, C. J.; Yelenosky, G.; Wodzinski, R. J. Identification, Characterization, and Partial Purification of Glucoamylase from Aspergillus Niger (Syn A. Ficuum) NRRL 3135. *Preparative Biochemistry* **1995**, *25*, 29–55.

(14) Ueberbacher, R.; Haimer, E.; Hahn, R.; Jungbauer, A. Hydrophobic interaction chromatography of proteins: V. Quantitative assessment of conformational changes. *Journal of Chromatography A* **2008**, *11981199*, 154–163.

(15) Grushka, E. Characterization of exponentially modified Gaussian peaks in chromatography. *Analytical Chemistry* **1972**, *44*, 1733–1738.

23

(16) Beck, J. V. *Heat conduction using Green's functions*; Hemisphere Pub. Corp.: London; Washington, DC, 1992.

(17) Gritti, F.; Guiochon, G. Perspectives on the Evolution of the Column Efficiency in Liquid Chromatography. *Analytical Chemistry* **2013**, *85*, 3017–3035.

(18) Bednar, I.; Tscheließnig, R.; Berger, E.; Podgornik, A.; Jungbauer, A. Surface energies of hydrophobic interaction chromatography media by inverse liquid chromatography. *Journal of Chromatography A* **2012**, *1220*, 115–121.

(19) Talukdar, K. K.; Lawing, W. D. Estimation of the parameters of the Rice distribution. *The Journal of the Acoustical Society of America* **1991**, *89*, 1193–1197.

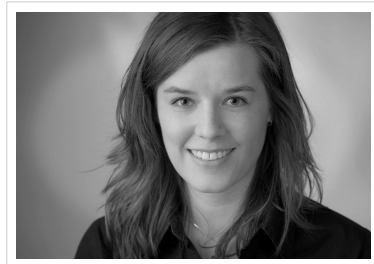(20) Egert, C. *Lineare statistische Modellierung und Interpretation in der Praxis*; Oldenbourg: München, 2013.

Graphical TOC Entry
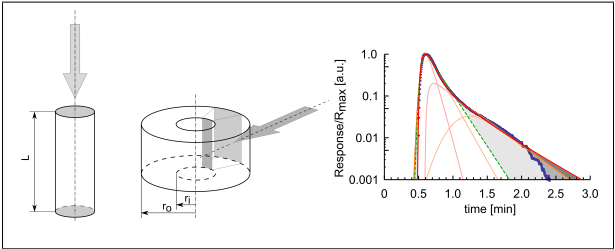
D. Curriculum vitae

DI Ingeborg Bednar

Ausbildung:

ab 09/10   **Doktoratsstudium der Ingenieurwissenschaften, BOKU Wien**
Dissertation: *Surface energy of hydrophobic chromatographic media and the impact of radial flow direction to the peak distribution in chromatography*

10/01 – 11/09   **Studium der Technischen Physik, TU Wien**
Diplomarbeit: *Thermoelectric properties of novel clathrates* $Ba_8T_xT'_yGe_{46-x-y}$ *(T=Cu, Si, Pd; T'=Zn) and* $Ba_8Ag_zGe_{46-z}$ *(z=2, 3, 4, 5)*

09/96 – 06/01   **HTL-Ausbildung, TGM** (Technologisches Gewerbemuseum), Wien
Abteilung Werkstoffingenieurwesen
Ausbildungsschwerpunkt: *Keramik, Glas und Baustofftechnik*

Berufserfahrung:

06/10 – 06/13   **Junior Researcher, ACIB** (Austrian Centre of Industrial Biotechnology), Wien
Projekt *Ligand and Surface Characterization*

09/01 – 04/10   **Sachbearbeiterin Lichtmikroskopie, Staatliche Versuchsanstalt – TGM**, Wien
Fachbereich *Kunststoff- und Umwelttechnik*

01/09 – 09/09   **Projektassistentin, Institut für Festkörperphysik, TU Wien**
Projekt *THECLA - Thermoelektrizität in Clathraten*

10/07 - 02/08   **Tutorin, TU Wien**
Lehrveranstaltung: *Physik für ElektrotechnikerInnen*

Praktika:

07/00 – 08/00   Ferialpraktikum als **Kunststofftechnikerin, Great Lakes**, Belgien

07/99 & 07/98   Ferialpraktikum als **Silikattechnikerin, Gmundner Keramik**

Weiterbildungen:

01/10   Schulung zur **Produktauditorin, ÖVGW** (Österreichische Vereinigung für das Gas und Wasserfach)

12/07   Ausbildung zur **ÖVGW – Auditorin**

Soziales Engagement:

09/97 – 06/12   Jungscharleiterin

DI Ingeborg Bednar

Publikationen (peer reviewed):

Bednar, I., Berger, E., Lendero Krajnc, N., Podgornik, A., Jungbauer, A. & Tscheliessnig, R. (2014).
Surface energies of monoliths by inverse liquid chromatography and contact angles,
Langmuir, 30 (19), 5435–5440.

Bednar, I., Tscheließnig, R., Berger, E., Podgornik, A., & Jungbauer, A. (2012).
Surface energies of hydrophobic interaction chromatography media by inverse liquid
chromatography. *Journal of Chromatography A*, *1220*, 115-121.

Zeiringer, I., Chen, M., Bednar, I., Royanian, E., Bauer, E., Podloucky, R., ... & Effenberger, H. (2011).
Phase equilibria, crystal chemistry, electronic structure and physical properties of Ag–Ba–Ge
clathrates. *Acta Materialia*, *59* (6), 2368-2384.

Nasir, N., Grytsiv, A., Melnychenko-Koblyuk, N., Rogl, P., Bednar, I., & Bauer, E. (2010).
Crystal structure and physical properties of quaternary clathrates $Ba_8Zn_xGe_{46-x-y}Si_y$,
$Ba_8(Zn, Cu)_xGe_{46-x}$ and $Ba_8(Zn, Pd)_xGe_{46-x}$. *Journal of Solid State Chemistry*, *183* (10), 2329-2342.

Bednar, I., Royanian, E., Bühler-Paschen, S., Bauer, E., Nasir, N., Grytsiv, A., ... & Rogl, P. (2010).
Giant Thermopower at Low Temperatures in Novel Clathrates $Ba_8\{Cu, Zn\}_xGe_{46-x}$.
Journal of electronic materials, *39* (9), 1687-1691.

Konferenzbeiträge:

06/13	Affinity 2013, 20th Biennial Meeting of the International Society for Molecular Recognition, Vienna/Austria, *Poster*
03/13	8th HIC/RPC Bioseparation Conference, Savannah/GA, *Vortrag*
06/12	MSS 2012, 5th Monolith Summer School & Symposium, Ajdovščina & Portorož/Slovenia, *Vortrag*
06/11	HPLC 2011, 36th International Symposium on High Performance and Liquid Phase Separations and Related Techniques, Budapest/Hungary, *Poster*
07/09	ICT2009 & ECT2009, The 28th International Conference on Thermoelectrics and The 7th European Conference on Thermoelectrics, Freiburg/Germany, *Vortrag*